DAVID W. TAYLOR NAVAL SHIP RESEARCH AND DEVELOPMENT CENTER

Bethesda, Maryland 20084

EXPERIMENTAL PERFORMANCE OF A FLAPPED HYDROFOIL IN CALM WATER AT LOW FROUDE NUMBERS

by

Michael B. Wilson

APPROVED FOR PUBLIC RELEASE: DISTRIBUTION UNLIMITED

SHIP PERFORMANCE DEPARTMENT
RESEARCH AND DEVELOPMENT REPORT

June 1982

DTNSRDC-82/002

NOW-DTNSRDC 5602129 (2-80)
(supersedes 3960144)

MAJOR DTNSRDC ORGANIZATIONAL COMPONENTS

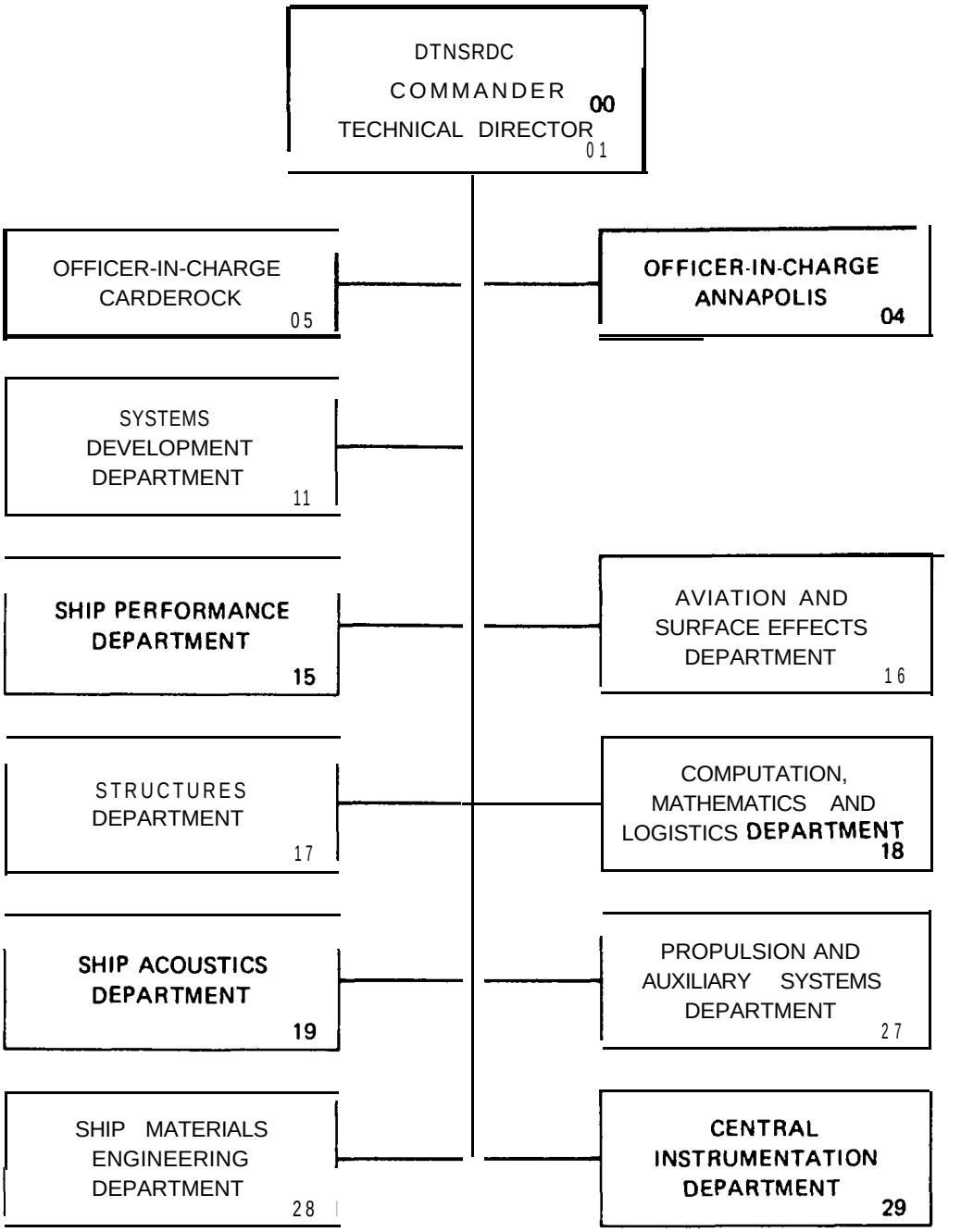

UNCLASSIFIED

SECURITY CLASSIFICATION OF THIS PAGE (When Data Entered)

REPORTDOCUMENTATION PAGE		READ INSTRUCTIONS BEFORECOMPLETINGFORM
1. REPORT NUMBER DTNSRDC-82/002	2. GOVT ACCESSION NO.	3. RECIPIENT'S CATALOG NUMBER
4. TITLE (end Subtitle) EXPERIMENTAL PERFORMANCE OF A FLAPPED HYDRO-FOIL IN CALM WATER AT LOW FROUDE NUMBERS		5. TYPE OF REPORT & PERIOD COVERED Final 6. PERFORMING ORG. REPORT NUMBER
7. AUTHOR(e) Michael B. Wilson		8. CONTRACT OR GRANT NUMBER(s)
9. PERFORMING ORGANIZATION NAME AND ADDRESS David W. Taylor Naval Ship Research and Development Center Bethesda,, Maryland 20084		10. PROGRAM ELEMENT. PROJECT, TASK AREA & WORK UNIT NUMBERS (See reverse side)
1. CONTROLLING OFFICE NAME AND ADDRESS Naval Material Command Navy Department Washington, D.C. 20360		12. REPORT DATE June 1982 13. NUMBER OF PAGES 98
14. MONITORING AGENCY NAME & ADDRESS(if different from Controlling Office)		15. SECURITY CLASS. (of this report) UNCLASSIFIED 15a. DECLASSIFICATION/DOWNGRADING SCHEDULE

16. DISTRIBUTION STATEMENT (of this Report)

APPROVED FOR PUBLIC RELEASE: DISTRIBUTION UNLIMITED

17. DISTRIBUTION STATEMENT (of the abstract entered in Block 20, if different from Report)

18. SUPPLEMENTARY NOTES

19. KEY WORDS (Continue on reverse side if necessary and identify by block number)

Hydrofoil
Low Froude Number
Lift
Drag
Lift-Dependent Drag
Near Surface Effect
Flap Effectiveness

20. ABSTRACT (Continue on reverse side if necessary and identify by block number)

Results of an experimental investigation are presented for the subcavitating hydrodynamic force performance of an aspect ratio 6, NACA'64 A010 foil section, plain-flapped, rectangular planform hydrofoil. The forward-leading sting-supported foil model was operated in calm water in the speed range of chord Froude numbers 1.22 to 4.23, at five depth-to-chord submergence ratios varying from 0.25 to 4.0. The results, presented in coefficient form,

(Continued on reverse side)

DD FORM 1473 JAN 73 EDITION OF 1 NOV 65 IS OBSOLETE
S/N 0102-LF-014-6601

UNCLASSIFIED

SECURITY CLASSIFICATION OF THIS PAGE (When Data Entered)

(Block 10)

Program Element 62543N
Task Area ZF43-421
Work Units 1500-102 and 1500-103

(Block 20 continued).

include the basic measured foil-alone lift and drag, lift increments and flap effectiveness due to flap deflection, and the inferred variation of hydrofoil drag-due-to-lift for lift coefficients as high as 1.0. These data cover an important low Froude number speed regime not normally included in published hydrofoil performance experiments. Comparisons are made between the experimental results for residual drag and two different analytical prediction schemes for the hydrofoil total drag-due-to-lift. It is shown that experimental values for residual drag are bounded below and above by the two prediction methods considered, and that the discrepancies are, largest at low Froude numbers.

TABLE OF CONTENTS

LIST OF FIGURES

LIST OF TABLES

NOTATION

		Units*
A	Hydrofoil planform aspect ratio; $b^2/S = b/c$	--
a_0	Foil section two-dimensional lift-curve slope	degree:: or radian
b	Hydrofoil span	L
b_f	Hydrofoil flap span (total)	L
C_D	Drag coefficient; $D/\frac{1}{2}\rho U^2 S$	
$C_{D,L}$	Drag-due-to-lift coefficient, sum of induced drag plus wavemaking drag-due-to-lift	--
$C_{D,L_{TOT}}$	Total hydrofoil drag-due-to-lift, sum of induced drag plus wavemaking drag due-to-lift plus additional induced drag due to partial span flap arrangement; $C_{D,L} + K_f(\Delta C_L/\pi A)$	--
$C_{D_{p,min}}$	Minimum wing profile drag coefficient, sum of friction drag plus foil drag that includes simulator wire drag	--
$C_{D_{tare}}$	Tare drag coefficient of pipe sting based on hydrofoil planform area; $D_{tare}/\frac{1}{2}\rho U^2 S$	--
$C_{DRAG_{IND}}$	Hydrofoil induced drag coefficient, including biplane effect for large Froude number; estimated using HANDE formula	--
$C_{\Delta DRAG_{WAVE}}$	Hydrofoil wave resistance coefficient; estimated using HANDE formula	--
C_L	Lift coefficient; $L/\frac{1}{2}\rho U^2 S$	--
C_{L_α}	Hydrofoil wing lift-curve slope at any submergence	degree^{-1} or radian
$(C_{L_\alpha})_\infty$	Wind lift-curve slope in unbounded flow	degree^{-1} or radian^{-1}

*L = length, M = mass, T = time, F = force = ML/T^2

		Units
$C_{L_{tare}}$	Tare lift coefficient of pipe sting based on hydrofoil planform area; $L_{tare}/\frac{1}{2}\rho U^2 S$	--
C_{L_0}	Wing reference lift coefficient for elliptic circulation distribution at infinite depth	--
C_r	Hydrofoil residual drag coefficient, measured drag less all estimated parasitic drag components	
C_W	Hydrofoil wavemaking drag coefficient due-to-lift	
C_{W_t}	Hydrofoil wavemaking drag coefficient due to thickness (displacement, nonlifting)	
c	Hydrofoil chord length	L
c_f	Flap chord length	L
c_{tip}	Chord length at foil tip	L
D	Hydrofoil drag force	F
E_S	Edge correction factor for wing, semiperimeter-to-span ratio; $1 + A^{-1}$ for rectangular planform	
F_{n_c}	Froude number based on chord length; $U/(gc)^4$	
F_{nh}	Froude number based on depth of submergence of quarter chord	
g	Acceleration due to gravity	L/T^2
h	Depth of submergence to hydrofoil quarter chord	L
K_f	Induced drag factor for partial span flap	
L	Hydrofoil lift force	F
R_{n_c}	Reynolds number based on chord length; Uc/ν	--
S	Hydrofoil planform area, bc	L^2
S_f	Planform area of flaps; $b_f c_f$	L^2
t	Hydrofoil section maximum thickness	L

		Units
U	Freestream velocity, speed of hydrofoil	L/T
x	Distance along chordline of foil, measured from leading edge	L
Y	Ordinate (half thickness) of foil section shape	L
α	Hydrofoil resultant angle of attack of chord line with respect to freestream direction; $\alpha_N + (\Delta\alpha/L)L$	degree
α_N	Nose piece angle of attack	degree
δ_f	Flap deflection angle	degree
δ_P	Glauert planform shape correction factor for induced drag	
$\Delta\alpha/L$	Change of angle of attack-per-lift due to sting deformation under lift load	degree/F
ΔC_{D_p}	Incremental profile drag coefficient (due to angle of attack), without flap	--
$\Delta C_{D_{p,flap}}$	Incremental profile drag coefficient due to flap deflection	--
$\Delta C_{D_{tips}}$	Parasitic drag coefficient due to tip shape	--
ΔC_L	Incremental lift coefficient due to flap deflection	
$\Delta DRAG_{tips}$	Incremental drag force due to tip shape	
ν	Kinematic viscosity	L^2/T
ρ	Mass density of water	M/L^3
σ_i	Biplane factor for induced drag	
τ	Glauert planform shape correction factor for lift-slope	

ABSTRACT

-Results of an experimental investigation are presented for the subcavitating hydrodynamic force performance of an-aspect ratio 6, NACA 64 A010 foil section, plain-flapped, rectangular planformhydrofoil. The forward-leading sting-supported foil model, was operated in calm water in the speed range of chord Froude numbers 1.22 to 4.23, at five depth-to-chord submergence ratios. varying from 0.25 to 4.0. The results, presented in coefficient form, include the basic measured foil-alone lift and drag, lift increments and flap effectiveness due to flap deflection, and the inferred variation of hydrofoil drag-due-to-lift for lift coefficients as high as 1.0. These data cover an important low Froude number speed regime not normally included in published hydrofoil performance experiments. Comparisons are made between the experimental results for residual drag and two different analytical prediction schemes for the hydrofoil total drag-due-to-lift. It is shown that experimental values for residual drag are bounded below and above by the two prediction methods considered, and that the discrepancies are largest at low Froude numbers.

ADMINISTRATIVE INFORMATION

This work was authorized by the Naval Material Command (08T), funded under the Ships, Subs and Boats Program, Program Element 62543N, Task Area ZF43-421, and administered by the Ship Performance Department under Work Units 1500-102 and 1500-103.

INTRODUCTION

In response to design considerations for large hydrofoil ships, for partial hydrofoil supported craft, for application as antipitch and antiroll fins on surface ships, and for control foils on small waterplane area twin hull (SWATH) ships the physical size of possible or proposed subcavitating hydrofoil systems has grown in recent years. This has focused attention on a low Froude number range that has received little attention in most of the hydrofoil experimental literature that provides basic performance data. Chord Froude numbers as small as 1.5 to 2 at submergence ratios of h/c = 0.5 to 2 are conceivable operational values of interest in practical applications for large hydrofoil craft takeoff or for cruising SWATH ships.

A hydrofoil operating near the free surface at low Froude numbers at a fixed geometric angle of attack experiences an accentuated drag-due-toylift (or total induced drag) caused by a hump of the wavemaking resistance coefficient centered

around a depth Froude number $F_{n_h} \cong 1.4$. The accompanying lift coefficient shows a local minimum or dip at about the same Froude number. These effects are exaggerated as the submergence ratio decreases. Predictions of general properties of hydrofoil force performance using linearized potential theory have been available for a long time and are described for instance by Wu,[1*] Nishiyama,[2] Breslin,[3] and by numerous other authors noted in the bibliographies of these works.

Some of the general trends of these predicted features have been illustrated in the classic foil-alone performance experiments by Wadlin et al.[4] for an aspect ratio 10 rectangular planform hydrofoil operated at submergence ratios h/c = 0.84 and 3.84, at chord Froude numbers in the range F_{n_c} = 1.08 to 9.72, and at chord length Reynolds numbers in the range 0.18×10^6 to 1.64×10^6 with turbulence stimulation. Force data for an aspect ratio 4 rectangular planform hydrofoil are also included in Reference 4 at five submergences h/c = 0.59 to 4.09, in the chord Froude number range of 3.24 to 7.56.

The foil-alone performance experiments reported on by Wilson and Kelley[5] for an aspect ratio 4 rectangular planform hydrofoil at seven submergence ratios h/c = 0.25 to 3.5 cover chord Froude numbers in the range 0.5 to 3.5, at chord length Reynolds numbers in the range 0.74×10^6 to 5.2×10^6 with trip wire turbulence stimulation. "The results'of Reference 5 provide perhaps the most complete data available in the low Froude number range and seem to verify the interesting trends of predicted free surface influence on the low Froude number performance of a hydrofoil. There are present in these results suspected influences of interference velocities from the nacelle-like fairing that covered the block gauge dynamometer that connected the hydrofoil to the supporting strut and measured the forces on the foil.

Most instances of published hydrofoil force data cover a relatively high range of chord Froude numbers and deal with foil-plus-strut performance. Some examples are noted here for reference. Jones[6] has reported results for an aspect ratio 6 rectangular planform hydrofoil at h/c = 1, operated at chord Froude numbers F_{n_c} = 4.8 to 9.2 without turbulence stimulation. These data include unflapped and flapped performance, for several flap span arrangements. Feldman[7] has presented a considerable body of data for a series of rectangular planform hydrofoils having

*A complete listing of references is given on page 83.

the same cambered foil section shape with six different aspect ratios and various strut arrangements at six submergences in the chord Froude number range F_{n_c} = 2.06 to 9.63, without turbulence stimulation. Layne[8] has carried out experiments on tapered planform hydrofoils having two different NACA section shapes in the chord Froude number range F_{n_c} = 7.44 to 23.2, without turbulence stimulation. Finally, a very extensive program of performance evaluation for a hydrofoil-nacelle-strut arrangement has been outlined by Dixon et al.[9] Variable pressure water channel experiments were performed with an aspect ratio 6.5 tapered planform, flapped hydrofoil at three submergences, with simultaneous scaling of both Froude number and vapor cavitation number. The tested chord Froude number range was 3.97 to 6.81, at chord length Reynolds numbers in the range 0.96×10^6 to 1.65×10^6, without turbulence stimulation.

The experiments described here were designed to provide force data for foil-alone performance specifically covering a low Froude number range of interest, at sufficiently large Reynolds numbers, with a guarantee of turbulent boundary layer flow, and with minimal hydrodynamic interference from the support system. As an example application, for a 20 ft (6.1 m) chord hydrofoil operated in the speed range 23 to 55 knots, the Froude number range is F_{n_c} = 1.527 to 3.665; and with a nominal foil loading L/S = 1200 lbf/ft^2 (57.5 kN/m^2), the corresponding range of required net lift coefficient is 0.8 to 0.139.

DESCRIPTION OF MODEL, INSTRUMENTATION, AND EXPERIMENT FACILITY

The experiments reported on here were conducted on Carriage 2 in the deep water basin at the David W. Taylor Naval Ship Research and Development Center, Carderock. This towing tank is 1886-ft (574.8-m) long, 51-ft (15.5-m) wide, with a water depth of 22 ft (6.71 m). Figure 1 is a photograph of the model hydrofoil and its forward-leading sting support system mounted on the vertical rails of the towing carriage.

MODEL AND MOUNTING EQUIPMENT

The hydrofoil model manufactured for these experiments is an aspect ratio 6, rectangular planform wing, with a chord length of 16 in. (40.64 cm), span of 96 in. (2.44 m), squared-off tips, and a maximum thickness of 1.6 in. (4.064 cm).

The NACA 64 A010 section shape was machined from a solid piece of aluminum, and the final surface finish was produced with emery cloth. Table 1 gives the model one-half thickness ordinates for this uncambered symmetric foil section. Table 2 summarizes the important characteristics of the hydrofoil.

It was important with these experiments to achieve total foil lift coefficients of at least 0.8 to cover conditions expected at low speed takeoff of a hydrofoil system, so a trailing-edge flap configuration was provided with a flap chord ratio of $c_f/c = 0.25$ and with a generous flap span extending across nearly the full foil span, $b_f/b = 0.934$. The flap was actually cut from the trailing edge portion of the complete profiled foil. The flap deflection angles were fixed using a series of 14 angled flap pads spaced across the upper and lower sides of the foil, and screwed into place flush with the surfaces of the foil and flap. Plastiline putty was forced into the gaps at the flap knee and was smoothed even with the surface, so the flap system can be described as a "sealed plain flap." Figure 2 is a sketch of the hydrofoil section showing a flap pad and the definition of the flap deflection angle δ_f.

Turbulence stimulation was provided by 0.016 in. (0.0406 cm) diameter piano. wires stretched taut and touching both the upper and lower nose surfaces of the foil at a distance of 0.02c, or 0.32 in. (0.813 cm), back from the leading edge. Each wire was held in place at l-ft (30.48-cm) intervals across the span, and was, thus permitted to strum in the flow over the foil.

The forward-leading sting support system for the hydrofoil consists of a long horizontal pipe instrumented for the measurement of lift and drag force through two support points and connected to struts through corresponding stacks of modular force gauges. Angle of attack variation for the foil is provided by a series of steel nose pieces, each with an angled slot that accommodates the rear end of the foil. The after end of the nose piece fits into the forward end of the pipe, with a pin key to ensure a horizontal foil position. There is a different nose piece for each angle of attack considered, and the slot in each is positioned such that the foil quarter-chord point always lies along the centerline of the sting-nose combination. With this scheme, the sting was always towed submerged in a level orientation, for every angle of attack. This allowed for very simple and relatively small magnitude tare forces to be removed from the measured data.

TABLE 1 - HYDROFOIL ONE-HALF THICKNESS ORDINATES
FOR NACA 64 A010 SECTION

x (inch)	x/c	Y (inch)	y/c
0	0	0	0
0.08	0.005	0.1286	0.00804
0.12	0.0075	0.155	0.00969
0.2	0.0125	0.196	0.01225
0.4	0.025	0.2701	0.01688
0.8	0.05	0.3723	0.02327
1.2	0.075	0.4488	0.02805
1.6	0.10	0.5118	0.03199
2.4	0.15	0.6101	0.03813
3.2	0.20	0.6835	0.04272
4.0	0.25	0.737	0.04606
4.8	0.30	0.7739	0.04837
5.6	0.35	0.7949	0.04968
6.4	0.40	0.7992	0.04995
7.2	0.45	0.783	0.04894
8.0	0.50	0.7494	0.04684
8.8	0.55	0.7021	0.04388
9.6	0.60	0.6434	0.04021
10.4	0.65	0.5755	0.03597
11.2	0.70	0.5003	0.03127
12.0	0.75	0.4197	0.02623
12.8	0.80	0.3365	0.02103
13.6	0.85	0.2531	0.01582
14.4	0.90	0.1699	0.01062
15.2	0.95	0.0866	0.00541
16.0	1.0	0.00336	0.00021

TABLE 2 - HYDROFOIL GEOMETRY AND PARTICULARS

Aspect ratio	A = 6
Foil thickness ratio	t/c = 0.10
Span.	b = 8 ft (2.438 m)
Chord length	c = 1.333 ft (0.406 m)
Flap -chord ratio	$c_f/c = 0.25$
Flap span ratio	$b_f/b = 0.934$
Flap planform area ratios	$S_f/S = 0.2357$
Planform area; shape	S = 10.67 ft^2 (0.991 m^2); Rectangular, squared-off tips
Foil material	6061-T6 aluminum
Section shape	NACA 64 A010
Turbulence stimulator wire	0.016 in. (0.041 cm)

The dynamometer for this set-up was designed to measure the hydrodynamic forces on the sting-plus-foil and, of course, the sting-alone. It consists of an assemblage of three standard four-inch DTNSRDC differential reluctance block gauges, together. with a double-neck flexure in the after gauge stack that was designed to transmit mainly a vertical force with very small horizontal force and moment. A single pin joint hinge is positioned in the forward gauge stack. Drag force was measured using a single block gauge located in the forward gauge stack. Two different capacity gauges were employed for different portions of the experimental program. A 100 lb (445 N) range gauge was used for measuring the sting tare forces and for the low drag part of the foil-plus-sting tests. This was replaced by a 500 lb (2.224 kN) capacity gauge for the higher drag part of the tests.

The lift force was determined by the sum of the fore and aft lift gauges, having capacities of 5,000 lb (22.24 kN) and 2,000 lb (8.896 kN), respectively. For positive values'of foil lift, the forward gauge stack was loaded in compression and the aft in tension. A nominal maximum allowable value of total foil lift of 3,000 lb (13.34 kN) was adhered to during the tests so as not to exceed the rated capacities of any of the force gauges in the system.

Instrumentation for the collection of three channels of force data consisted of ENDEVCO signal conditioners for the differential reluctance block gauges and DANA amplifiers. Voltage output from the amplifiers was digitized using ANALOGIC analog-to-digital converters. All the data were collected and processed on-line using an INTERDATA computer, with data storage on magnetic tape using a Tri-Data Cartrifile recorder. Data sheets were obtained during the tests from a VERSATEC printer on board the carriage."

Simple streamlined fairings, each with a maximum width of 6 in. (15.24 cm) were fitted around the two block gauge stacks. These were fastened at the top end only., with gaps at the lower end, so that no forces were transferred through the fairings that would interfere with the force measurements on the sting-plus-hydrofoil combination. Hydrodynamic interference from the elliptically shaped nose piece and from the sting are believed to be very small. Figure 3 is a sketch of the sting and dynamometer support system.

CALIBRATION, INTERACTIONS, INACCURACIES

Set up and calibration of this experiment consisted of first calibrating the individual block gauges, then recalibrating and adjusting the arrangement of the

dynamometer components in the assembled condition using the heavy bridge of, Carriage 5 as a calibration stand. Without disassembly, the dynamometer was then moved to Carriage 2 to be fastened to the tilt table and support bracket that connect to the vertical rails of the carriage. The final calibration factors were obtained with the model support system completely assembled and in position on the carriage.

Owing to the large physical dimensions of the dynamometer, there are small but important elastic deformations of the pipe sting, the struts, and cross support beam that occur under the application of large lift forces typical of this experiment. The resultant force measurement interaction appears predominantly as changes in the drag force.readings due to varying levels of lift force. After extensive calibration, the interaction effect of lift into drag was found to be conveniently repeatable and subject to simple removal from the directly measured values. Interaction of drag force into the indicated lift was found to be negligibly small as was the effect of applied moment upon drag. All the final force data presented in this report have been systematically corrected for dynamometer interaction.

Elastic deformation of the sting under load also causes a change in the effective angle of attack, $\Delta\alpha$, measured at the quarter-chord of the hydrofoil. With the assembled dynamometer mounted on Carriage 2, a final deformation calibration was obtained as angle of attack-change-per-unit lift $\Delta\alpha/L = 0.0005222$ deg/lb (0.00232 deg/N), with the lift force applied at the quarter-chord position.

Measurement inaccuracies are inherent to the mechanical and electrical systems employed. Expected magnitudes of errors for the force measurements have been estimated from the maximum scatter band observed from repeated calibration of the assembled dynamometer. For all the basic measurements, including the forces, the characteristic accuracies are summarized in Table 3.

A careful check of the precision of the final machined foil section shape was made using a profile measurement machine (Brown and Sharp VALIDATOR) at DTNSRDC. Chordwise surveys of the profile were conducted along lines on either side of the planform centerline, at a distance of 0.4583 (b/2) from the centerline. The results are shown plotted in Figures 4 and 5, for the starboard and.port sides, respectively, with the scale for the ordinate (offset ratio, y/c) expanded by a factor of 10 compared with the chordwise distance scale for x/c. Comparisons are displayed between the offsets specified for the NACA 64 A010 profile and those measured on the hydrofoil as machined, for both the top and bottom surfaces. In

TABLE 3 - EXPECTED MEASUREMENT ERROR BOUNDS

Measured Quantity	Expected Range of Error
Drag (both gauges)	± 2% of measured value, D < 50 lb
	± 0.5% of measured value, D > 50 lb
Lift	± 1.5% of measured value, L < 800 lb
	± 1% of measured value, L > 800 lb
Speed	± 0.01 knot (± 0.02 ft/sec, ± 0.006 m/s)
Depth of submergence	± 0.01 ft (3 mm)
Angle of attack	± 0.01 deg

general, the deviations of offsets of the machined surface from the specified surface are very small, almost everywhere less than 0.5% of the maximum section offset Y_{max} = 0.8 in. (2.03 cm). On the starboard side, the maximum deviation of any offset on the upper surface was found to be 0.0236 y_{max} near the nose $(x/c = 0.005)$, and on the lower surface, it was measured as 0.012 y_{max} at x/c = 0.35. On the port side, the maximum measured deviation on both the top and bottom surfaces amounts to 0.0154 y_{max} near the nose $(x/c = 0.005)$.

PROCEDURE

Overall, the experiment was directed at obtaining the hydrodynamic force characteristics on the submerged hydrofoil alone, so that contributions from the supporting sting had to be collected separately, then subtracted away as tares. A deep submergence case of h/c = 4 was chosen to provide reference performance levels for the wing that contain only minimal influence of the free surface. This was especially important for establishing certain drag components. The operating procedure consisted of making towing carriage runs over the range of test speeds at each fixed depth of submergence h measured to the location of the hydrofoil quarter chord (submergence of sting-pipe centerline). The first series of tests were run with the sting alone, and fitted with a faired plug having the same shape as the slotted nose pieces at the leading end of the sting. These tests covered the complete speed range and all the submergences h/c = 0.25, 0.5, 1.0, 2.0, and 4.0.

The second series of tests were run with the sting-plus-foil, at the various wing angles of attack established with the slotted nose pieces α_N = 0, 2, 4, 6, and 8 deg, and with zero flap deflection. The third series of tests were run with flap deflection angles δ_f = 7.5 and 15 deg at two different nose piece angles of attack α_N = 4 and 8 deg. 'Table 4 summarizes the nominal matrix of experiments for the data presented in this report.

Measured water temperature was 68°F (20°C); therefore, the density and kinematic viscosity values used in the data reduction were ρ = 1.9367 slug/ft^3 (998.13 kg/m^3) and ν = 1.0836 x 10^{-5} ft^2/sec (1.0067 x 10^{-6} m^2/s), respectively. For the speed range of U = 8 to 27.7 ft/sec (2.44 to 8.44 m/s), the corresponding range of chord length Reynolds number is R_{n_c} = 0.984 x 10^6 to 3.41 x 10^6; the range of chord length Froude number is F_{n_c} = 1.22 to 4.27.

STING TARE FORCES

Results of the lift and drag measurements on the sting alone are displayed in Figure 6 in terms of lift and drag coefficients CL_{tare} and CD_{tare} based on the hydrofoil planform area S, plotted versus speed U or chord length Froude number F_{n_c}. These tare forces were systematically subtracted from the raw force data measured for the sting-plus-foil in order to obtain the hydrofoil-alone measured data presented in the tables of Appendices A and B and in the plots of the next section.

EXPERIMENTAL RESULTS

All the results of this investigation have been reduced to standard coefficient form using the familiar aerodynamic and hydrodynamic definitions for lift coefficient CL and drag coefficient CD given in the notation.

BASIC LIFT AND DRAG PERFORMANCE FOR ZERO FLAP

The basic measured lift and drag characteristics of the hydrofoil.with zero flap deflection are presented in Figures 7 through 16 in groups of three graphs for each submergence ratio. Displayed are the lift coefficient C_L versus α, the drag coefficient CD versus C_L, and the total lift-to-drag ratio L/D versus α plotted with contours of constant speed U. Data for the submergence ratios h/c = 4, 2, 1, 0.5, and 0.25 correspond to Figures 7 and 8; 9 and 10; 11 and 12; 13 and 14; and 15 and 16, respectively. Tabulated values of these measured force data for zero flap deflection are given in Appendix A, Tables A.1 through A.5.

TABLE 4 - NOMINAL TEST MATRIX FOR LOW FROUDE NUMBER HYDROFOIL EXPERIMENTS

Configuration	Parameter	Range
Sting alone	Speed	U = 8 to 27.7 ft/sec (2.44 to 8.44 m/s)
	Chord Froude number	F_{n_c} = 1.22 to 4.23
	Submergence ratio	h/c = 0.25, 0.5, 1, 2, 4
Hydrofoil mounted on sting with zero flap angle	Speed	U = 8 to 27.7 ft/sec (2.44 to 8.44 m/s>
	Chord Froude number angle of attack of nose piece	α_N = 0, 2, 4, 6, 8 deg
	Flap angle	δ_f = 0
	Submergence ratio	h/c = 0.25, 0.5, 1, 2, 4
Hydrofoil mounted on sting with flap deflection	Speed	U = 8 to 24 ft/sec (2.44 to 7.315 m/s>
	Chord Froude number angle of attack of nose piece	α_N = 4 and 8 deg
	Flap angle	δ_f = 7.5 and 15 deg
	Submergence ratio	'h/c = 0.5, 1, 2, 4

These performance diagrams are classical presentations of the lift and drag for airfoils. For unbounded flows, the results for a range of speeds typically collapse onto single curves in these types of plots. Of course, for a near free surface hydrofoil, this is not the case, and the effects of speed (Froude number) tend to become more pronounced as the submergence ratio is decreased, especially for the low range of Froude numbers of these experiments.

For the deepest submergence case of h/c = 4, the lift-curve CL versus α in Figure 7a follows a single straight line, indicating essentially wave-free operation. What speed variation is present in the drag coefficient for h/c = 4 appears to be due mainly to Reynolds number variation on friction drag. The foil lift-to-drag ratios at this deep submergence reach values exceeding 16 at the highest speeds. It appears then, that the h/c = 4 submergence provides a reasonable reference performance for the force characteristics of the foil having very small free surface effect.

LIFT

Lift-Curve Slope

The linear relationship between C_L and a is clearly evident in Figures 7a, 9a, lla, 13a, and 15a and justifies the usual definition for zero flap lift-curve slope C_{L_α} computed from

$$C_L = c_{L_\alpha}(a - \alpha_0) \qquad (1)$$

where $\alpha - \alpha_0$ is the angle of attack measured from zero lift. In general, the angle for.zero lift α_0 for a hydrofoil is a complicated function of speed and depth of submergence because of the free surface effect. Variation of the inferred values of lift-curve slope C_{L_α} with speed and submergence ratio is shown in Figures 17 and 18. These plots show most succinctly the characteristic reduction of lift with decreasing submergence (at constant α) and the tendency toward a local dip or minimum of lift at depth Froude number $F_{n_h} \cong 1.4$, in agreement with the trends observed in previous low Froude number results discussed in Reference 5.

From the deepest submergence case of h/c = 4, the reference lift-curve slope is a constant

$$(C_{L_\alpha})_\infty = 0.06905 \text{ deg}^{-1} \qquad (2)$$

According to the usual simplified wing analysis, the lift-curve slope in unbounded flow can be estimated from

$$(C_{L_\alpha})_\infty = \frac{a_0}{E_s + \frac{a_0}{\pi A}(1+\tau)} \tag{3}$$

where a_0 = effective section value of lift-curve slope

E_s = semiperimeter-to-span ratio (Jones edge correction factor)

τ = planform correction factor for lift slope for rectangular wing (Glauert)

For the aspect ratio 6 rectangular wing, Equation (3) can be rearranged to give a consistent value for the section lift slope a_0, together with the appropriate value of planform correction factor τ. With the observed value for the aspect ratio 6 wing at deep submergence of $(C_{L_\alpha})_\infty = 3.956$ radian^{-1}, the section lift-slope is

$$a_0 = 6.118 \text{ radian}^{-1}(0.1068 \text{ deg}^{-1})$$

with $\tau = 0.17$, so that $A/a_0 = 0.981$. These foil lift slope properties are consistent with the established characteristics of the foil section, Specifically, from Loftin,[10] the comparable section lift-slope, determined in wind tunnel tests with NACA 6A-Series foils having t/c = 0.1, is $a_0 = 6.13$ radian$^{-1}(0.107 \text{ deg}^{-1})$.

Lift Performance with Flap

Hydrofoil lift performance with flap deflection must be analyzed here with data taken at two nose piece angles of attack $\alpha_N = 4$ and 8 deg. Plots of measured C_L versus α for submergence ratios of h/c = 4, 2, 1, and 0.5 are assembled in Figures 19 through 22, respectively. Contours of speed (Froude number) are given for the two different flap deflections $\delta_f = 7.5$ and 15 deg, as well as for the zero flap configuration. This manner of presentation allows for the easy interpolation of values of C_L and $\Delta C_L = (C_L(\delta_f) - C_L(\delta_f=0))$ at any desired angle of attack α. High values of C_L, at times exceeding 1.0, were achieved at the largest flap deflection angle $\delta_f = 15$ deg. As expected, there is a nearly linear increase of flap lift increment ΔC_L with flap deflection δ_f. Tabulated values of the measured lift data with flap deflection are given in Appendix B, Tables B.l and B.2.

Values of flap lift increment ΔC_L, derived from Figures 19 through 22, are shown plotted versus submergence ratio in Figure 23 for flap angles δ_f = 7.5 and 15 deg, at selected contours of speed F_{n_c} = 1.22, 1.83, and 2.44. This shows the distinctive fall-off of flap lift increment with decreasing submergence ratio.

Flap Effectiveness

Flap effectiveness for a finite aspect ratio wing is often discussed in terms of the ratio of two lift-curve slopes measured with respect to flap deflection and angle of attack

$$\frac{d\alpha}{d\delta_f} = \frac{dC_L/d\delta_f}{dC_L/d\alpha} \tag{4}$$

Figure 24 shows the reference values of this flap effectiveness factor plotted versus speed for the hydrofoil at h/c = 4. The ideal value of $d\alpha/d\delta_f = 0.6$ has been estimated from Hoerner[11] for a flapped lifting surface $S_f/S = 0.236$.

DRAG

Drag Performance with Flap Deflection

Hydrofoil drag results with flap deflection are presented in Figures 25 through 28 for submergence ratios h/c = 4, 2, 1, and 0.5, respectively. These plots display the measured drag coefficient C_D versus α^2, with contours of speed. Results are shown for flap deflection angles of δ_f = 7.5 and 15 deg, as well as for zero flap cases at the same speeds. This presentation is based on the idea that the expected increments of induced drag and wavemaking drag due-to-lift are proportional to C_L^2, and because the linear relationship between C_L and α is well established, families of contours are expected for C_D versus α^2. This type of data trend has been verified using the flapped hydrofoil results of Jones.[6] All of the tabulated results for the measured drag data with nonzero flap deflection are given in Appendix B, Tables B.1 through B.4.

For the cases of h/c = 4 and 0.5, respectively, sample polar plots of C_D versus C_L in Figures 29 and 30 illustrate the unified trend of drag data for the range of unflapped and flapped configurations for this uncambered foil.

Analysis and Drag Components

The net total drag of a fully submerged subcavitating hydrofoil with flaps may be divided into components interpreted as the sum of total parasitic drag (or profile drag) plus the drag-due-to-lift (sum of induced and wavemaking drag); so that, in coefficient form,

$$C_D = (C_{D_{p,min}} + AC,_{tips} + \Delta C_{D_p} + AC_{D_{p,flap}}) + (C_{D,L_{TOT}} + C_{W_t}) \qquad (5)$$

where $C_{D_{p,min}}$ = minimum wing profile drag, sum of friction drag plus the form drag that includes effects of foil thickness and stimulator wire drag

$AC_{D_{tips}}$ = parasitic drag component due to squared-off tips

ΔC_{DP} = incremental profile drag, without flap

$Ac_{D_{p,flap}}$ = incremental profile drag due to flap deflection

$C_{D,L_{TOT}} = C_{D,L} + K_f(\Delta C_L)^2/\pi A$ = total of induced drag plus wavemaking drag-due-to-lift, plus additional induced drag due to partial span flap arrangement

K_f = induced drag factor for partial span flaps

ΔC_L = incremental lift coefficient due to flap deflection

C_{W_t} = wavemaking drag due to displacement effect of finite thickness foil

The first group of terms in parentheses in Equation (5) represents all the parasitic drag components, while the last two terms cover the induced drag plus wavemaking due to both lift and displacement effects.

This experiment was designed with the idea of using the results of the deepest submergence case in order to deduce the various parasitic components that are 'independent of free surface effects. To remove the drag-due-to-lift component, $C_{D\,L}$, the lifting line hydrofoil theory of Wu[1] has been employed, using the analytical' results for hydrofoils with elliptic circulation distributions. From the wing properties determined from the lift slope curve noted earlier, A/a, = 0.981, so that the Glauert correction factor for the induced drag on a rectangular planform wing is $\delta_p \cong 0.05$ (see Martin[12]).

For a hydrofoil with elliptic circulation distribution, the theoretical result for drag-due-to-lift takes the form

$$\left(\frac{C_{D,L}}{C_{L_0}^2}\right)_{ELLIP} = \frac{1}{\pi A}(1-\sigma_i) + \frac{C_W}{C_{L_0}^2} \tag{6}$$

where A = hydrofoil planform aspect ratio

σ_i = biplane factor for induced drag (see von Kármán and Burgers [13] and Wilson[14])

C_W = hydrofoil wave resistance coefficient (see Wu's[1] result for D_4)

C_{L_0} = wing reference lift coefficient for the elliptic circulation distribution at infinite depth

It should be noted that, in the limits of zero and infinite Froude number,

$$\begin{aligned} C_W &\to 0 && \text{as } F_{n_c} \to 0 \\ C_W &\to \frac{2\sigma_i}{\pi A} C_{L_0}^2 && \text{as } F_{n_c} \to \infty \end{aligned} \tag{7}$$

Thus, for the rectangular planform hydrofoil, the corresponding limits of drag-due-to-lift ratios are

$$\begin{aligned} \left(\frac{C_{D,L}}{C_{L_0}^2}\right)_{RECT} &\to (1+\delta_p)\frac{1-\sigma_i}{\pi A} && \text{as } F_{n_c} \to 0 \\ \left(\frac{C_{D,L}}{C_{L_0}^2}\right)_{RECT} &\to (1+\delta_p)\frac{1+\sigma_i}{\pi A} && \text{as } F_{n_c} \to \infty \end{aligned} \tag{8}$$

where δ_p is the Glauert planform shape correction factor for induced drag. From Martin,[12] $\delta_p = 0.05$ for aspect ratio 6 wings. At intermediate Froude numbers, the detailed calculated results for

$$\frac{C_W}{C_{L_0}^2} = \frac{8}{\pi A} \int_0^{\pi/2} e^{-2F_{n_h}^2 \sec^2\theta} J_1^2\left(\frac{1}{\beta}\sec^2\theta\sin\theta\right) \frac{\sec\theta}{\sin^2\theta}\, d\theta \tag{9}$$

compiled by Wilson,[14] have been used for all the systematic reduction of data from the h/c = 4 measurements, and in later comparisons. 'In this equation, Fnh = $U/(gh)^{\frac{1}{2}}$ is the submergence Froude number, Jl is the Bessel functionof the first kind, and $\beta = U^2/g(b/2)$.

Numerical values for the biplane factor σ_i valid for elliptic circulation distribution are given in Table C.l of Appendix C.

Parasitic Drag Components

All four of the parasitic drag components noted in Equation (5) have been estimated from published work or inferred from the present data.

1. The contribution of tip drag attributable to the two squared-off ends of the hydrofoil can be 'estimated from the empirical results of Hoerner[11]

$$\Delta DRAG_{tips} = \left[(0.15)\left(\frac{t}{c}\right)_{tip} + (0.37)C_L^3\right]\frac{1}{2}\rho U^2 c_{tip}^2 \qquad (10)$$

and expressed in coefficient form, based on foil planform area, as

$$\Delta C_{D_{tips}} = 0.00025 + (0.00617)C_L^3 \qquad (11)$$

2. The minimum profile drag $C_{Dp,min}$ consists of skin friction drag plus the form drag of the foil operating at zero lift. An adequate fit is given by

$$C_{D_{p,min}} = 2C_f(ITTC) + 0.0025 \qquad (12)$$

where $C_f(ITTC)$ denotes the flat plate turbulent friction coefficient determined from the 1957 ITTC correlation curve at chord length Reynolds number R_{n_c}.

3. The incremental profile drag contribution AC_{D_p} here represents the additional profile drag penaity incurred when the symmetric foil operates at nonzero lift due to angle of attack. This component should contain no wing induced drag, and has been estimated here at each speed over a range of lift coefficients from the zero flap measured data at h/c = 4 using

$$\Delta C_{D_p} = C_{D_{meas}} - (C_{D_{p,min}} + AC_{Dtips} + C_{D,L}) \qquad (13)$$

where all the induced drag and wavemaking effects are represented in the drag-due-to-lift given by $C_{D,L} = (C_{D,L}/C_{L_0}^2)_{RECT}\, C_L^2$. Figures 31a and 31b present the inferred

values of incremental drag coefficient ratio $AC_{D_p}/C_{D_{p,min}}$ plotted versus C_L^2 with contours of speed.

4. Application of flaps to reach high lift incurs a further incremental profile drag $AC_{D_{p,flap}}$. This term can be deduced in the same fashion as for $AC_{DP'}$ but must also account for an additional induced drag factor attributable to the partial span arrangement of the flap. Thus, from the h/c = 4 measured drag data with flaps, the incremental profile drag due to flap deflection has been estimated using

$$\Delta C_{D_{p,flap}} = C_{D_{meas}} - \left[C_{D_{p,min}} + AC_{D_{tips}} + AC_{D_p} + C_{D,L} + K_f \frac{(\Delta C_L)^2}{\pi A} \right] \quad (14)$$

where all the previous component definitions apply; $C_{D,L}$ is based on the total C_L with flap, and the added drag due to flap lift distribution on partial span flaps is accounted for using the flap drag factor, $K_f = 0.0429$, from Young[15]. Figure 32 is a plot of the inferred values of $AC_{D_{p,flap}}$ plotted versus speed, for the flap deflection angles δ_f = 7.5 and 15 deg. For purposes of the further data reduction at the shallower submergences, the constant (mean) values

$$AC_{D_{p,flap}} = 0.0033 \text{ at } \delta_f = 7.5 \text{ deg}$$

$$AC_{D_{p,flap}} = 0.011 \text{ at } \delta_f = 15 \text{ deg}$$

have been used.

Inferred Hydrofoil Drag-due-to-Lift: Residual Drag

With the assumption that the parasitic drag components discussed previously are independent of free surface effects regardless of the depth of submergence, the measured hydrofoil residual drag coefficient is obtained from measured total drag using

$$C_r = C_{D_{meas}} - (C_{D_{p,min}} + AC_{Dtips} + A C_{D_p} + C_{Dp,flap}) \quad (15)$$

where the $C_{D_{p,flap}}$ term is applied only for the cases with flap deflection. The residual drag C_r is supposed to be dominated by the drag-due-to-lift, but must include a small wavemaking resistance due to displacement effect (foil thickness).

Plots of the residual drag ratio C_r/C_L^2 versus speed (Froude number) are given in Figures 33 through 36 for the submergence ratios h/c = 2, 1, 0.5, and 0.25,

respectively. These graphs summarize the results for both the zero flap and the flapped configurations (high lift). Plotted for comparison are two prediction curves for drag-due-to-lift ratio C_{D_L}/C_L: (1) the hydrofoil lifting line theory for constant shape elliptic circulation distribution $(C_{D,L}/C^2_{L_0})_{ELLIP}$ and (2) an estimating formula derived from HANDE by the Boeing Company.[16] The presentation of the residual drag data in this manner puts a severe test on the cases with very low levels of foil lift, because even small drag errors or the presence of wave-making drag due to nonlifting origin are amplified by the factor $1/C^2_L$ as $C_L \rightarrow \pm 0$. Data for the small nose angle of attack, α_N = 2 deg, seem to suffer from this problem, as they do not fall into trends established by the results for the angles of attack α_N = 4, 6, and 8 deg. For the data with moderate to high levels of lift coefficient, the results at a given submergence coalesce toward a single curve, and are bounded below by the lifting line prediction $(C_{D,L}/C^2_{L_0})_{ELLIP}$, and seem to be bounded above by the HANDE[16] prediction curve. As discussed in the HANDE manual, the so-called "wave resistance" contribution has been adjusted empirically to fit the low Froude results obtained in the hydrofoil experiments by Wadlin et al.[4] In Figures 33 through 36, the present experimental results for C_r/C^2_L, and both the prediction curves for $C_{D,L}/C^2_L$ converge at the higher Froude numbers, typically $F_{n_c} > 2.5$.

Another method of data presentation for the residual drag coefficient results is given in the plots of C_r versus $C_L|C_L|$ shown in Figures 37 through 42 for chord Froude numbers of F_{n_c} = 1.22, 1.53, 1.83, 2.44, 3.055, and 3.665, respectively. Each of these plots shows the resultant experimental C_r values, and for reference, the $C_{D,L}$ from lifting line theory for four different submergence ratios h/c = 0.25, 0.5, 1, and 2.

There are two things worth noting in these comparisons. First, the expected proportionality of C_r with respect to C^2_L is put to a test, and is shown to hold fairly well for $C^2_L \leq 0.5$ and at the larger Froude numbers. However, for the higher levels of lift coefficient there is a noticeable but slight nonlinear increase of C_r versus C^2_L. Part of this could be the result of the nonlinear free surface effect upon wave drag of the sort predicted from the numerical computations of Salvesen and von Kerczek[17] for two-dimensional flow past a submerged vortex. Unfortunately, it is not known at this time what lift levels C_L would be required in the case of finite aspect ratio submerged wings for there to be an observable nonlinear effect.

Whatever the cause, similar slight nonlinear trends of drag coefficient versus $C_L|C_{L_I}$ can be determined, for example, from the hydrofoil performance results presented by Dixon et al.[9] at just moderate levels of foil lift coefficient, and in the higher range of Froude numbers of those experiments.

The second noteworthy feature in Figures 37 through 42 is that the difference between the measured values of C_r and the $C_{D,L}$ from the lifting line theory at low to moderate lift levels appear as small amounts of additional drag that do not affect the slope of the curve. The magnitude of the offsets of the C_r curve are larger at the small Froude numbers, and at the shallower submergences. Because the range of foil depth-to-thickness ratio is h/t = 2.5 to 20, corresponding to h/c = 0.25 to 2.0, it is plausible that there are contributions to the hydrofoil residual drag that are attributable to wavemaking resistance due to foil thickness (nonlifting, displacement effect), rather than strictly drag-due-to-lift. No theoretical estimates of the nonlifting wavemaking drag for a submerged, finite thickness foil were obtained for this work. .

Comparisons of the present measured C_r values with the two analytical predictions of $C_{D,L}$ variation plotted versus C_L^2 are given in Figures 43 through 45 for submergences h/c = 0.5, 1.0, and 2.0, respectively. In each of these sets of figures at constant submergence, there are three graphs for three different speeds corresponding to Froude numbers F_n = 1.22, 1.53, and 1.83. The measured data include both unflapped and flapped wing results. It appears that, although the lifting line theory is generally a little too low at the smaller Froude numbers shown, the HANDE[16] predictions based on

$$C_{D,L} = C_{DRAG_{IND}} + C_{\Delta DRAG_{WAVE}} \tag{16}$$

are too high. The differences between them diminish with increasing Froude number, and the experimental results are thereby bounded below and above by the two prediction schemes employed.

CONCLUSIONS

1. Extensive foil-alone experimental force data are presented for the low Froude number operation of a large hydrofoil model at several submergences.

2. The present results for deep submergence (reference values) of lift curve slope and flap effectiveness agree well with known properties of this foil section.

3. Experimental results for lift increments and the inferred drag-due-to-lift with flap deflection provide useful hydrofoil data at relatively high lift coefficients up to about 1.0.

4. Measured (inferred) values of the residual drag coefficients C_r for the entire range of lift coefficient, appear likely to contain wavemaking resistance contributions due to foil thickness that are noticeable only at the lowest Froude numbers $F_{n_c} < 2$, and for the shallower submergences. For the higher Froude numbers and deeper submergences, the C_r values appear to be predominantly drag-due-to-lift.

5. The two prediction schemes for hydrofoibdrag-due-to-lift considered here give results that coalesce and are both relatively accurate for chord Froude numbers larger than around $F_{n_c} \approx 3$. For lower Froude numbers, the lifting line estimate for elliptic circulation distributions gives $C_{D,L}$ values too low, while the HANDE prediction formula gives values that are too high. It would be useful to have readily available for prediction purposes the capability for complete lifting line computer calculations of drag-due-to-lift for hydrofoils at arbitrary Froude number, aspect ratio, planform shape, and flap span configuration.

ACKNOWLEDGMENTS

The work of Mr. Dennis Mullinix is gratefully acknowledged. for preparation of the instrumentation package and computer programs for data acquisition. Extensive calibration work and the experiments themselves were conducted with the able participation of Messers Allen Feller, Douglas Gregory, Gabor Karafiath, Pierre. Lafrance, James Peck, Alan Sobolewski, and Bernard Young.

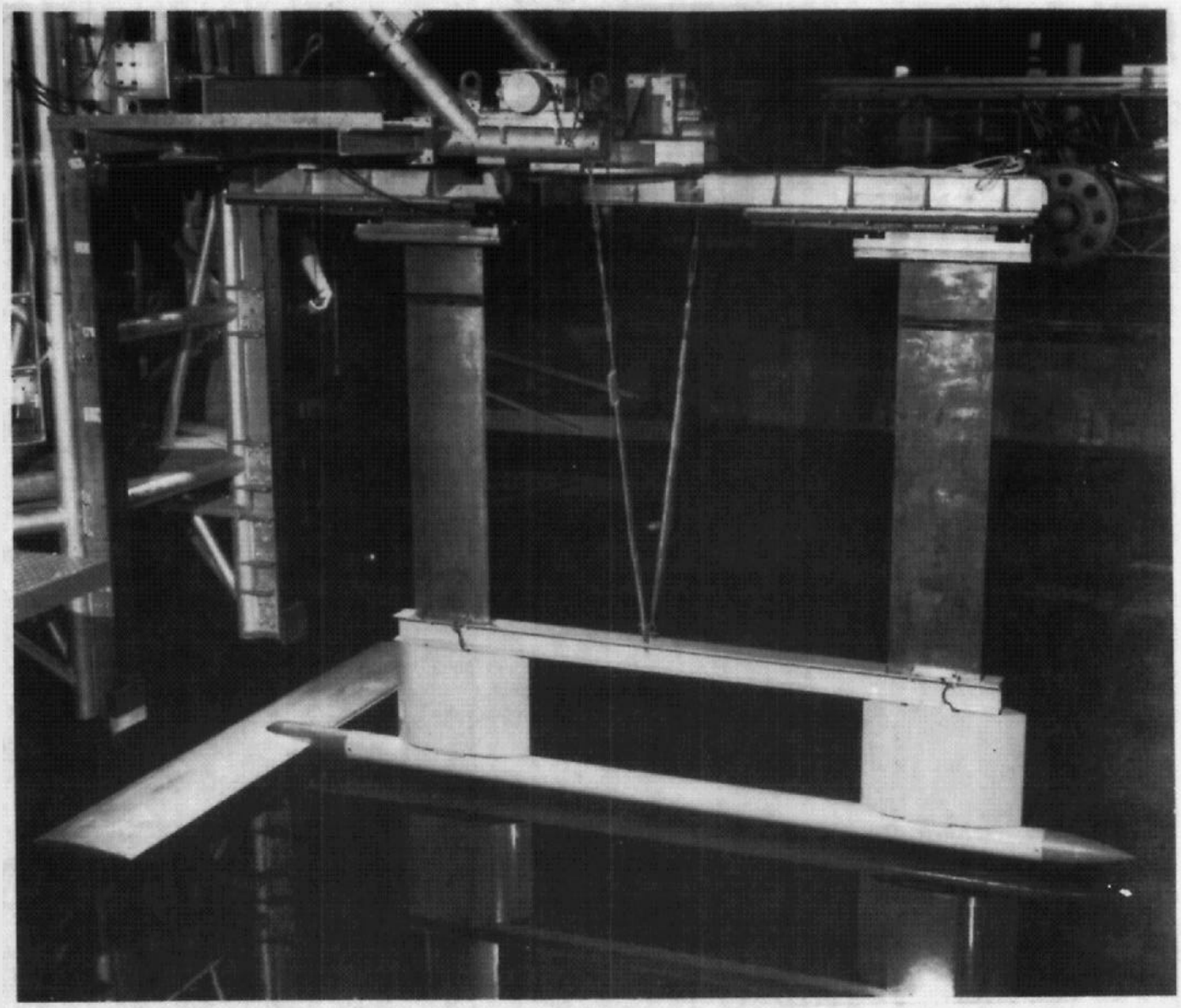

Figure 1 - Large Hydrofoil Model and Its Mounting System on Carriage 2 in the Deep Water Basin

(Foil and sting are shown here just above the water surface)

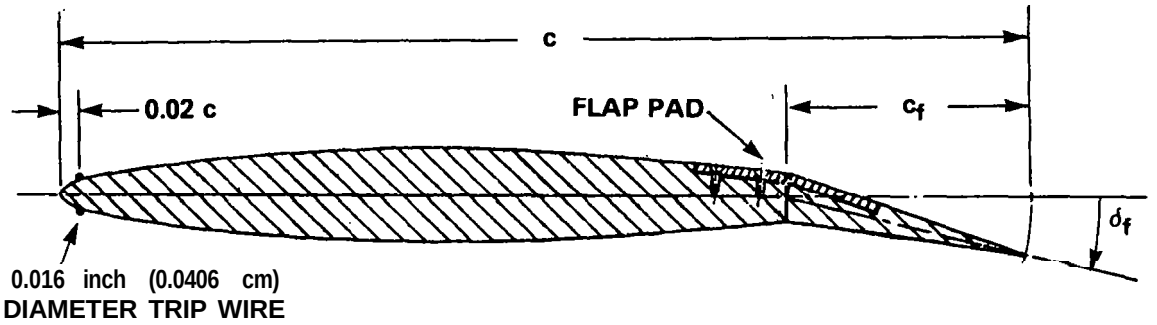

Figure 2 - Hydrofoil NACA 64 A010 Section With 0.25c Plain Flap

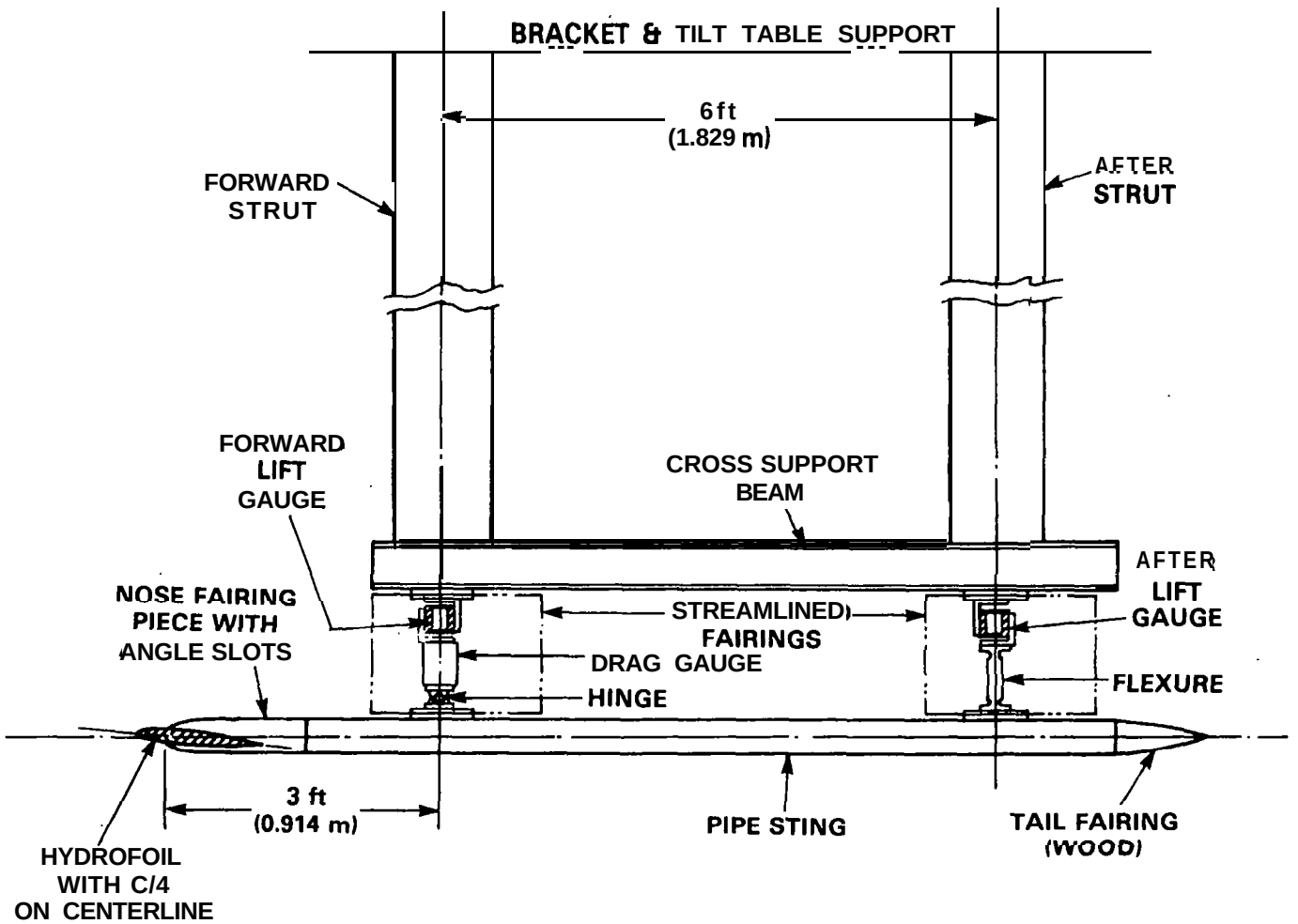

Figure 3 - Sketch of Hydrofoil Forward-Leading Sting and Dynamometer Support System

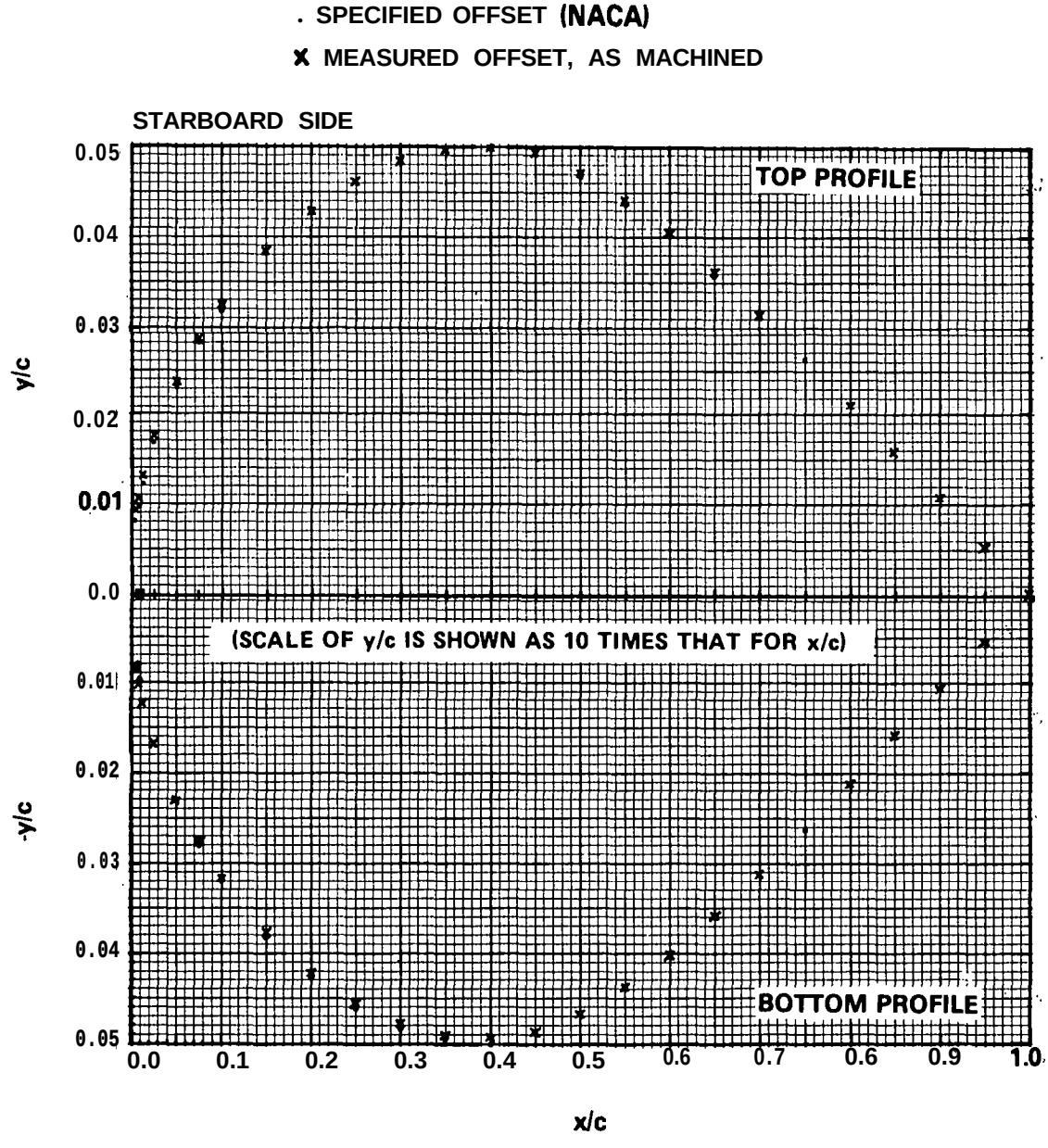

Figure 4 - Representation of Machined Foil Profile Accuracy--
Starboard Side, Top and Bottom

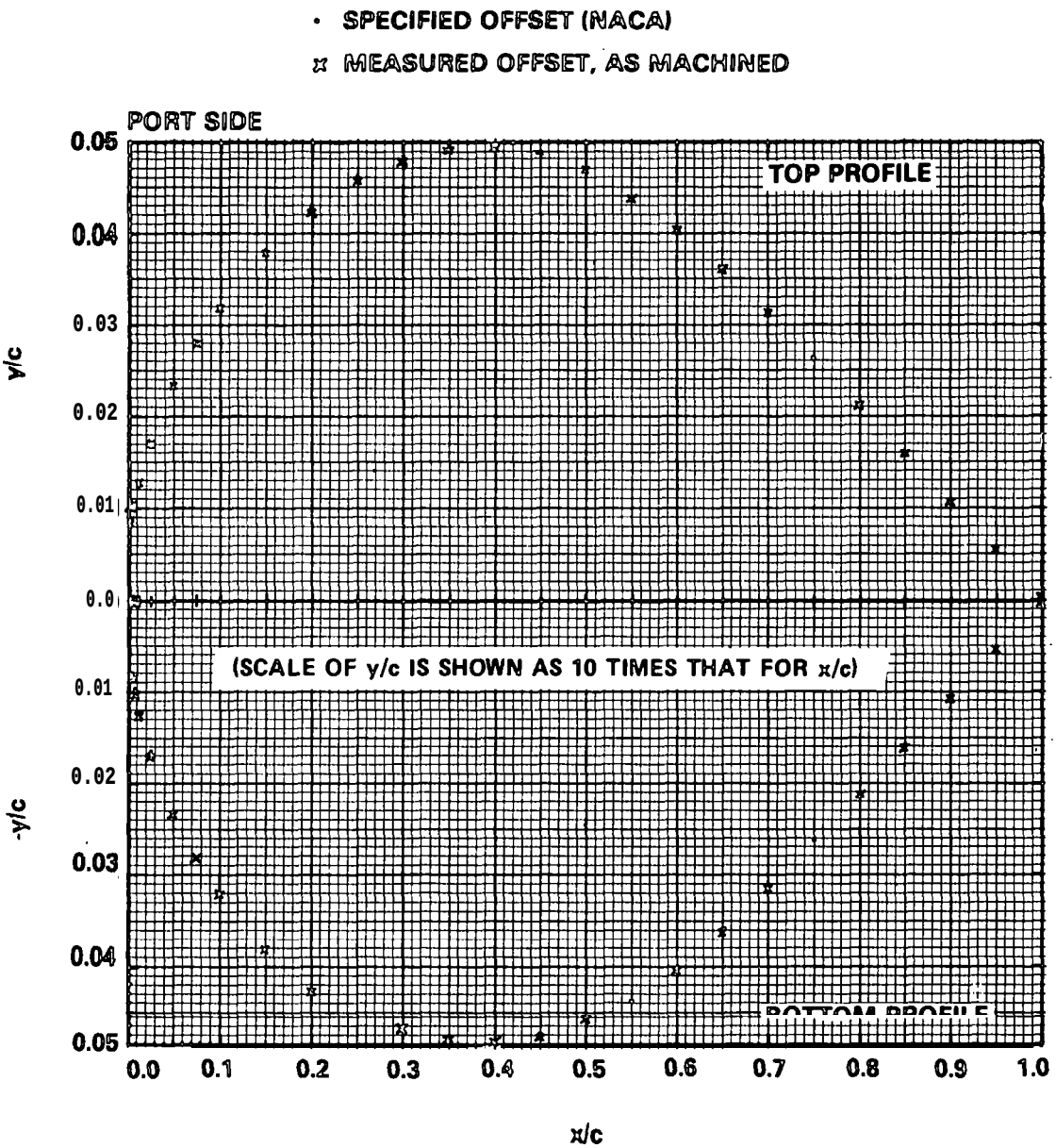

Figure 5 - Representation of Machined Foil Profile Accuracy -- Port Side, Top and Bottom

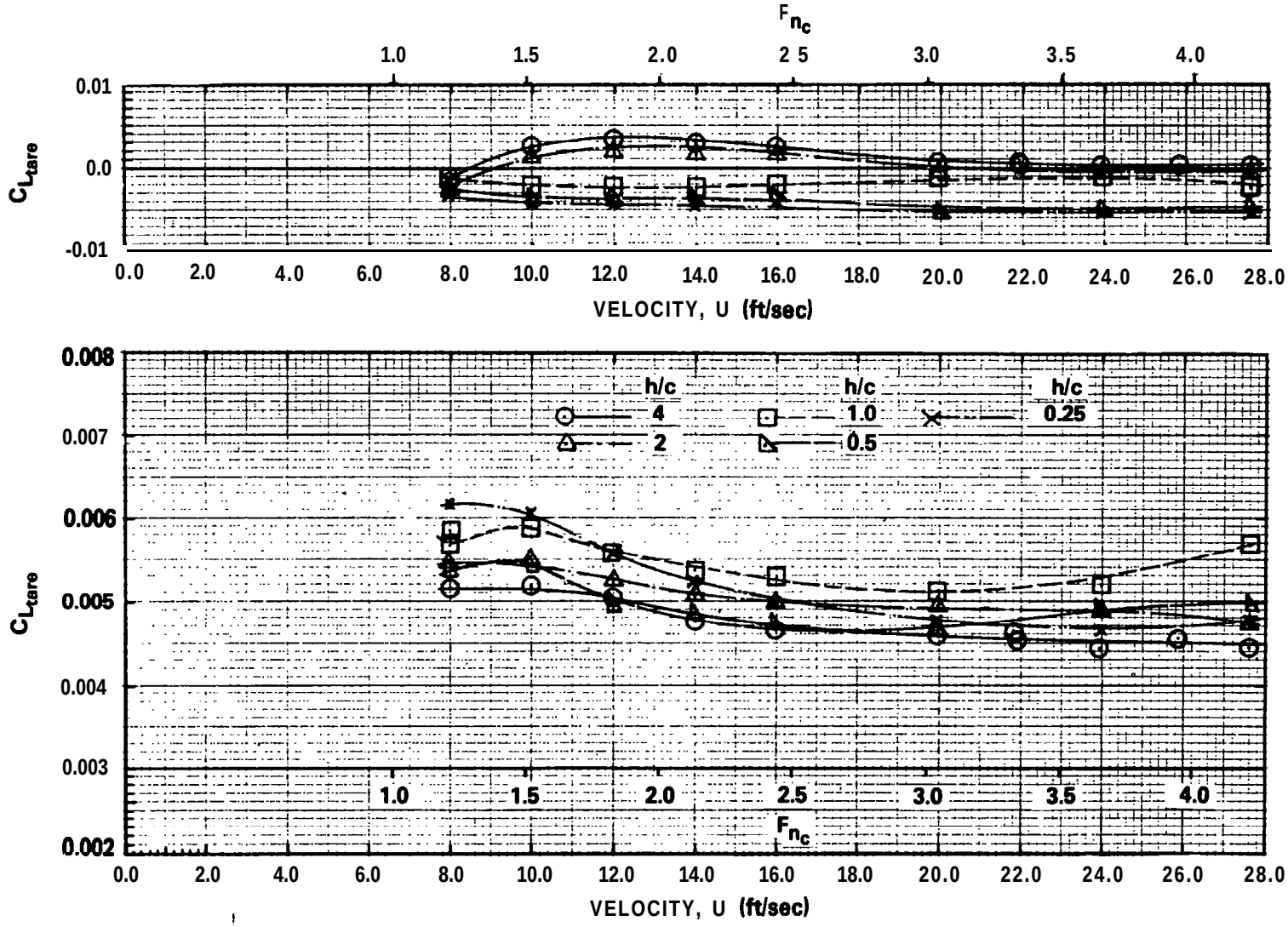

Figure 6 -'Variation of Sting Lift and Drag Tare Coefficients versus Speed, Contours of Submergence Ratio

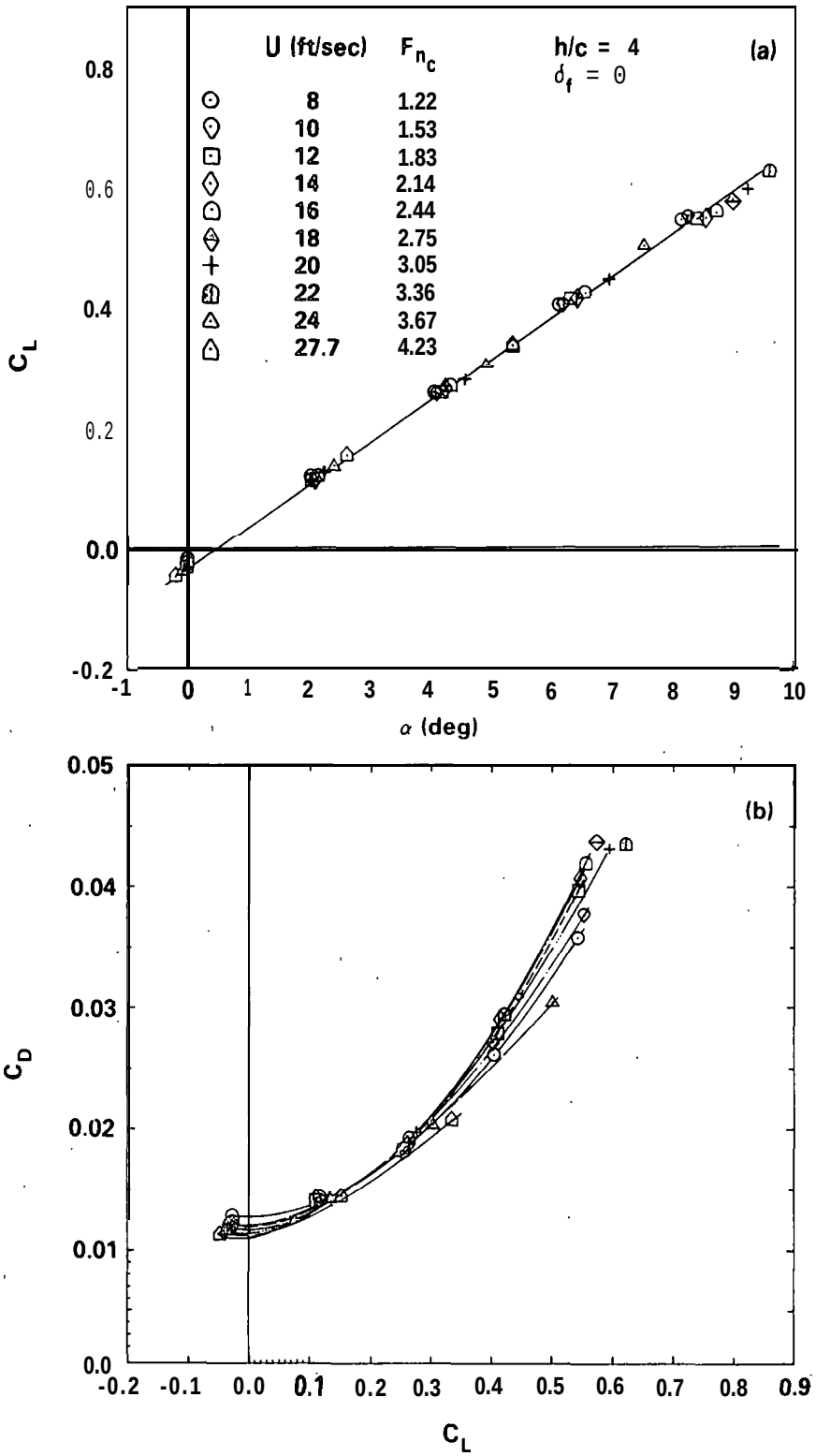

Figure 7 - Measured Hydrofoil Lift and Drag Coefficients for Submergence Ratio h/c = 4, Zero Flap, Contours of Speed

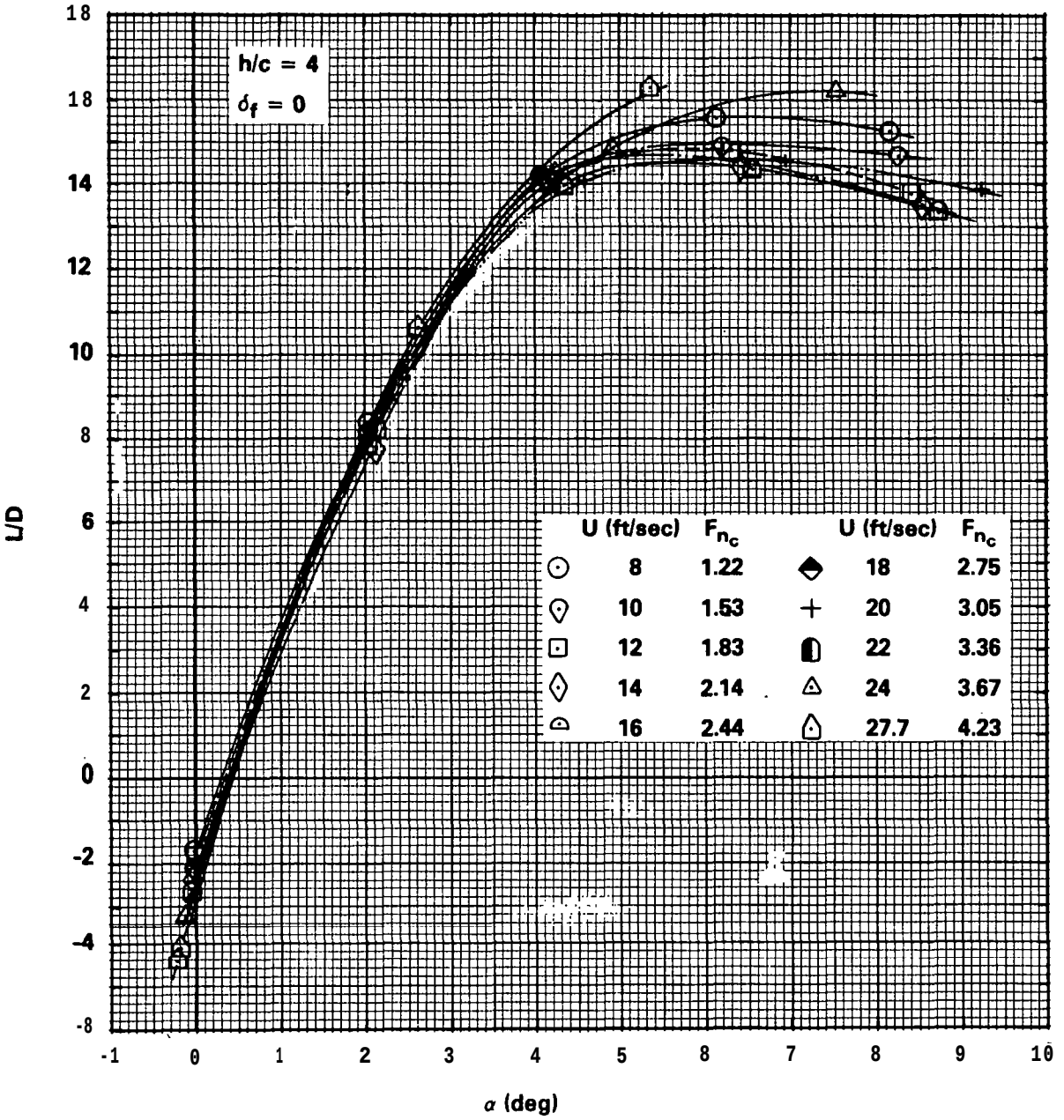

Figure 8 - Hydrofoil Lift-to-Drag Ratio versus Angle of Attack for Submergence Ratio h/c = 4, Contours of Speed

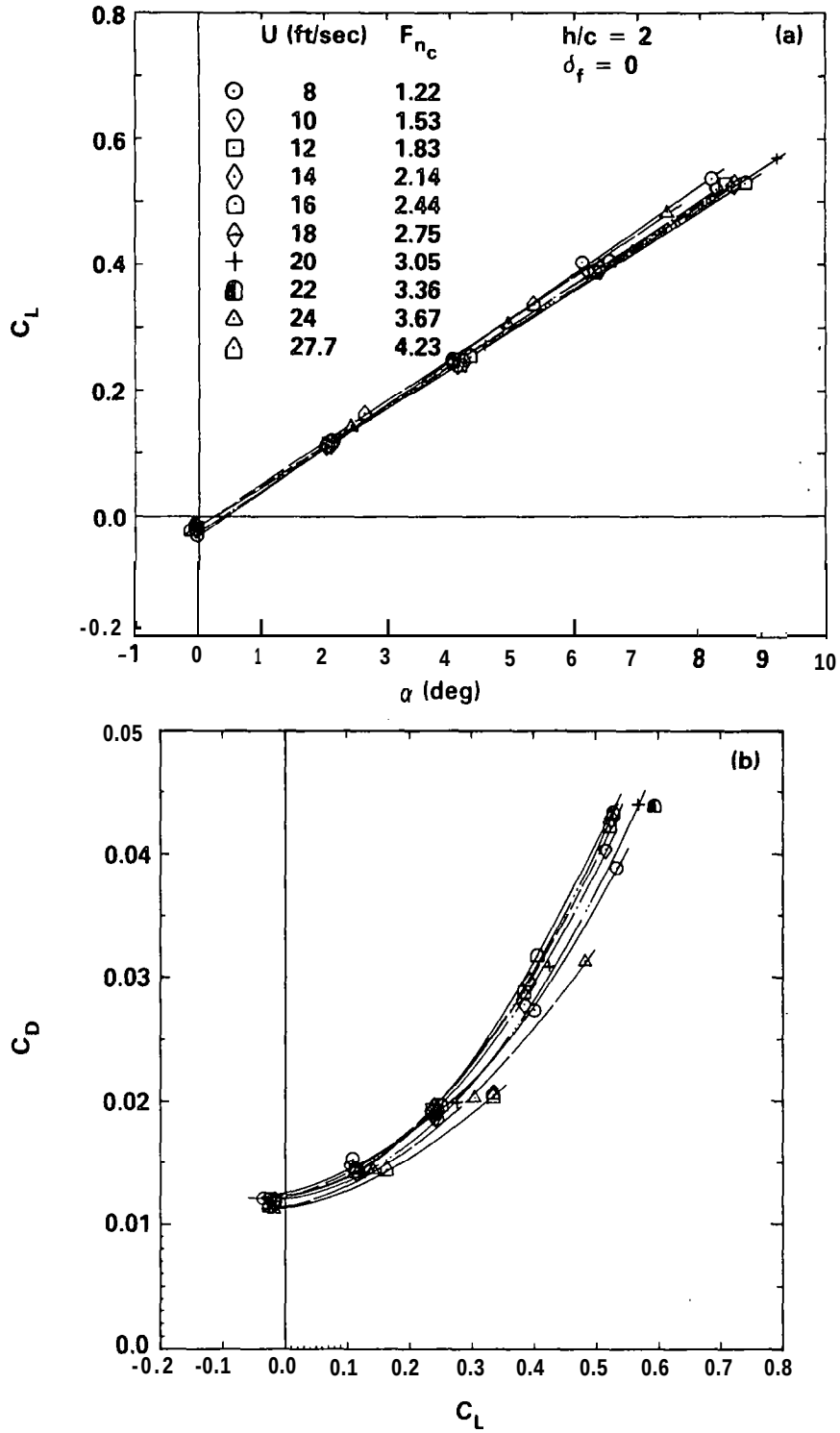

Figure 9 - Measured Hydrofoil Lift and Drag Coefficients for Submergence Ratio h/c = 2, Zero Flap, Contours of Speed

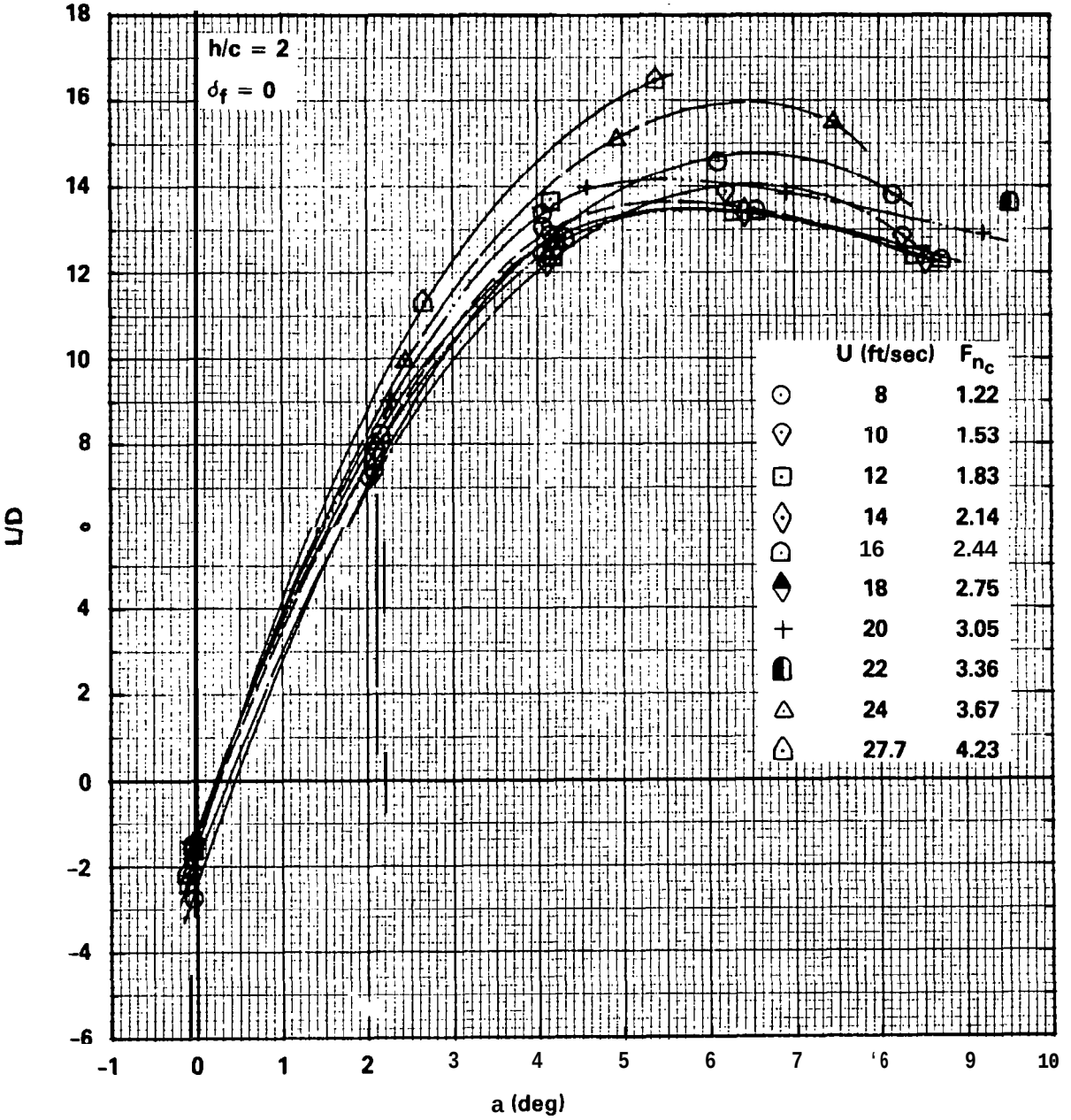

Figure 10 - Hydrofoil Lift-to-Drag Ratio versus Angle of Attack for Submergence Ratio h/c = 2, Contours of Speed

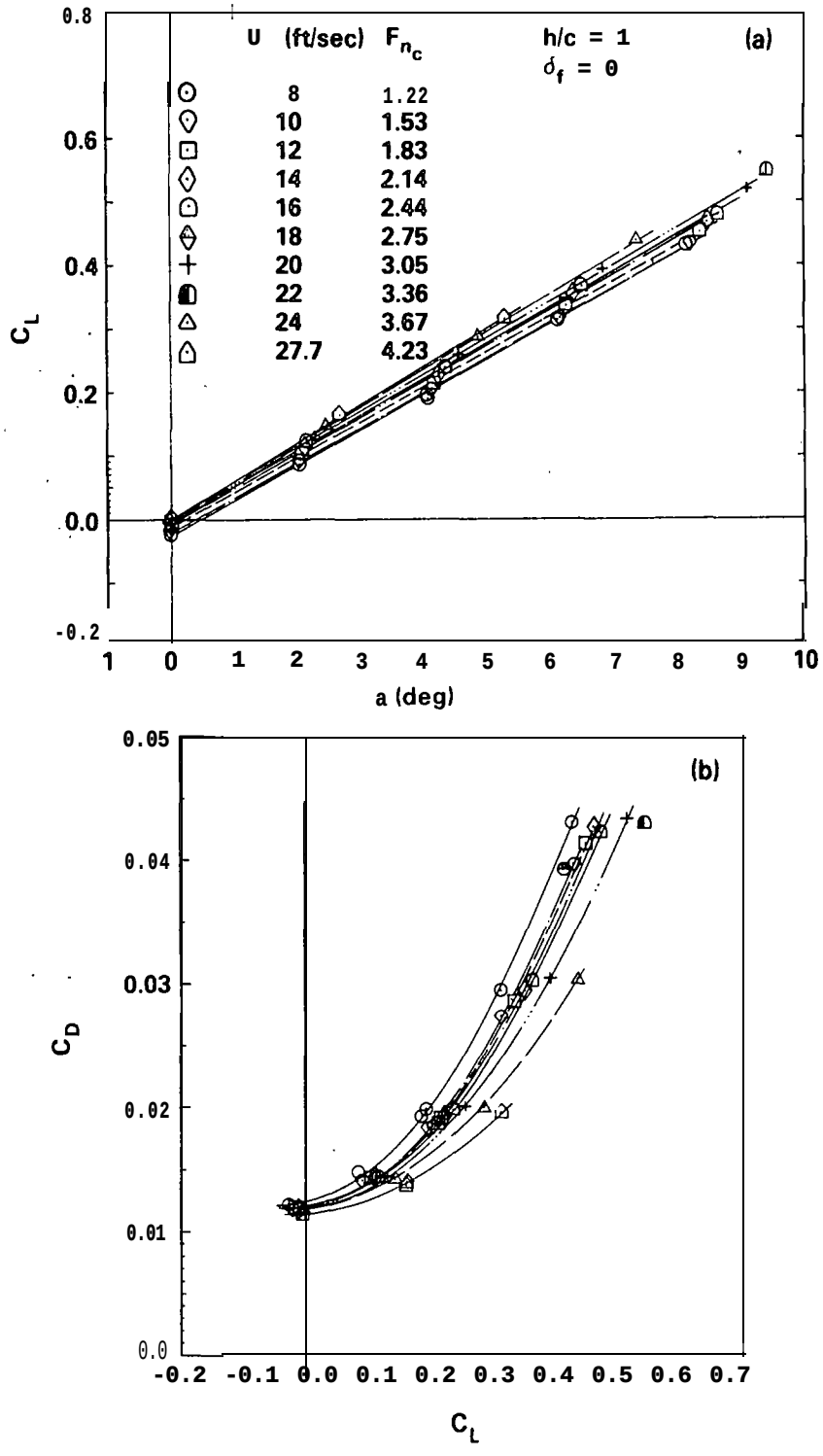

Figure 11 - Measured Hydrofoil Lift and Drag Coefficients for Submergence Ratio h/c = 1, Zero Flap, Contours of Speed

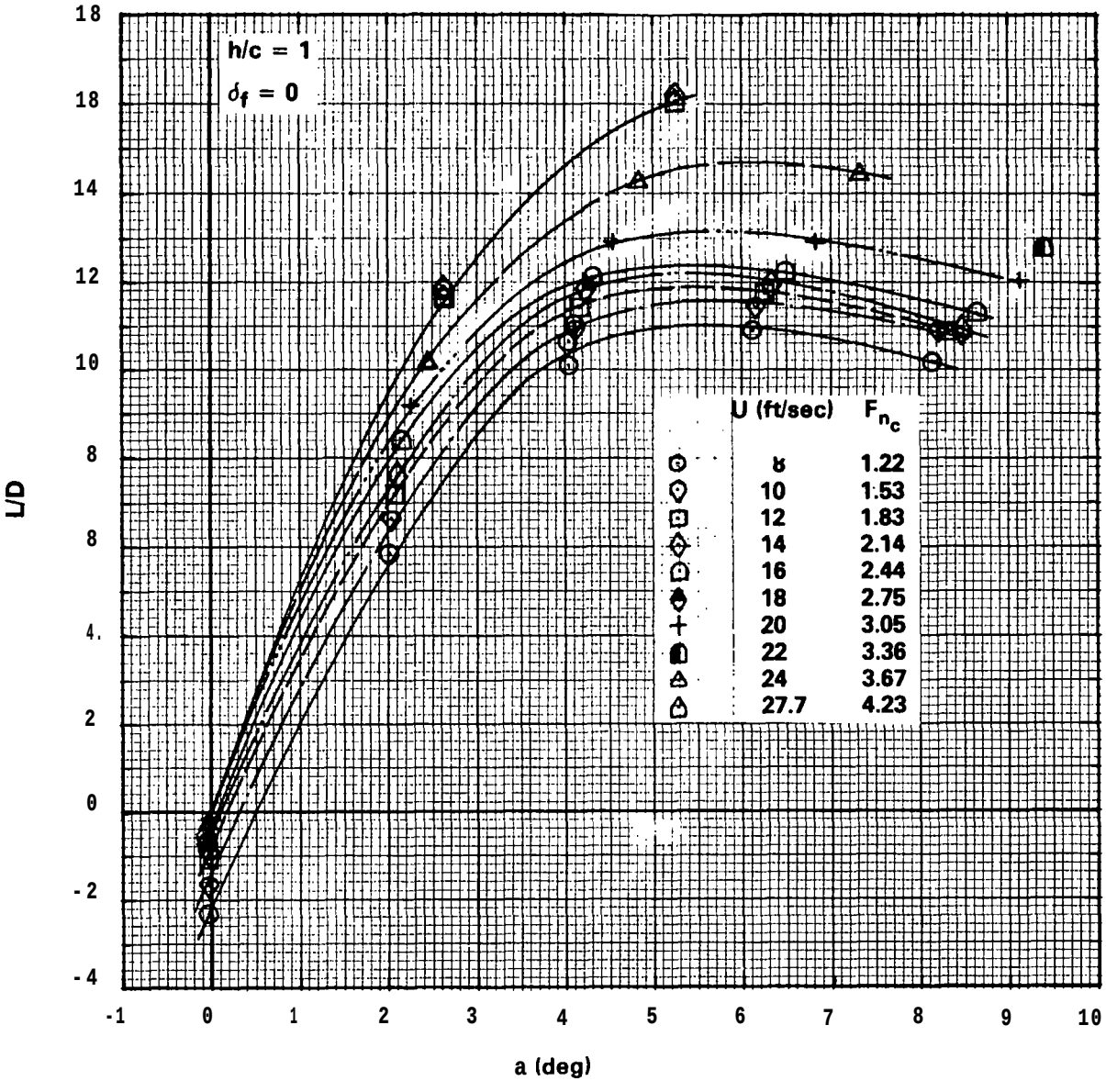

Figure 12 - Hydrofoil Lift-to.-Drag Ratio versus Angle of Attack for Submergence Ratio h/c = 1, Contours of Speed

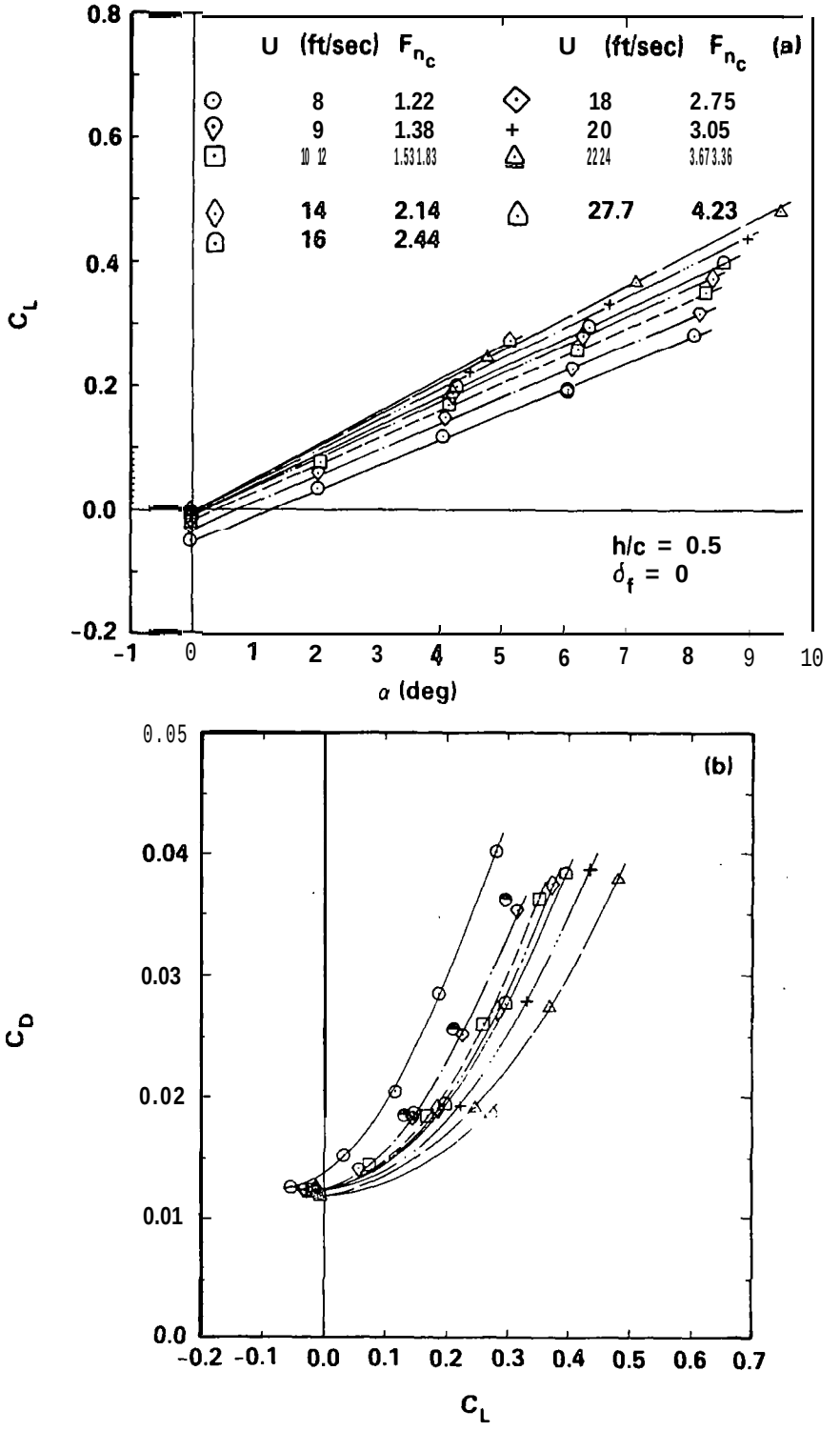

Figure 1.3 – Measured Hydrofoil Lift and Drag Coefficients for Submergence Ratio h/c = 0.5, Zero Flap, Contours of Speed

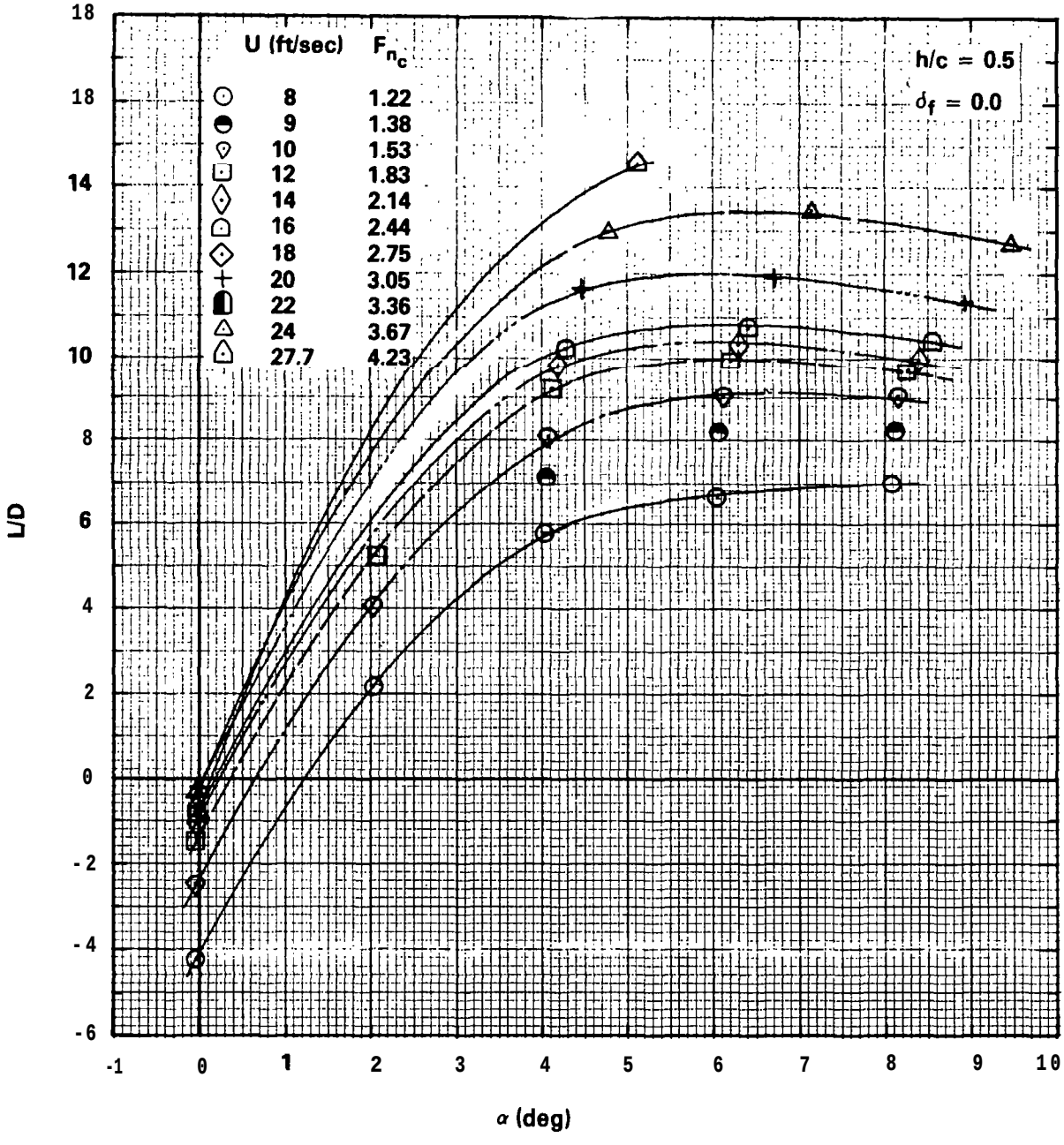

Figure 14 - Hydrofoil Lift-to-Drag Ratio versus Angle of Attack for Submergence Ratio h/c = 0.5, Contours of Speed

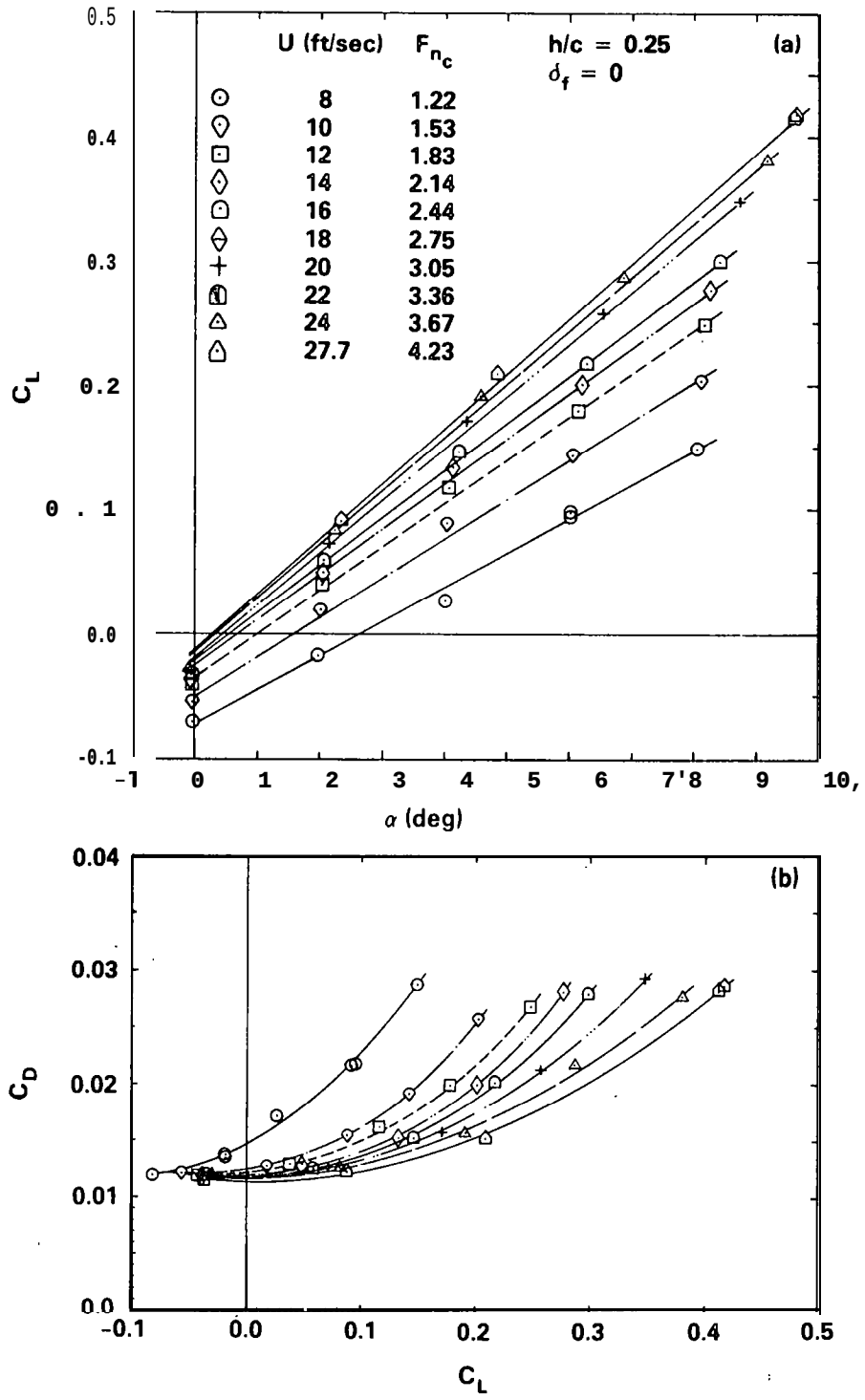

Figure 15 - Measured Hydrofoil Lift and Drag Coefficients for Submergence Ratio h/c = 0.25, Zero Flap, Contours of Speed

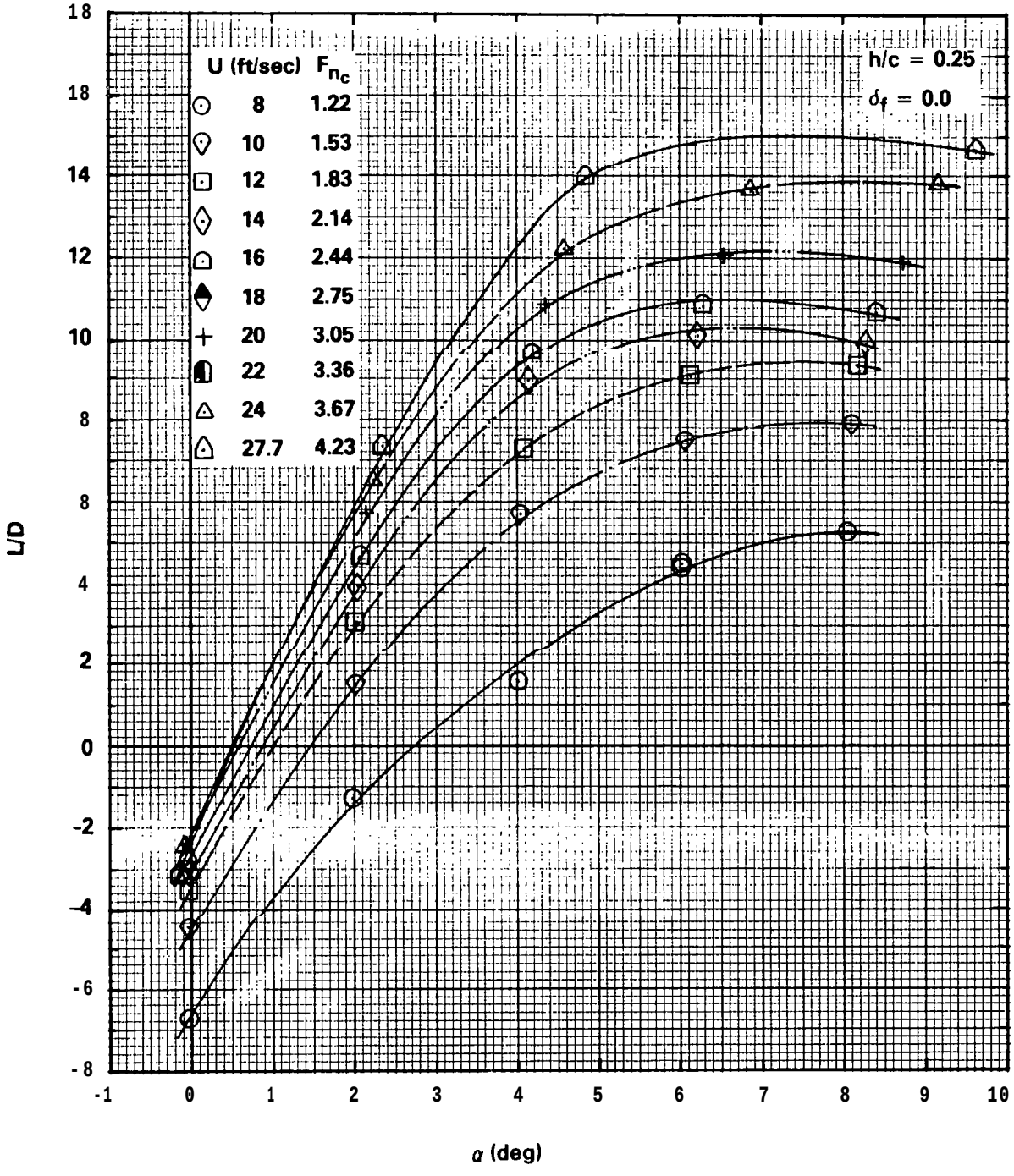

Figure 16 - Hydrofoil Lift-to-Drag Ratio versus Angle of Attack for Submergence Ratio h/c = 0.25, Contours of Speed

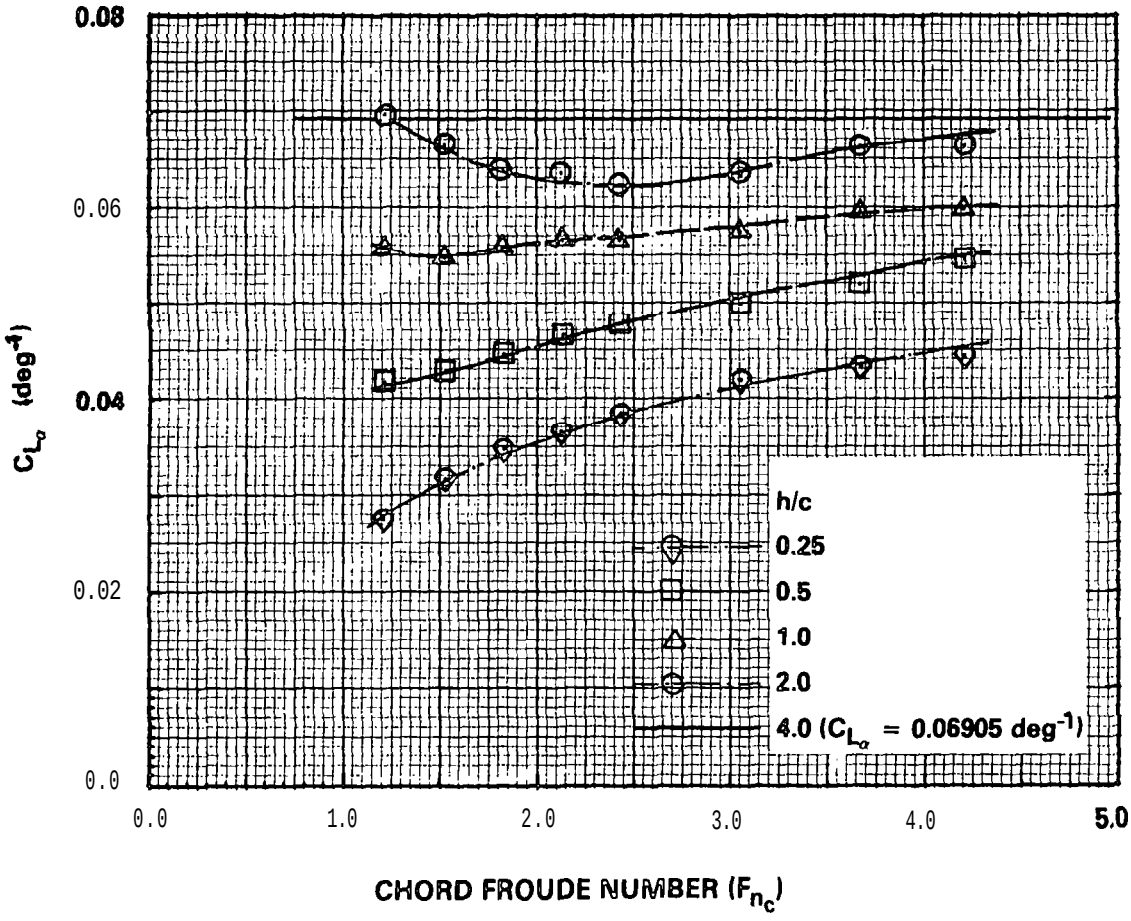

Figure 17 - Variation of Hydrofoil Lift-Curve Slope versus Chord Froude Number, Contours of Submergence

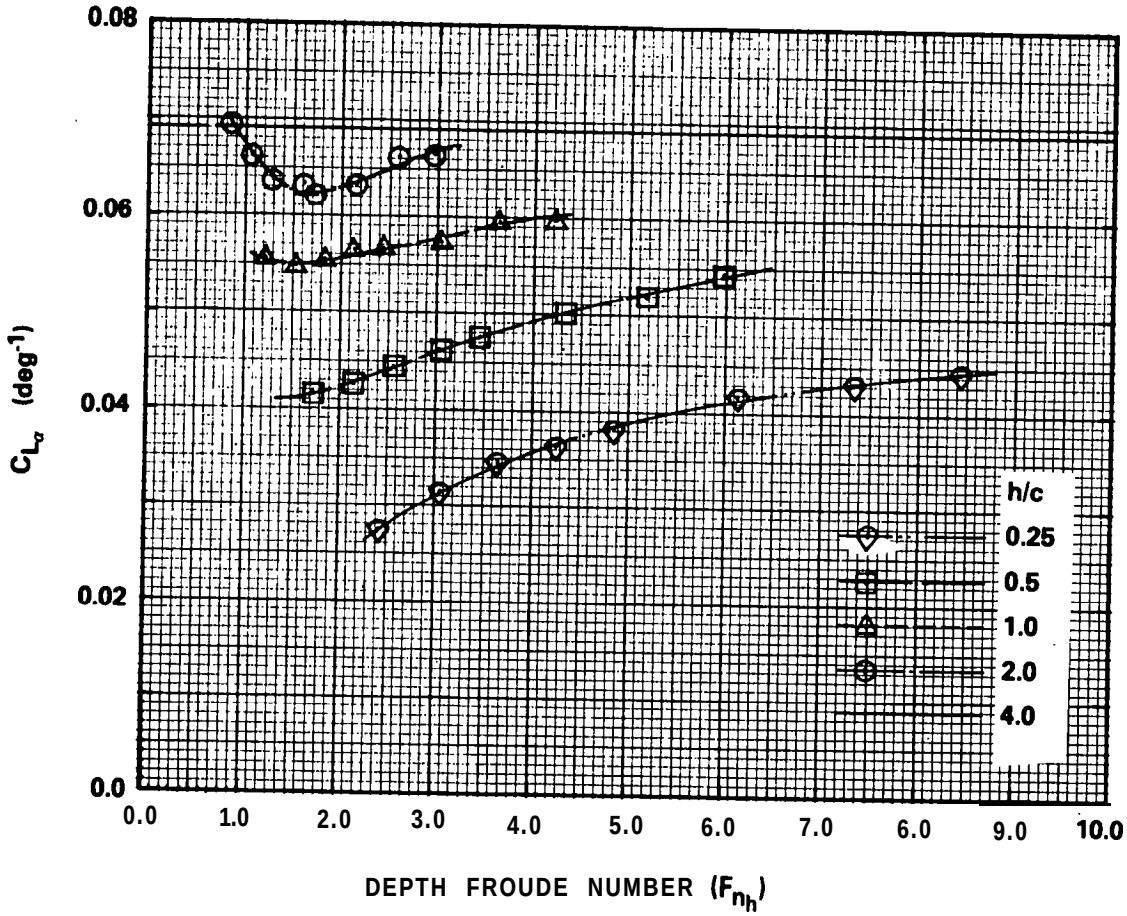

Figure 18 - Variation of Hydrofoil Lift-Curve Slope versus Depth Froude Number, Contours of Submergence

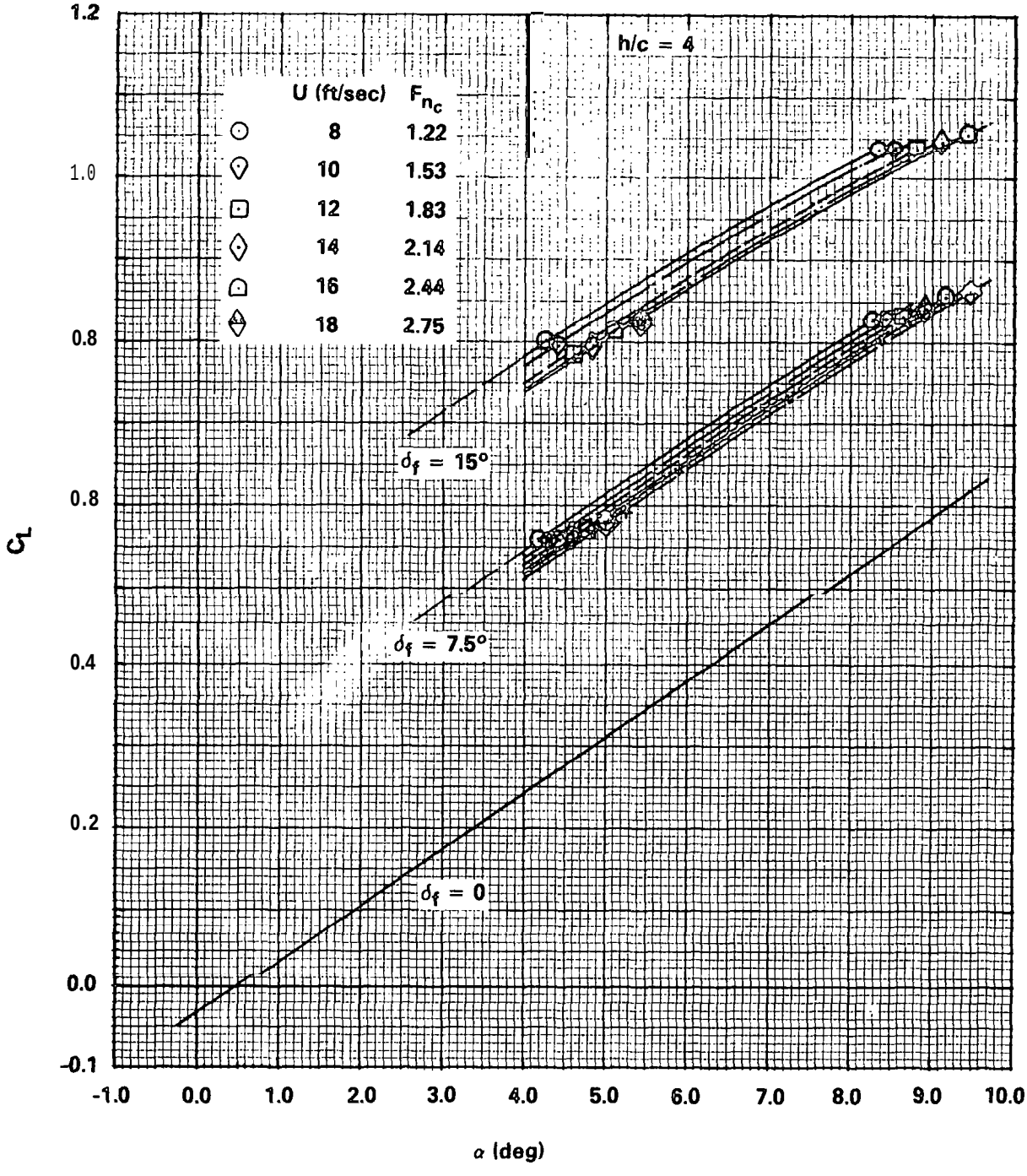

Figure 19 - Effect of Flap Deflection on Lift Coefficient versus Angle of Attack for Submergence Ratio h/c = 4

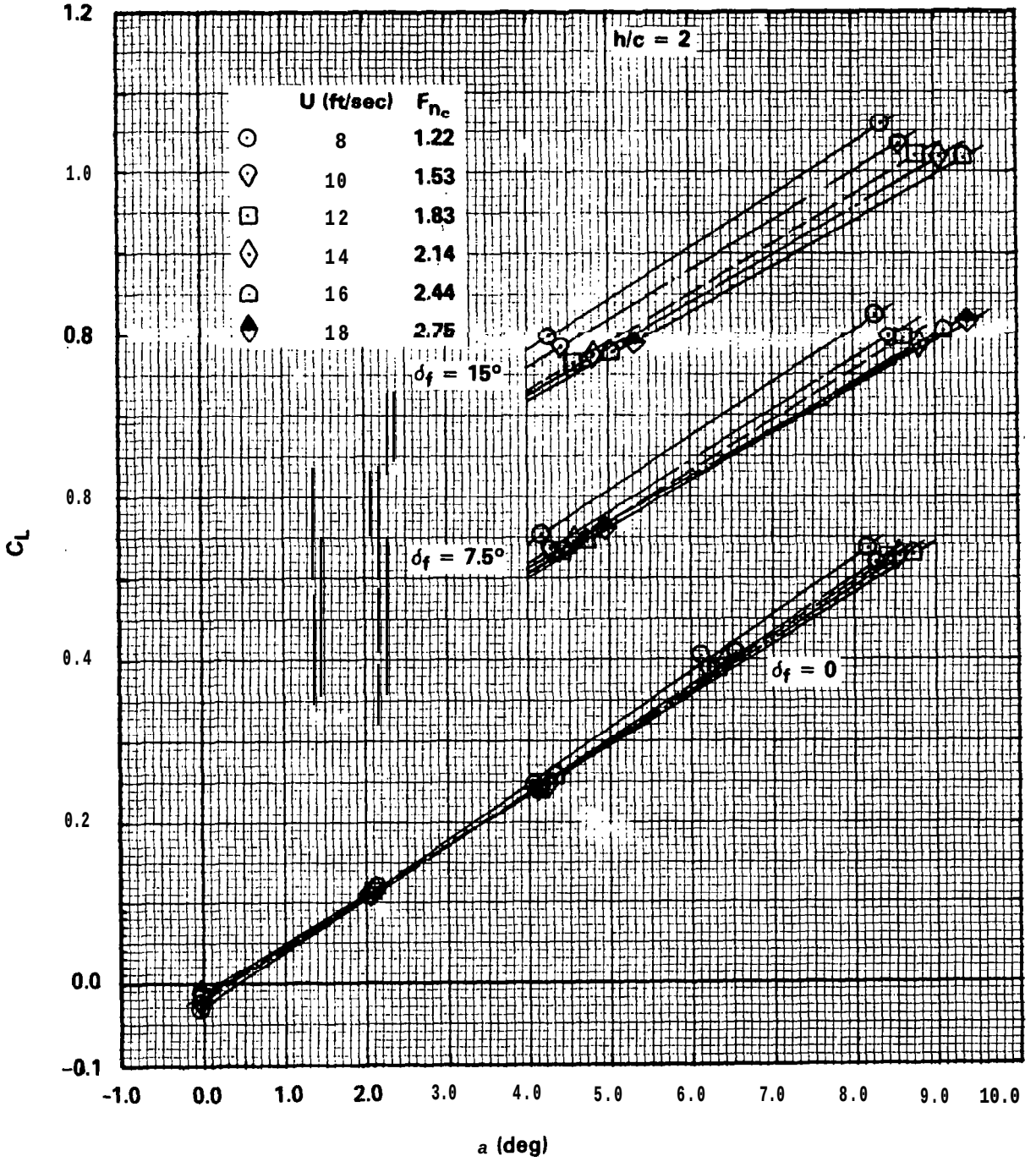

Figure 20 - Effect of Flap Deflection on Lift Coefficient versus Angle of Attack for Submergence Ratio h/c = 2

Figure 21 - Effect of Flap Deflection on Lift Coefficient versus Angle of Attack for Submergence Ratio h/c = 1

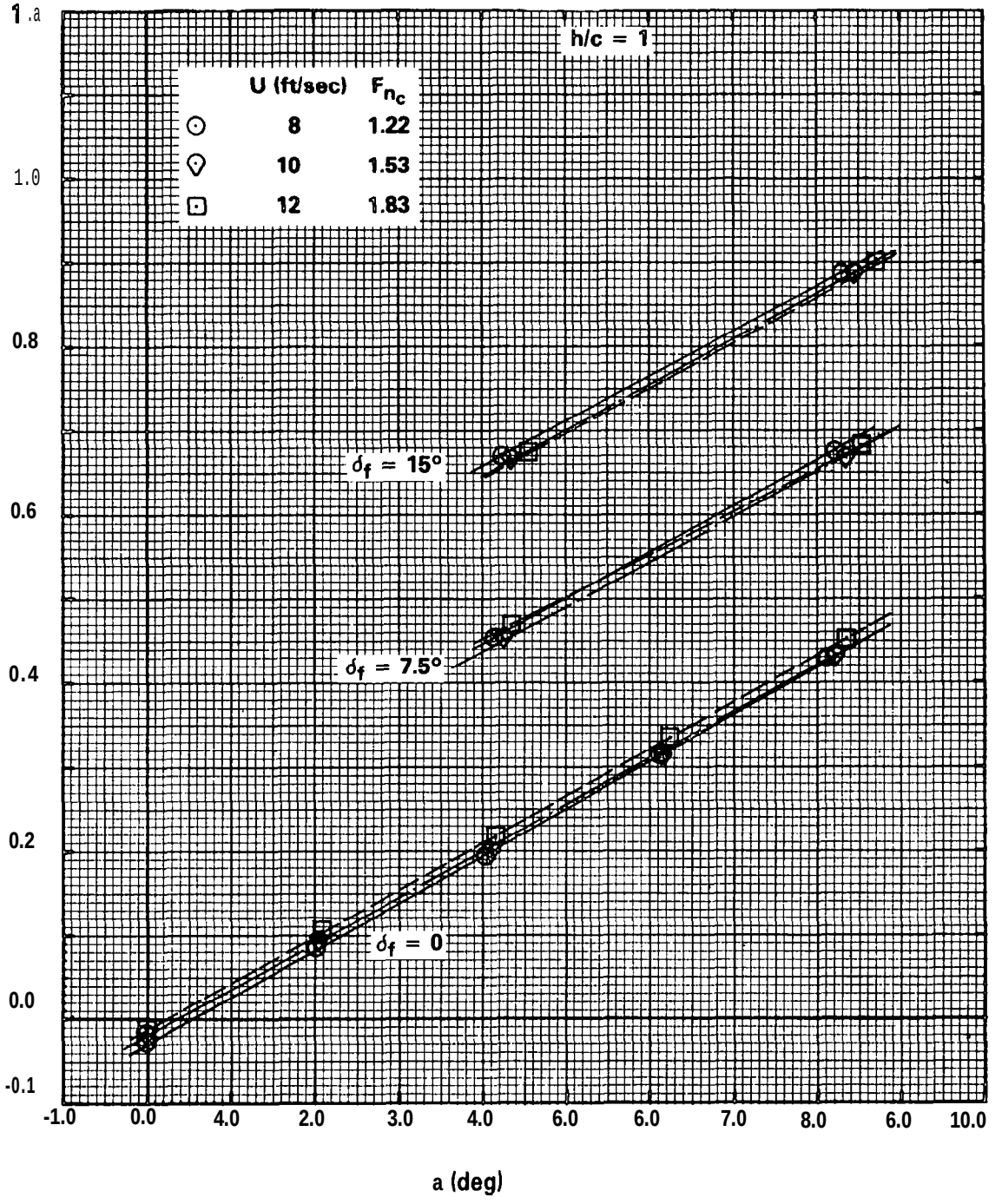

Figure 21a - F_{n_c} = 1.22, 1.53, and 1.83

Figure 21 (Continued)

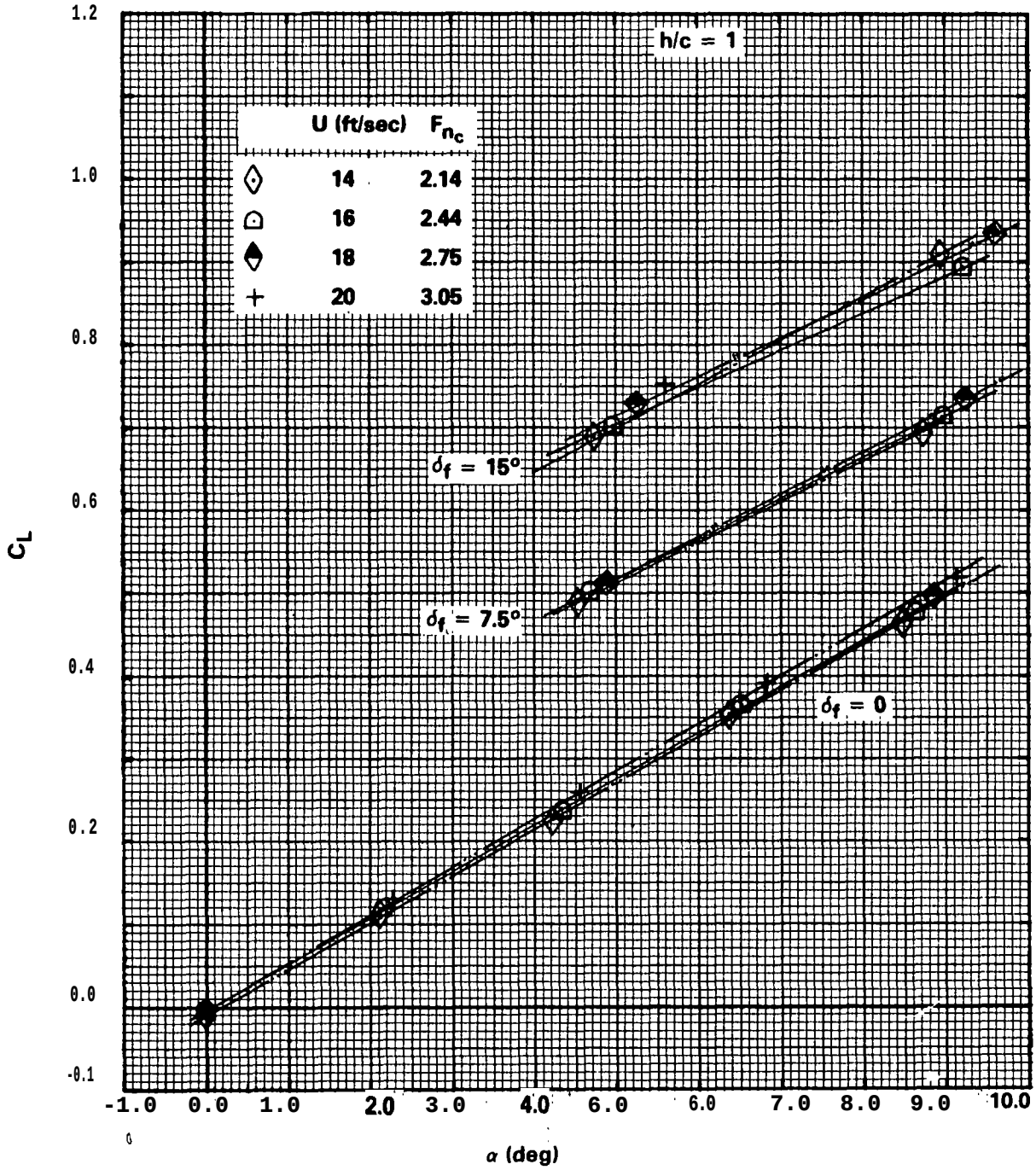

Figure 21b - F_{n_c} = 2.14, 2.44, 2.75, and 3.05

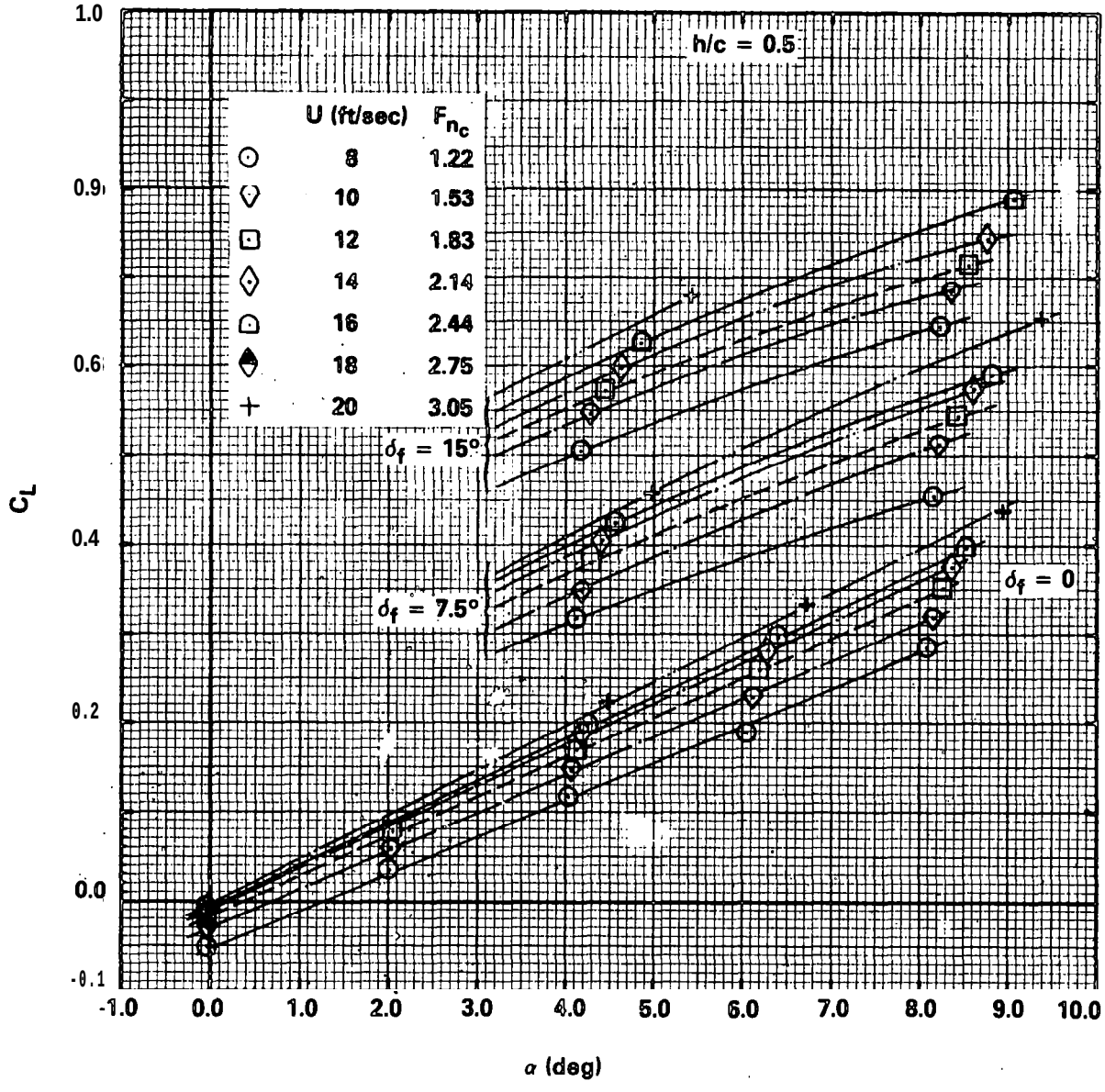

Figure 22 - Effect of Flap Deflection on Lift Coefficient versus Angle of Attack for Submergence Ratio h/c = 0.5

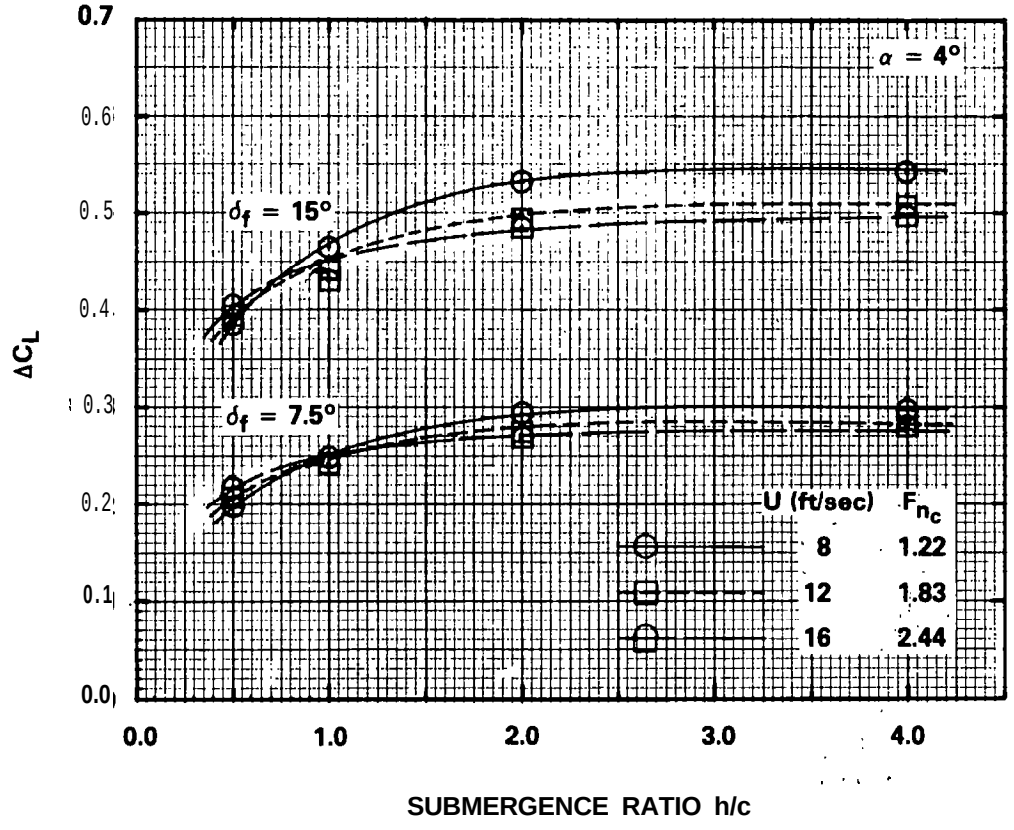

Figure 23 - Flap Lift Coefficient Increment versus Submergence Ratio, Contours of Speed

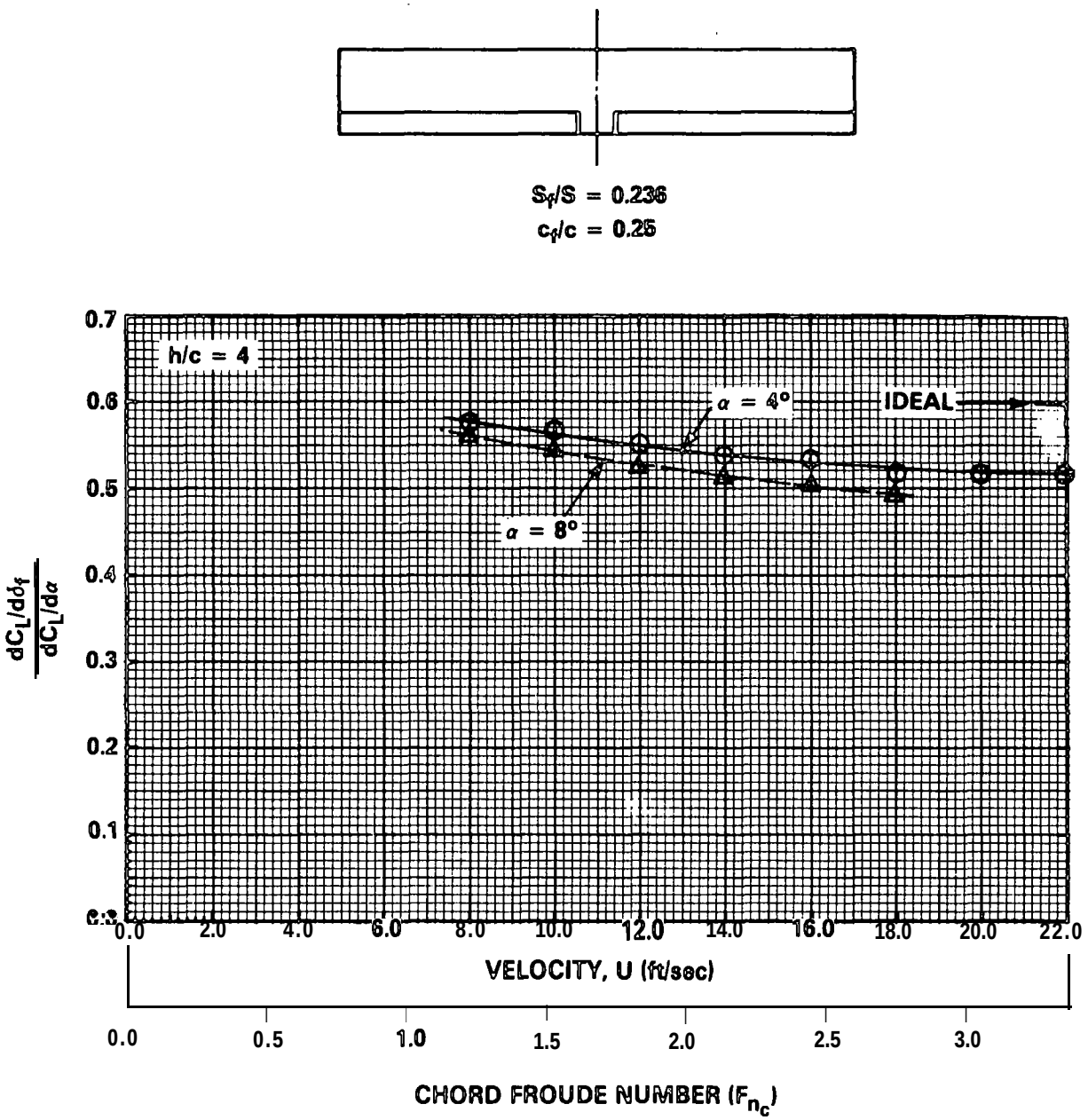

Figure 24 - Reference Flap Effectiveness (at Submergence h/c = 4) versus Speed

Figure 25 - Effect of Flap Deflection on Drag Coefficient versus Angle of Attack Squared for Submergence Ratio h/c = 4

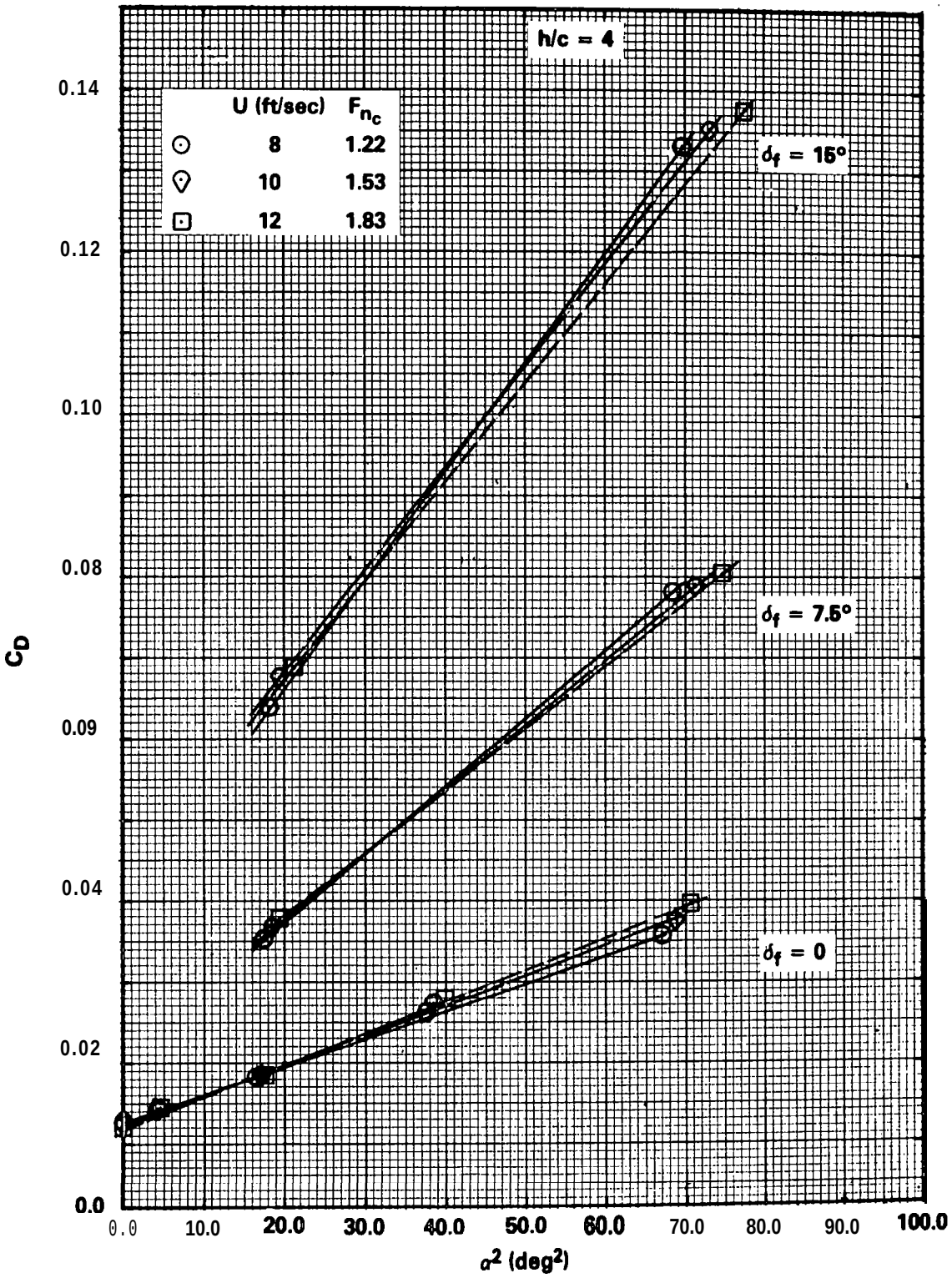

Figure 25a - F_{n_c} = 1.22, 1.53 and 1.83

Figure 25 (Continued)

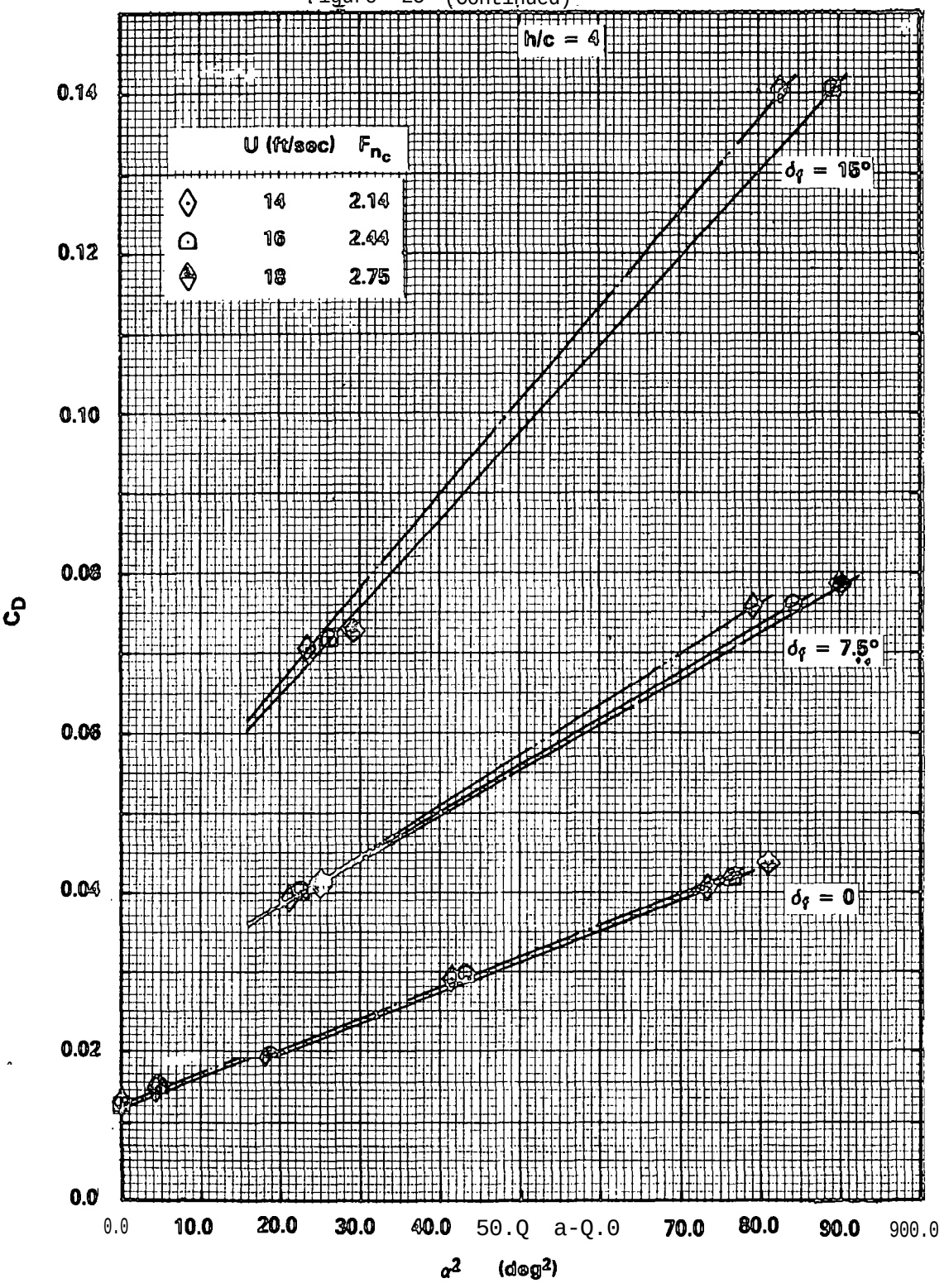

Figure 25b - F_{n_c} = 2.14, 2.44, and 2.75

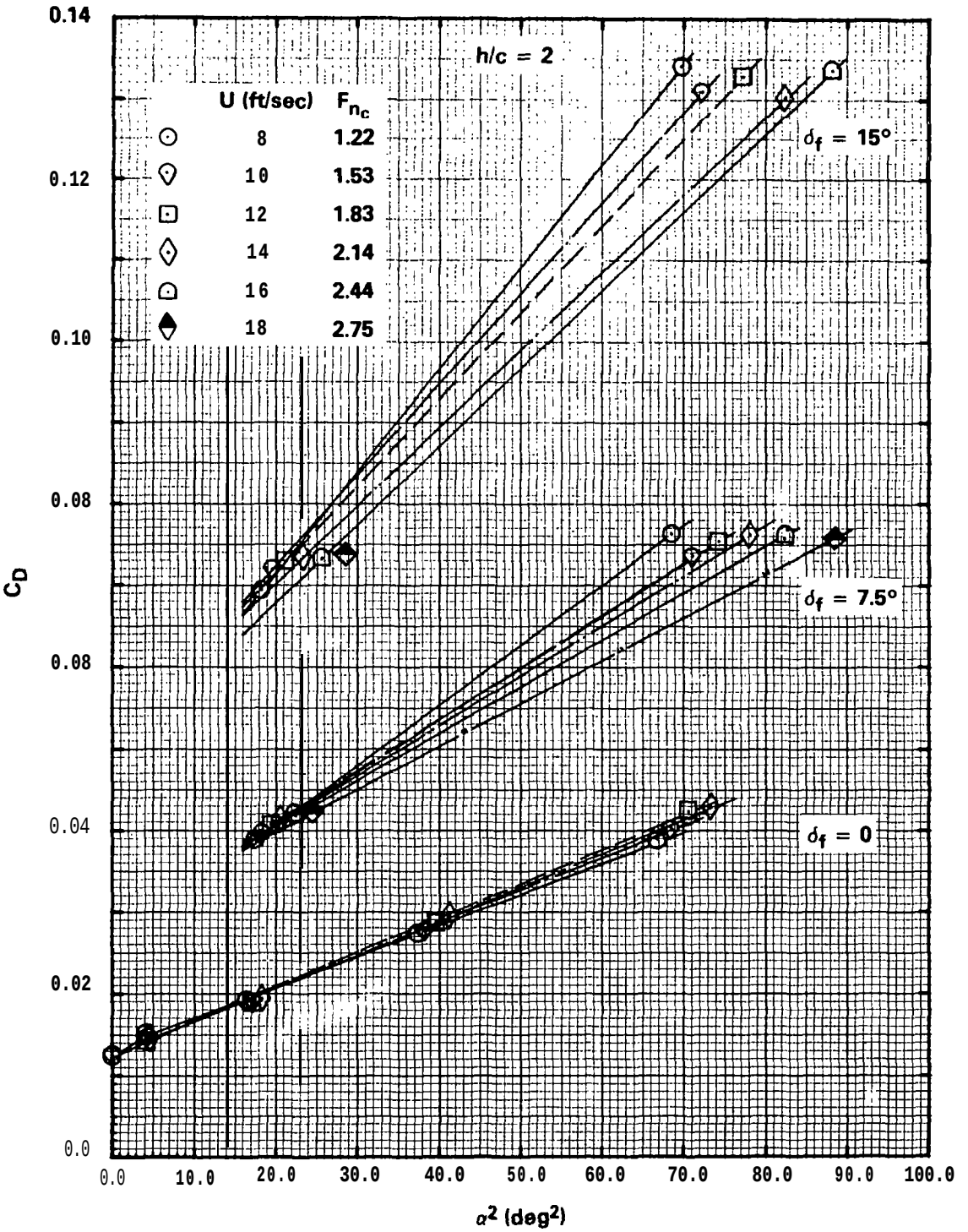

Figure 26 - Effect of Flap Deflection on Drag Coefficient versus Angle of Attack Squared for Submergence Ratio h/c = 2

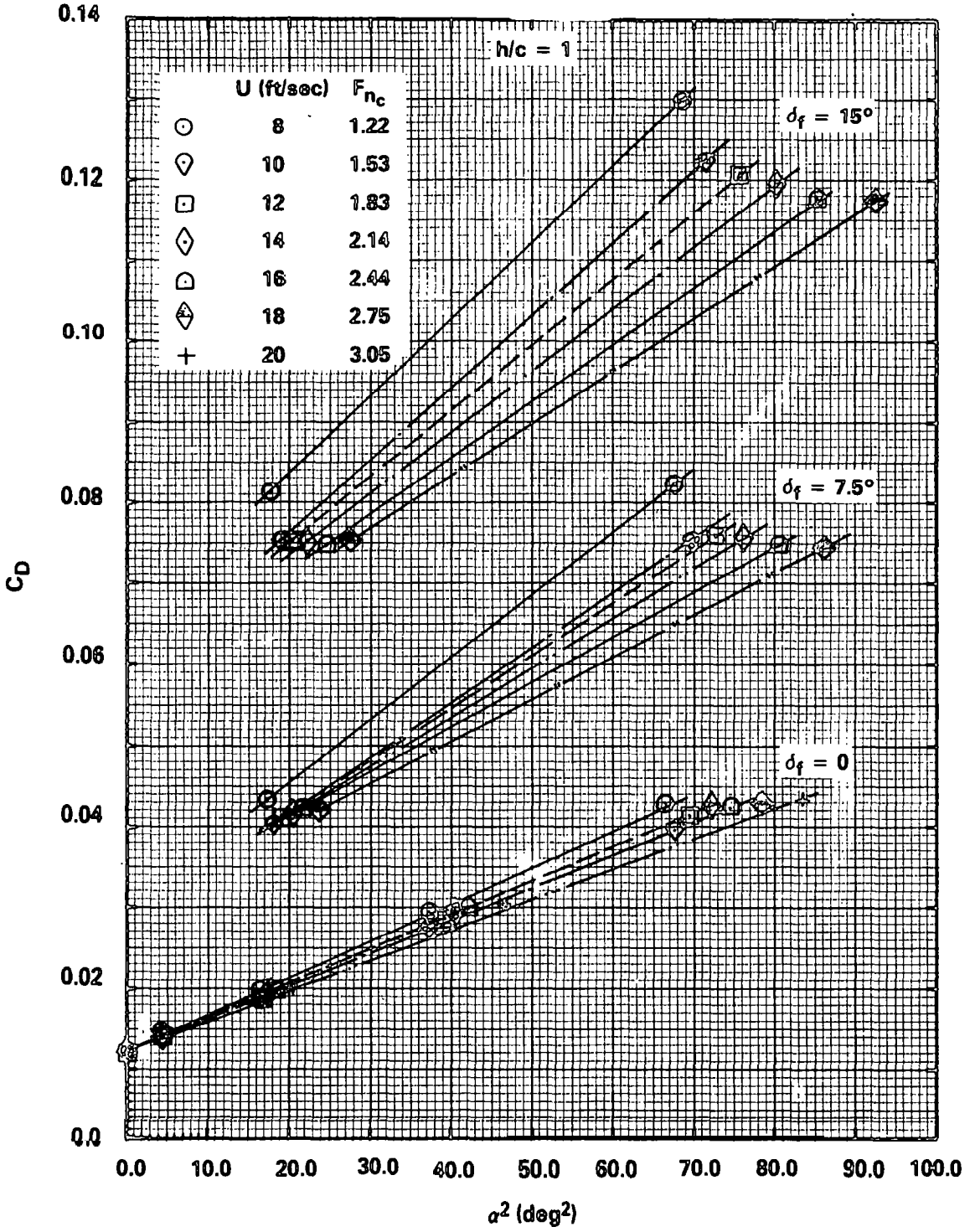

Figure 27 - Effect of Flap Deflection on Drag Coefficient versus Angle of Attack Squared for Submergence Ratio h/c = 1

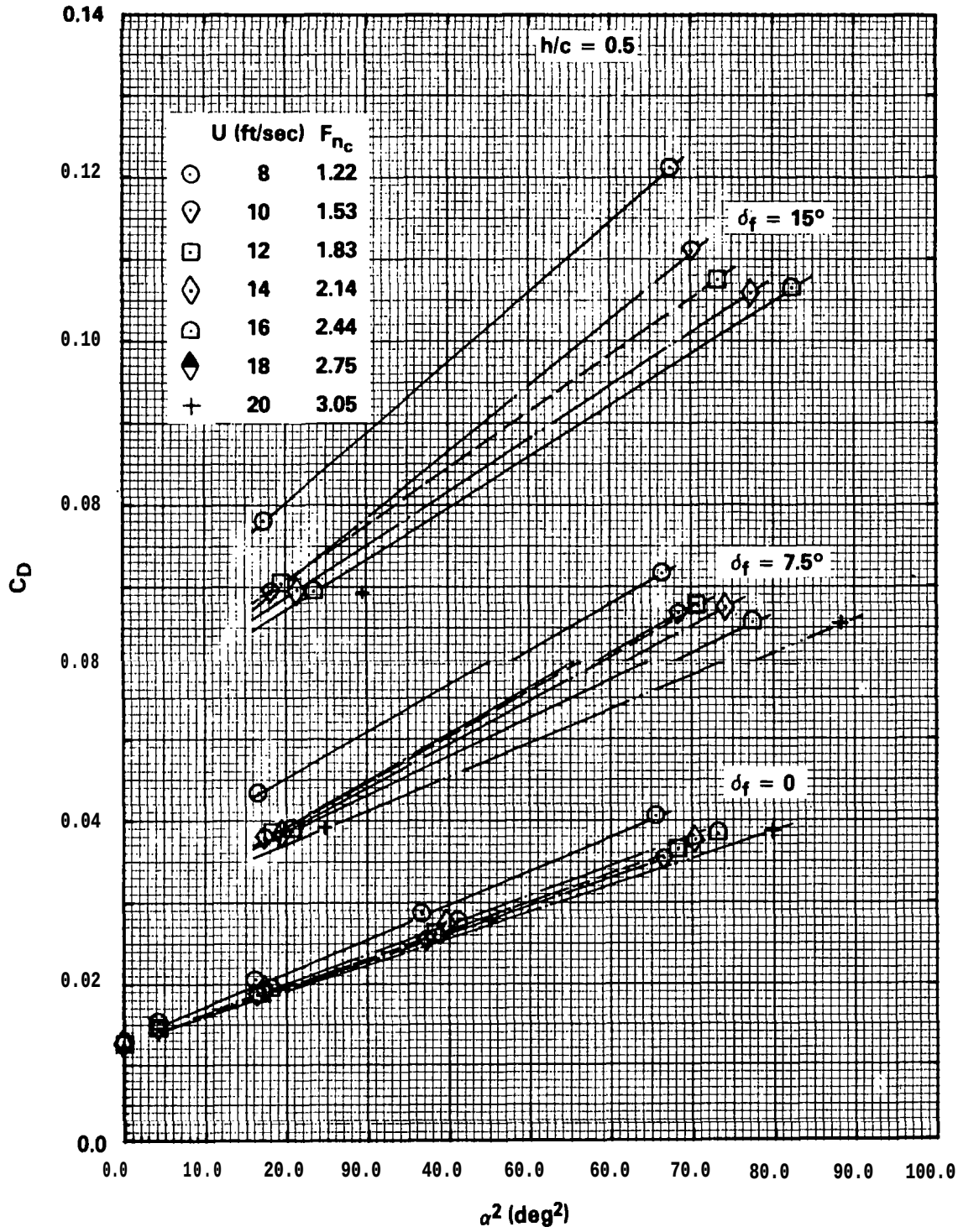

Figure 28 - Effect of Flap Deflection on Drag Coefficient versus Angle of Attack Squared for Submergence Ratio h/c = 0.5

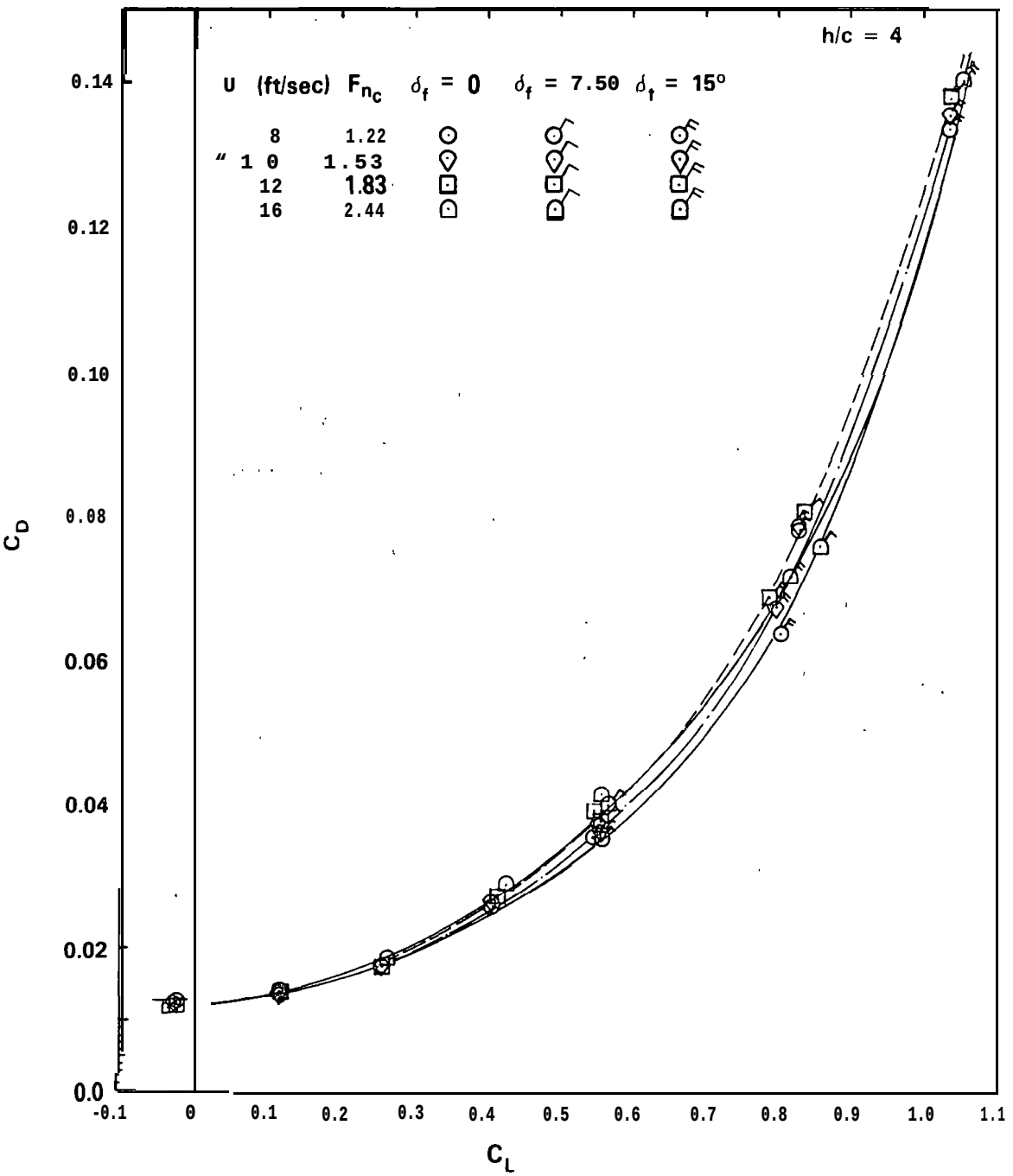

Figure 29 - Drag Polar of Measured CD versus C_L for Flapped and Zero Flapped Hydrofoil at Submergence Ratio h/c = 4

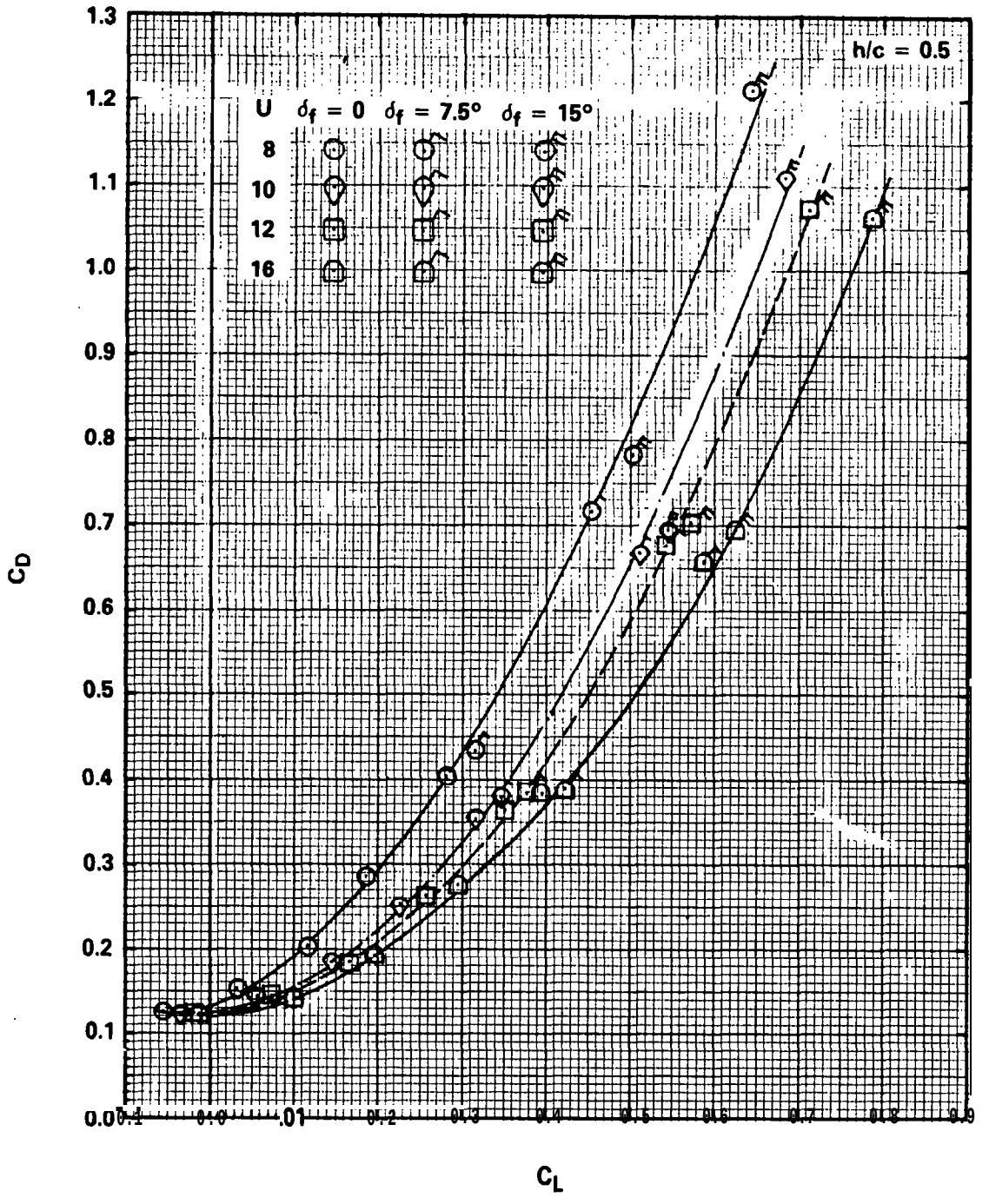

Figure 30 - Drag Polar of Measured CD versus C_L for Flapped and Zero Flapped Hydrofoil at Submergence Ratio h/c = 0.5

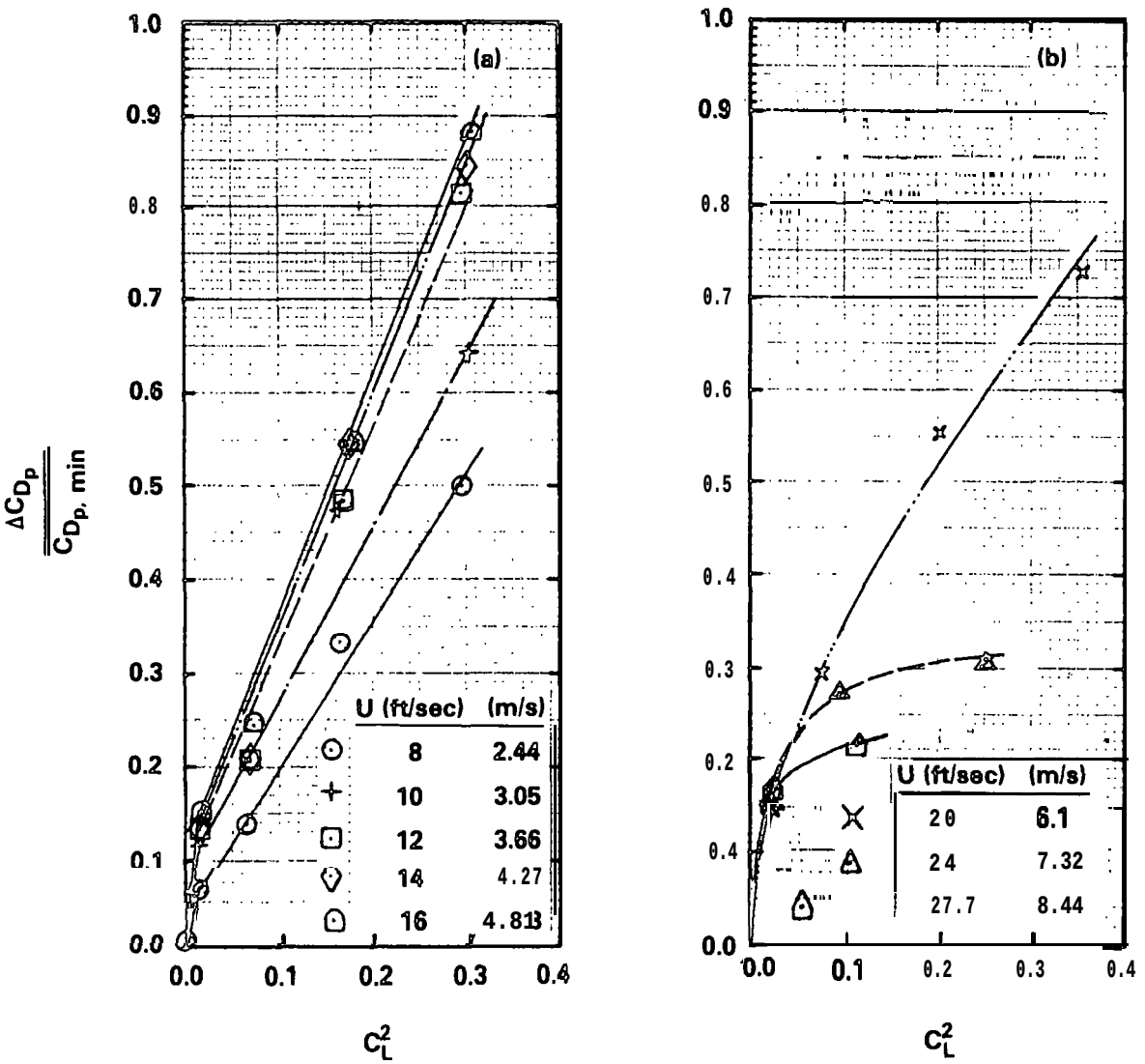

Figure 31 - Inferred Incremental Profile Drag Ratio versus C_L^2, Contours of Speed

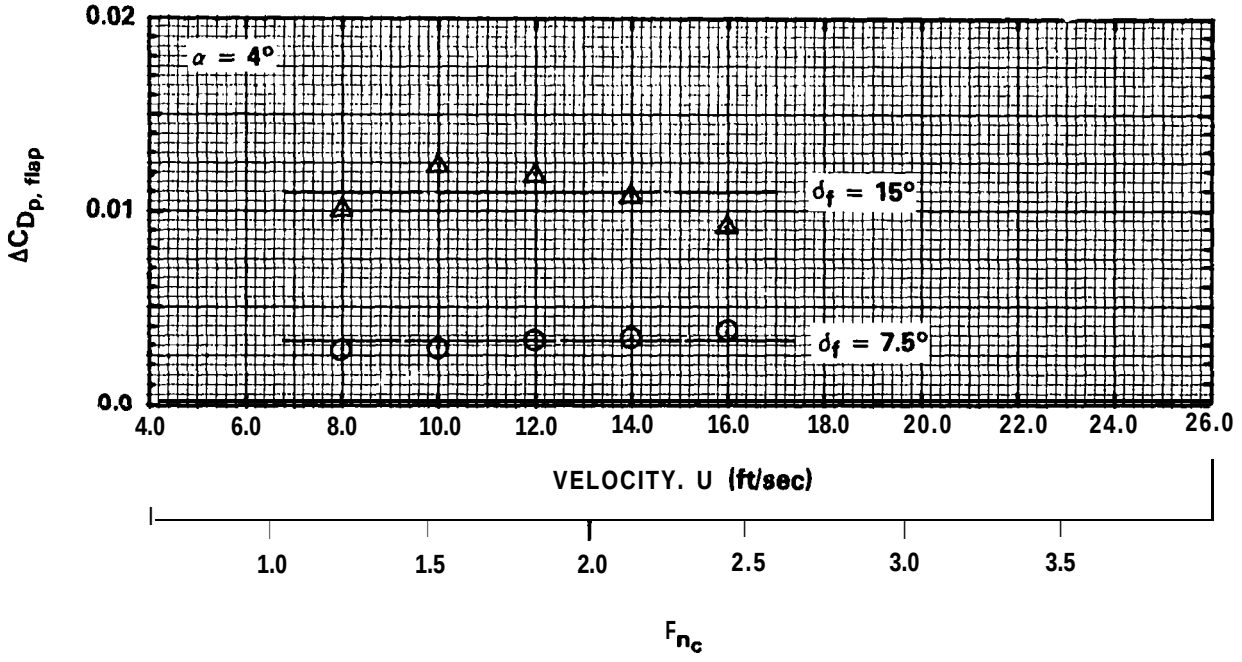

Figure 32 - Inferred Incremental Profile Drag Coefficient due to Flap Deflection versus Speed

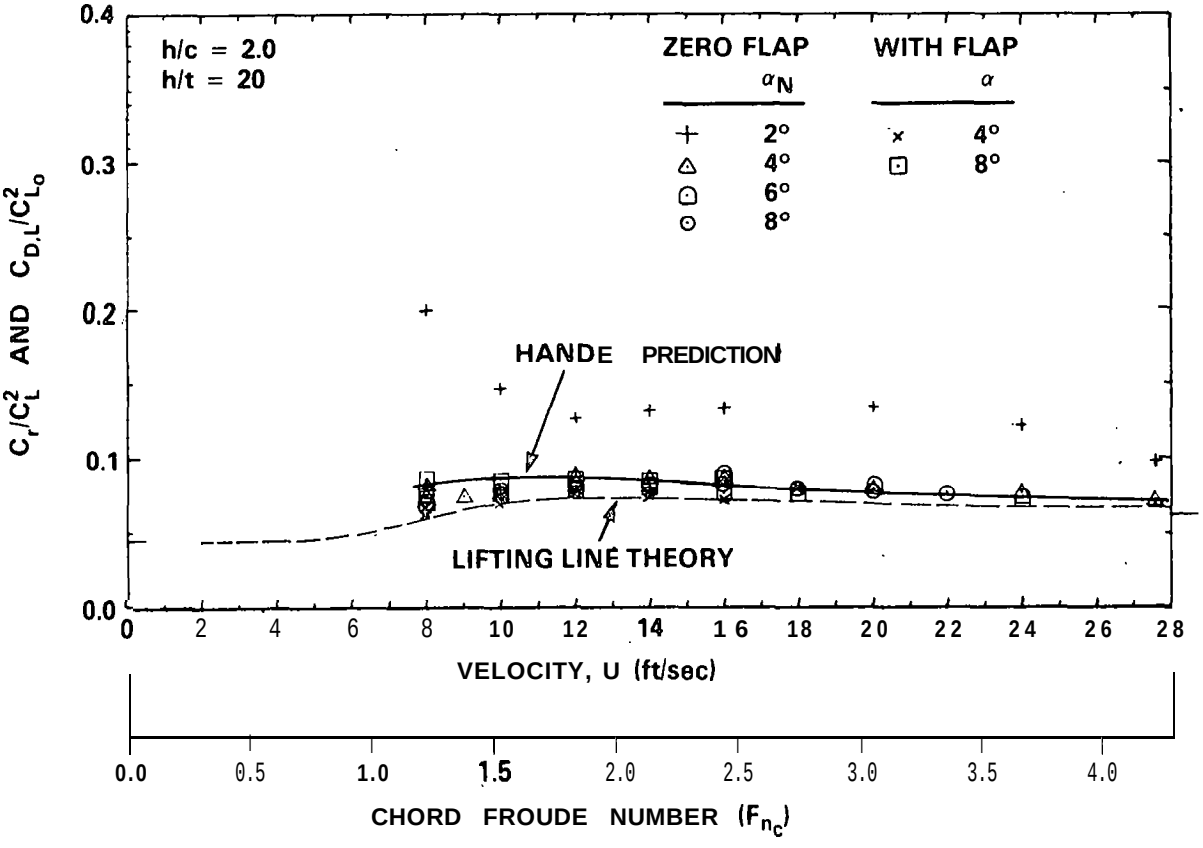

Figure 33 - Summary Plot of Total Drag-due-to-Lift Ratio versus Speed; Experiment and Predictions, at Submergence Ratio h/c = 2

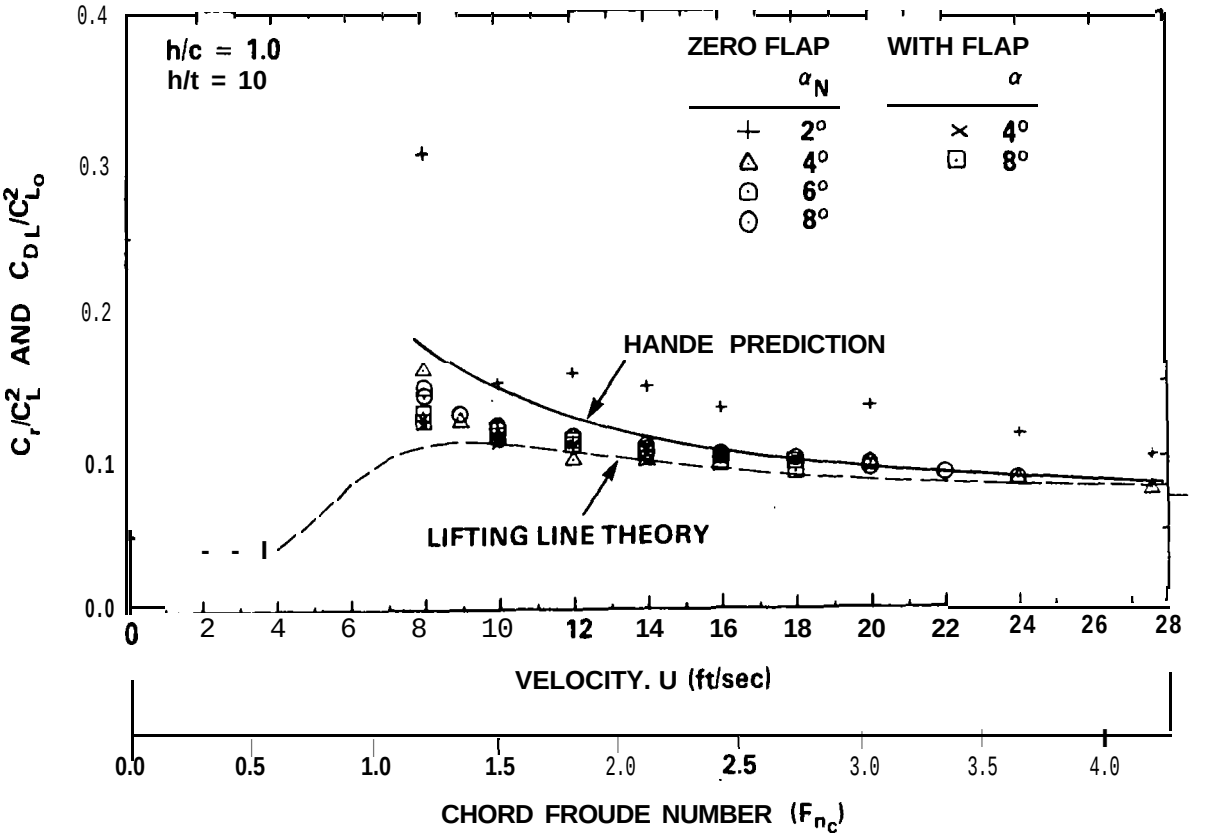

Figure 34 – Summary Plot of Total Drag-due-to-Lift Ratio versus Speed; Experiment and Predictions, at Submergence Ratio h/c = 1

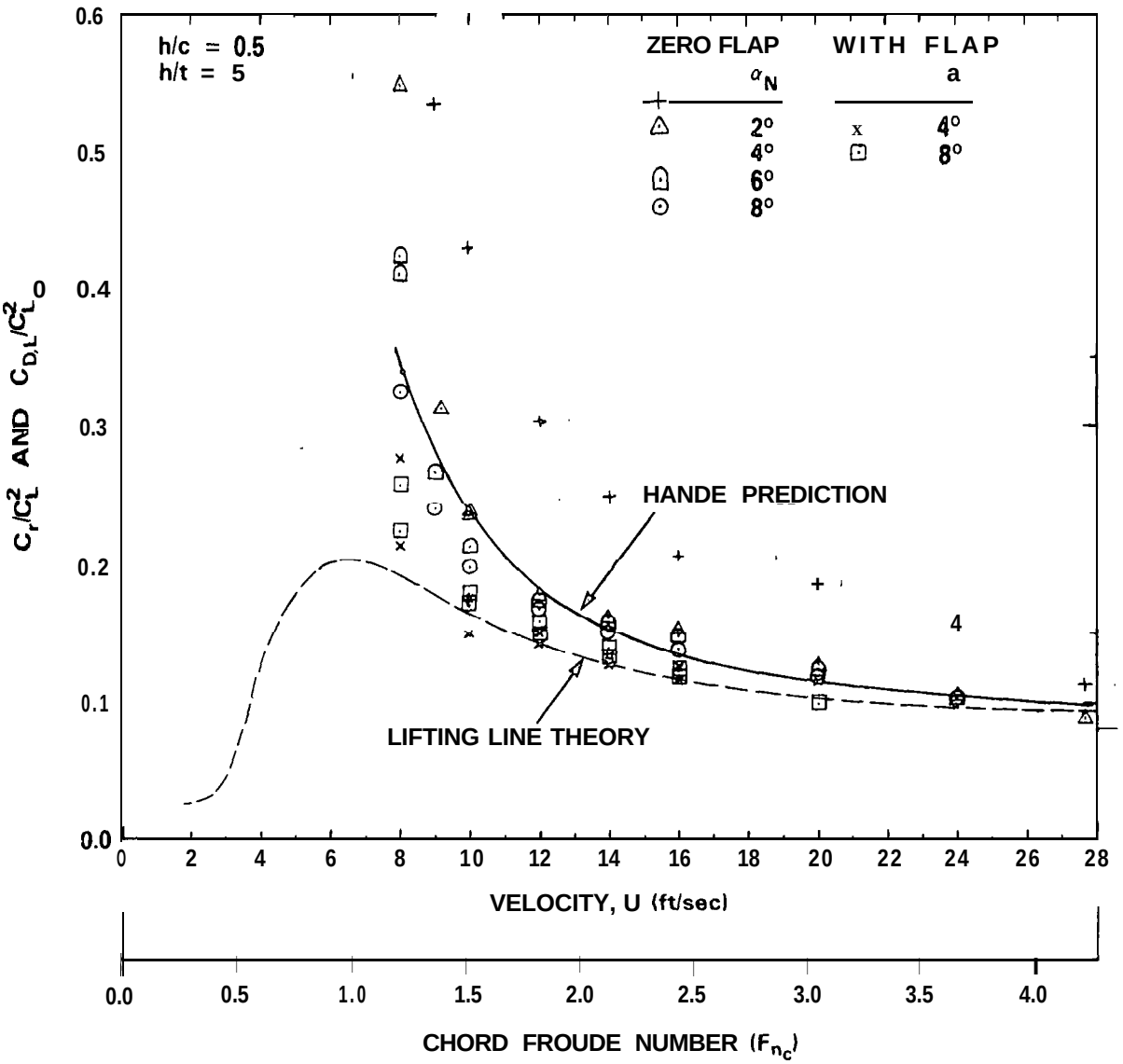

Figure 35 - Summary Plot of Total Drag-due-to-Lift Ratio versus Speed; Experiment and Predictions, at Submergence Ratio h/c = 0.5

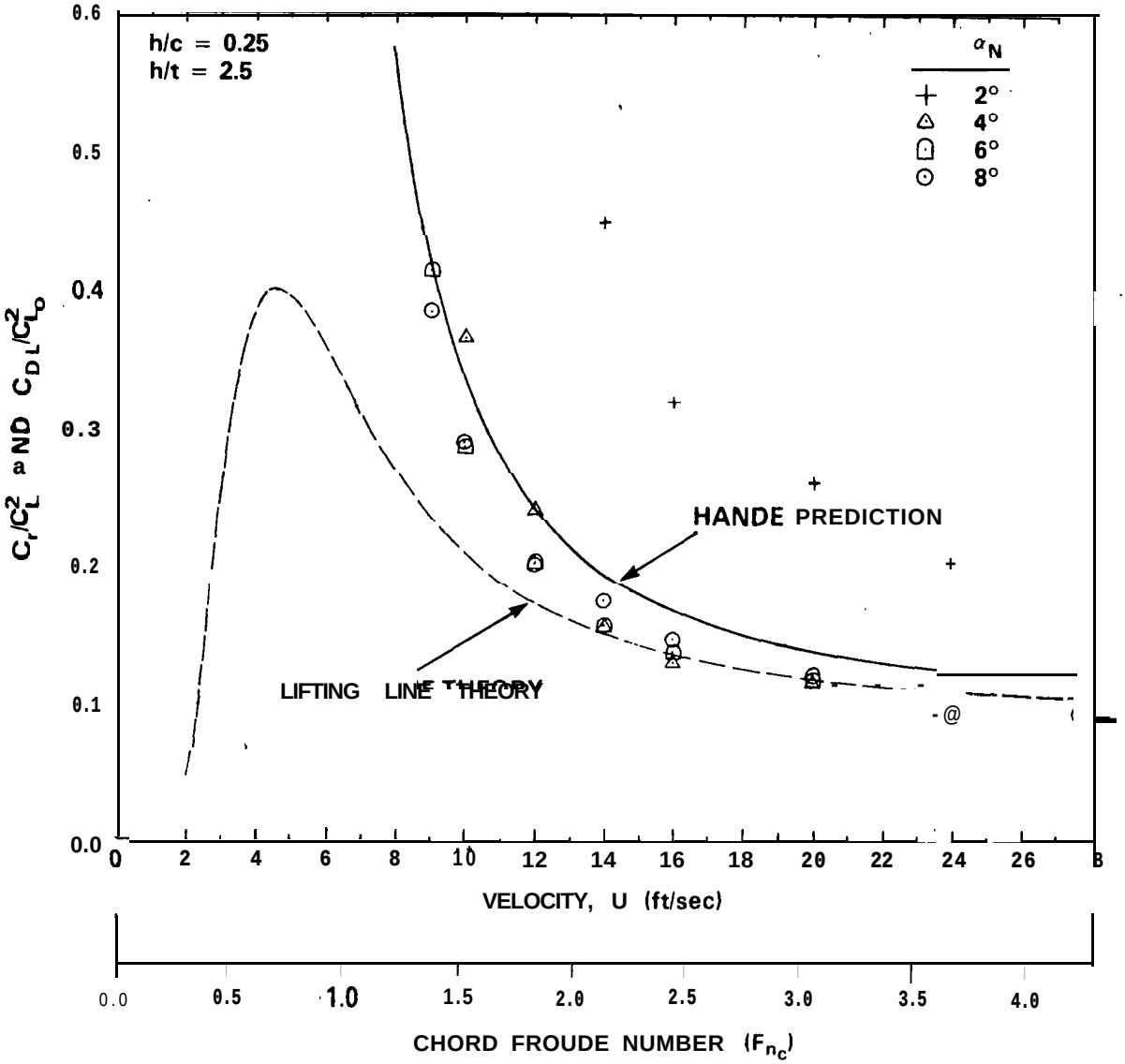

Figure 36 - Summary Plot of Total. Drag-due-to-Lift Ratio versus Speed; Experiment and Predictions, at Submergence Ratio h/c = 0.25

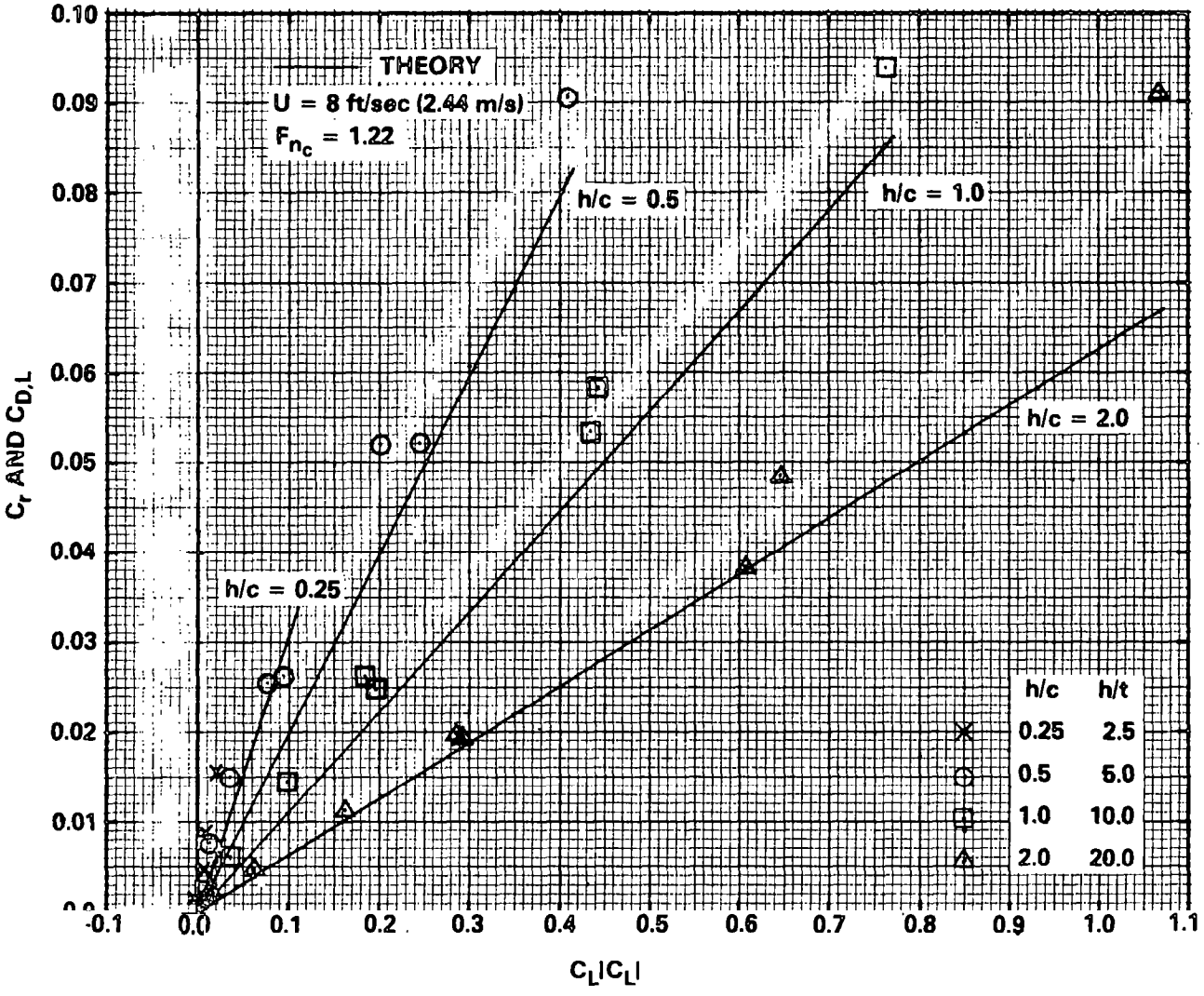

Figure 37 - Comparison of Measured Cr with Calculated C_D L from Lifting Line Theor'y versus C_L^2, for F_{n_c} = 1.22'

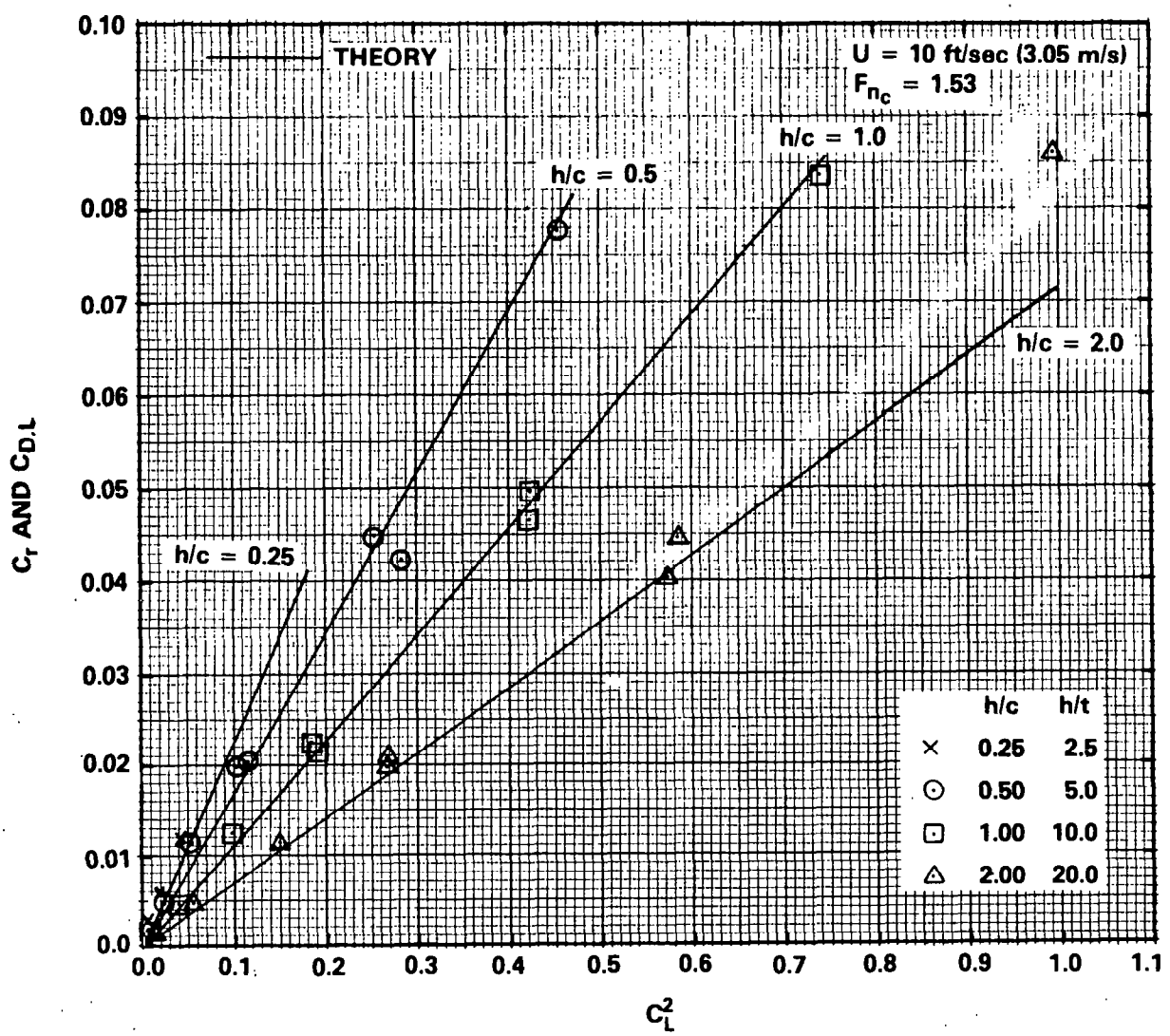

Figure 38 - Comparison of Measured C_{r_2} with Calculated $C_{D,L}$ from Lifting Line Theory versus C_L^2, for Fnc = 1.53

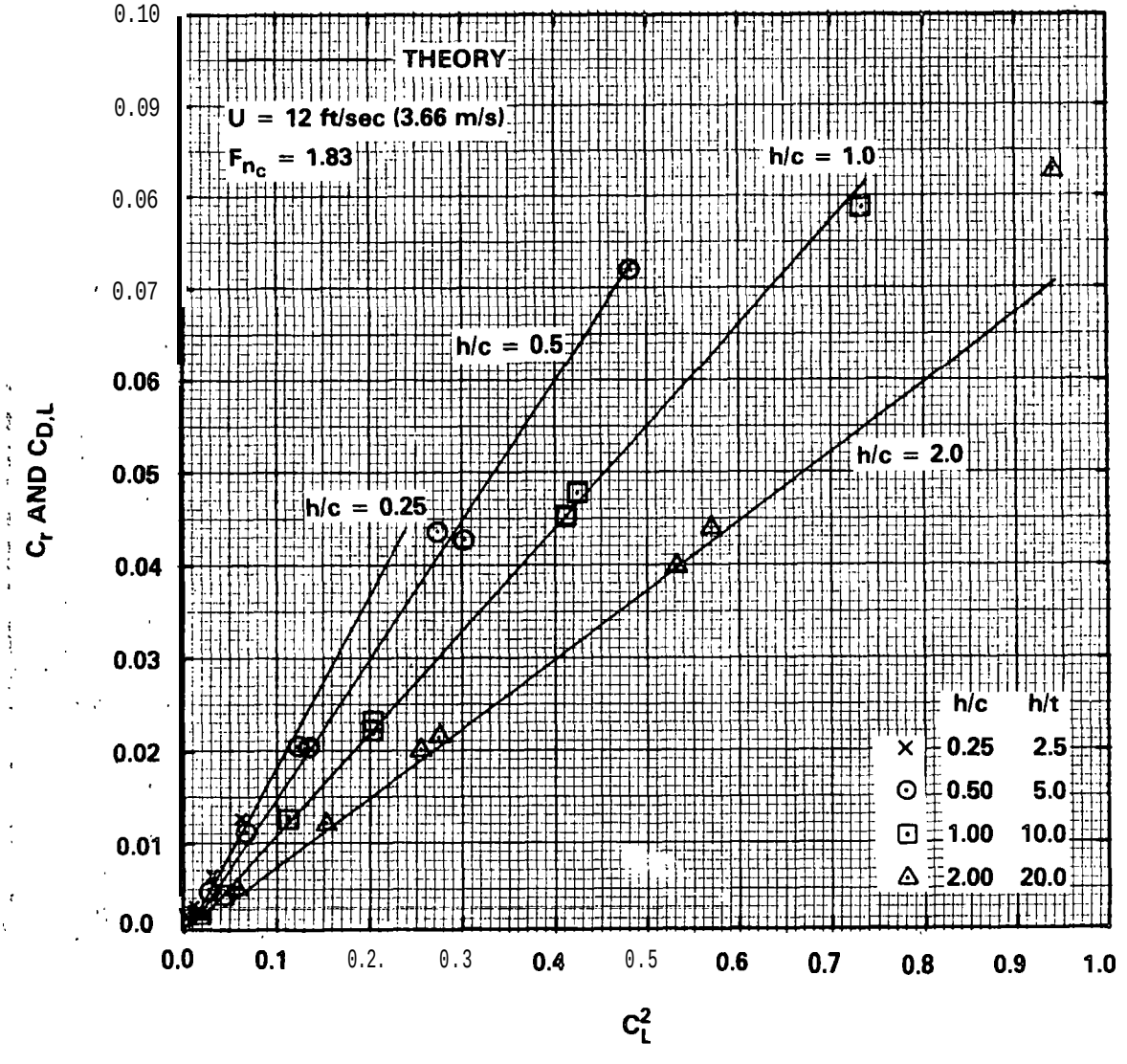

Figure 39 - Comparison of Measured C_r with Calculated $C_{D,L}$ from Lifting Line Theory versus C_L^2, fbr F_{n_c} = 1.83

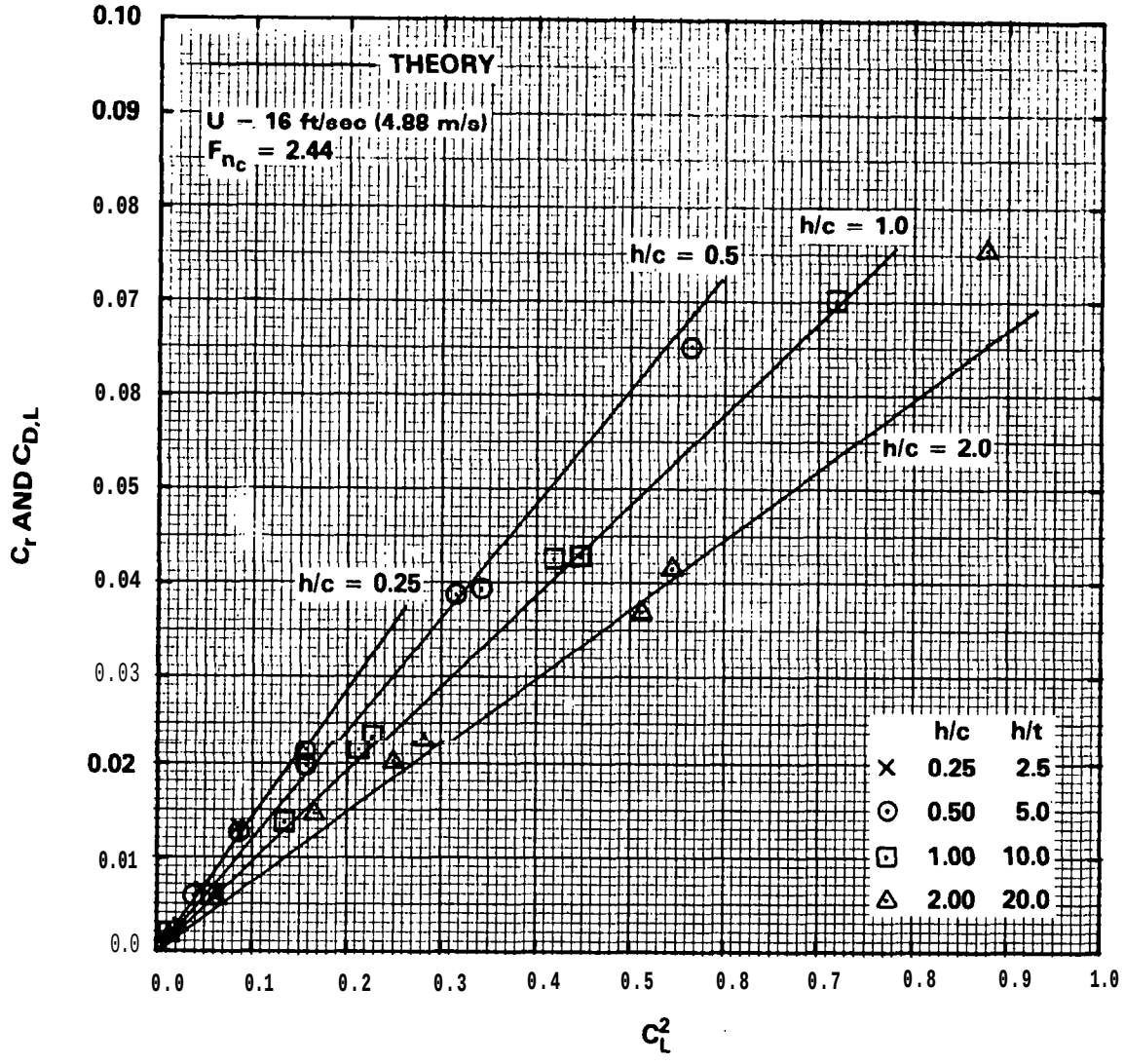

Figure 40 - Comparison of Measured C_r with Calculated $C_{D,L}$ from Lifting Line Theory versus C_L^2, for F_{n_c} = 2.44

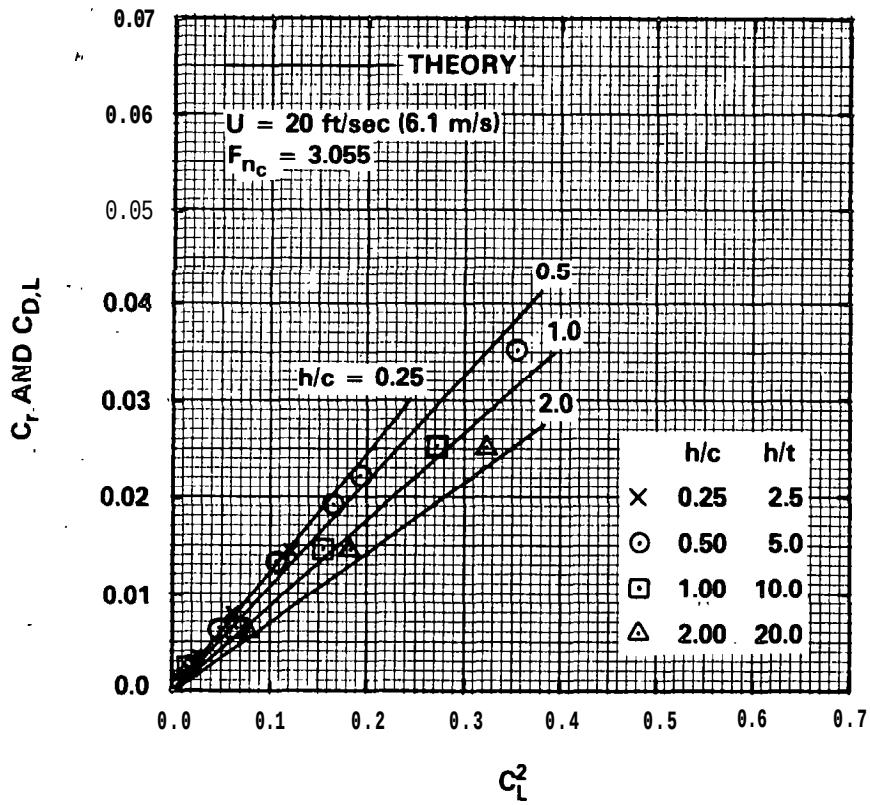

Figure 41 - Comparison of Measured Cr with Calculated $C_{D,L}$ from Lifting Line 'Theory versus C_L^2, for F_{n_c} = 3.055

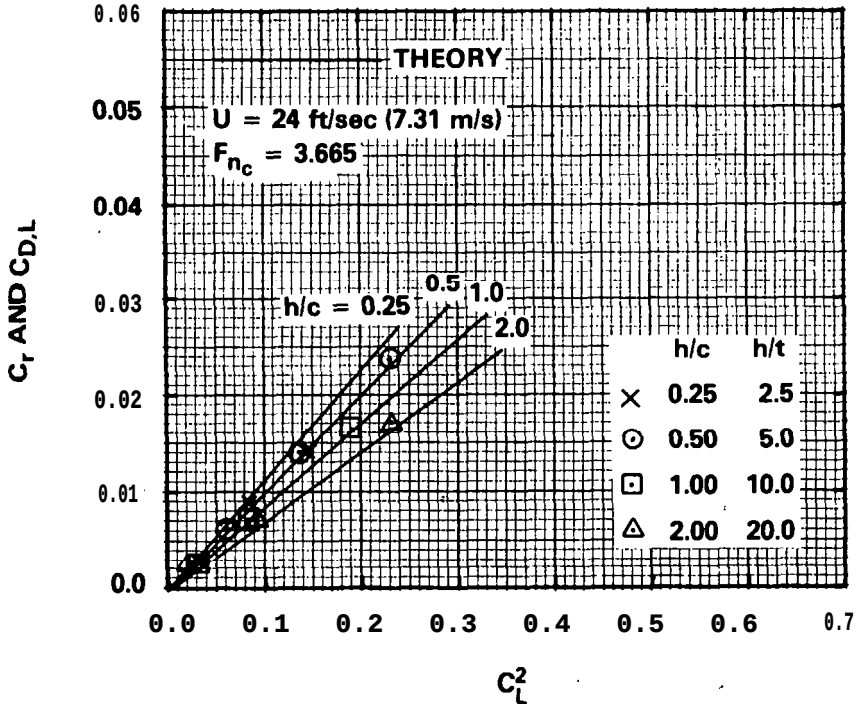

Figure 42 - Comparison of Measured C_r with Calculated $C_{D,L}$ from Lifting Line Theory versus C_L^2, for F_{n_c} = 3.665

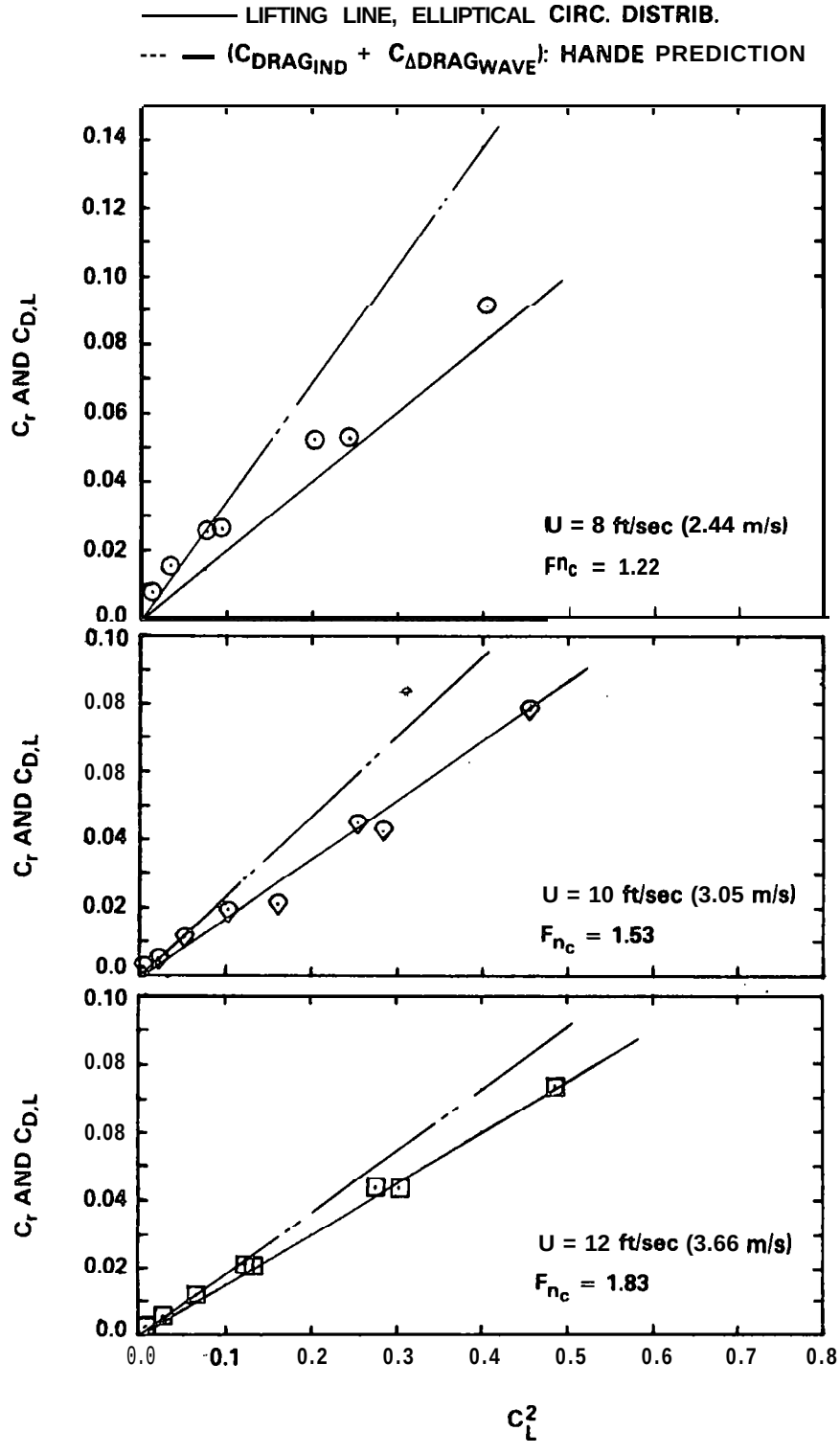

Figure 43 - Comparison of Measured C_r with Predictions of $C_{D,L}$ versus C_L^2, for Submergence Ratio h/c = 0.5

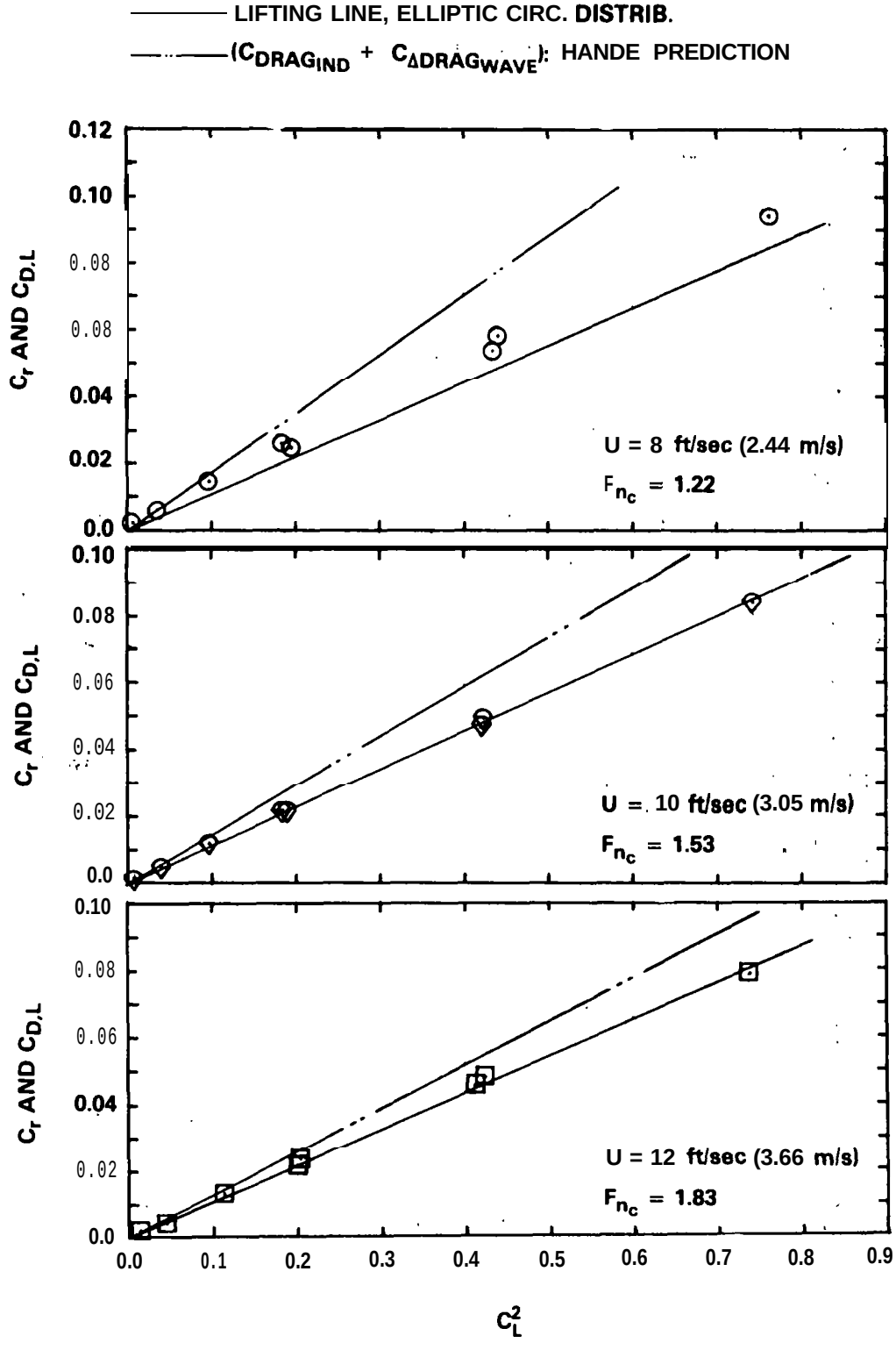

Figure 44 - Comparison of Measured Cr with Predictions of $C_{D,L}$ versus C_L^2, for Submergence Ratio h/c = 1

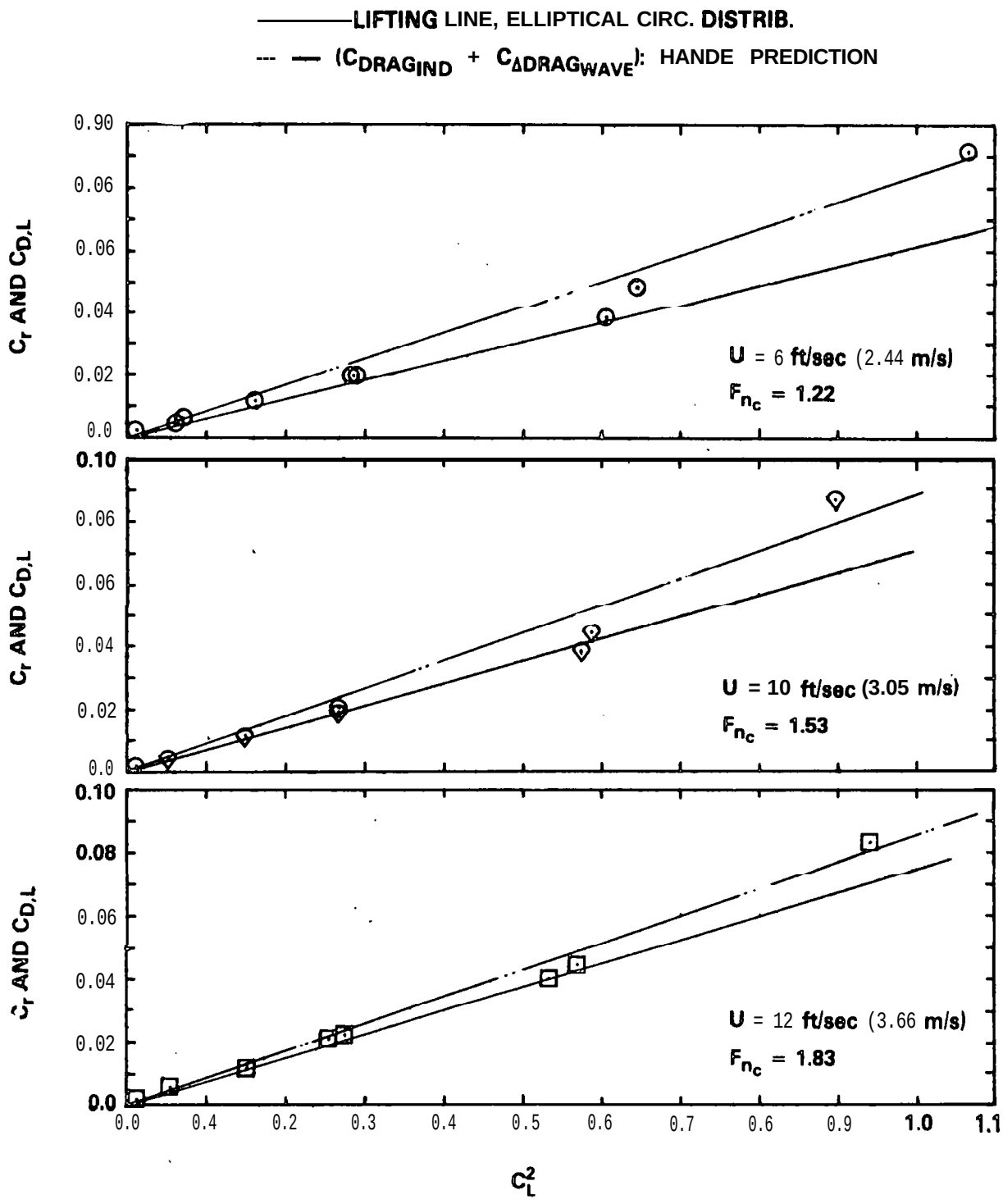

Figure'45 - Comparison of Measured C_r with Predictions of $C_{D,L}$ versus C_L^2, for Submergence Ratio h/c = 2

APPENDIX A

MEASURED HYDROFOIL FORCE DATA FOR ZERO FLAP DEFLECTION

TABLE A.1 - LIFT AND DRAG DATA FOR $\delta_f = 0$; h/c = 4

Angle of Attack α (deg)	Nominal Velocity u_∞ (ft/sec)	(m/s)	F_{n_c}	C_L	C_D
$\alpha_N = 0$					
-0.0075	a	2.44	1.22	-0.0219	0.01286
-0.0145	10	3.05	1.53	-0.0268	0.01224
-0.0179	12	3.66	1.83	-0.0229	0.012
-0.03	14	4.27	2.14	-0.0288	0.012
-0.044	16	4.88	2.44	-0.03167	0.0119
-0.071	20	6.1	3.05	-0.033	0.01167
-0.117	24	7.32	3.67	-0.03783	0.01154
-0.204	27.6	8.41	4.21	-0.04966	0.01125
-0.192	27.6	8.41	4.21	-0.04683	0.01137
$\alpha_N = 2$					
2.04	a	2.44	1.22	0.1195	0.01433
2.062	10	3.05	1.53	0.1151	0.01428
2.088	12	3.66	1.83	0.1119	0.01424
2.117	14	4.27	2.14	0.1102	0.0142
2.163	16	4.88	2.44	0.1181	0.0144
2.274	20	6.1	3.05	0.1274	0.01429
2.424	24	7.32	3.67	0.1368	0.01436
2.635	27.8	a.47	4.25	0.1529	0.01442
$\alpha_N = 4$					
4.088	a	2.44	1.22	0.2556	0.01806
4.139	10	3.05	1.53	0.2555	0.01823
4.201	12	3.66	1.83	0.2571	0.01832
4.281	14	4.27	2.14	0.2627	0.01851
4.367	16	4.88	2.44	0.2659	0.01902
4.598	20	6.1	3.05	0.2785	0.01984
4.942	24	7.32	3.67	0.3039	0.02034
5.387	27.6	8.41	4.21	0.3372	0.02068
5.386	27.6	8.41	4.21	0.3368	0.02062
$\alpha_N = 6$					
6.1401	a	2.44	1.22	0.406	0.02608
6.219	10	3.05	1.53	0.4035	0.02718
6.322	12	3.66	1.83	0.4116	0.02785
6.443	14	4.27	2.14	0.4164	0.029
6.583	16	4.88	2.44	0.4226	0.02945
6.96	20	6.1	3.05	0.4479	0.03077
7.549	24	7.32	3.67	0.5011	0.03093
$\alpha_N = a$					
8.187	a	2.44	1.22	0.5438	0.03567
8.298	10	3.05	1.53	0.551	0.0376
a.425	12	3.66	1.83	0.5441	0.03956
a.583	14	4.27	2.14	0.5482	0.04061
8.764	16	4.88	2.44	0.5562	0.04182
9.001	18	5.49	2.75	0.5766	0.04356
9.274	20	6.1	3.05	0.5959	0.043
9.605	22	6.71	3.36	0.6222	0.04348

TABLE A.2 - LIFT AND DRAG DATA FOR δ_f = 0; h/c = 2

Angle of Attack α (deg)	Nominal Velocity U (ft/sec)	(m/s)	F_{n_c}	C_L	C_D
α_N = 0					
-0.0113	8	2.44	1.22	-0.03288	0.01203
-0.0138	10	3.05	1.53	-0.02537	0.01215
-0.0144	12	3.66	1.83	-0.01834	0.01194
-0.0202	14	4.27	2.14	-0.0189	0.01192
-0.0246	16	4.88	2.44	-0.01781	0.01177
-0.0366	20	6.1	3.05	-0.01706	0.01169
-0.06	24	7.32	3.67	-0.01934	0.01166
-0.106	27.6	8.41	4.21	-0.0256	0.01151
-0.113	27.6	8.41	4.21	-0.02747	0.01142
α_N = 2					
2.038	8	2.44	1.22	0.110	0.01522
2.058	10	3.05	1.53	0.1067	0.0146
2.087	12	3.66	1.83	0.1111	0.01438
2.122	14	4.27	2.14	0.1149	0.01438
2.163	16	4.88	2.44	0.1183	0.01433
2.275	20	6.1	3.05	0.1281	0.01417
2.444	24	7.32	3.67	0.1433	0.0144
2.669	27.6	8.41	4.21	0.1623	0.0143
2.67	27.6	8.41	4.21	0.1625	0.0143
α_N = 4					
4.086	8	2.44	1.22	0.2488	0.01904
4.086	8	2.44	1.22	0.2476	0.0185
4.084	8	2.44	1.22	0.2448	0.01871
4.105	9	2.74	1.38	0.2409	0.01848
4.13	10	3.05	1.53	0.2406	0.01866
4.127	10	3.05	1.53	0.2338	0.0192
4.187	12	3.66	1.83	0.2386	0.01926
4.259	14	4.27	2.14	0.2433	0.01928
4.347	16	4.88	2.44	0.2512	0.01965
4.596	20	6.1	3.05	0.2773	0.01982
4.95	24	7.32	3.67	0.3065	0.02022
5.39	27.6	8.41	4.21	0.3379	0.02046
5.39	27.6	8.41	4.21	0.3387	0.02034
α_N = 6					
6.138	8	2.44	1.22	0.4014	0.02748
6.21	10	3.05	1.53	0.3873	0.02789
6.303	12	3.66	1.83	0.3882	0.02888
6.422	14	4.27	2.14	0.3967	0.02962
6.56	16	4.88	2.44	0.4065	0.03169
6.914	20	6.1	3.05	0.4263	0.03082
7.495	24	7.32	3.67	0.4835	0.03124
α_N = 8					
8.184	8	2.44	1.22	0.5357	0.03884
8.281	10	3.05	1.53	0.5193	0.04034
8.41	12	3.66	1.83	0.5246	0.04226
8.56	14	4.27	2.14	0.5273	0.0429
8.728	16	4.88	2.44	0.5294	0.04321
8.96	18	5.49	2.75	0.5524	0.04381
9.22	20	6.1	3.05	0.5693	0.04398
9.544	22	6.71	3.36	0.5974	0.04383

TABLE A.3 - LIFT AND DRAG DATA FOR δ_f = Cl; h/c = 1

Angle of Attack α (deg)	Nominal Velocity U (ft/sec)	(m/s)	F_{n_c}	C_L	C_D
α_N = 0					
-0.009	8	2.44	1.22	-0.02676	0.01202
-0.01	10	3.05	1.53	-0.0192	0.01166
-0.009	12	3.66	1.83	-0.01196	0.01161
-0.01	14	4.27	2.14	-0.00964	0.01169
-0.012	16	4.80	2.44	-0.00858	0.01166
-0.004	20	6.1	3.05	-0.00192	0.01187
-0.009	24	7.32	3.67	-0.00292	0.01166
-0.027	27.7	8.44	4.23	-0.00652	0.01135
-0.026	27.7	8.44	4.23	-0.00631	0.01137
α_N = 2					
2.03	8	2.44	1.22	0.084	0.01485
2.05	10	3.05	1.53	0.0926	0.01401
2.08	12	3.66	1.83	0.1028	0.01428
2.118	14	4.27	2.14	0.1102	0.01449
2.163	16	4.88	2.44	0.1183	0.0144
2.281	20	6.1	3.05	0.1307	0.01425
2.451	24	7.32	3.67	0.1452	0.01422
2.665	27.6	8.41	4.23	0.1614	0.01393
2.663	27.6	8.41	4.23	0.1609	0.01359
α_N = 4					
4.067	8	2.44	1.22	0.1937	0.01974
4.085	9	2.74	1.38	0.194	0.01809
4.11	10	3.05	1.53	0.2026	0.01837
4.11	10	3.05	1.53	0.1989	0.01816
4.166	12	3.66	1.83	0.2127	0.01851
4.17	12	3.66	1.83	0.2173	0.019
4.24	14	4.27	2.14	0.2266	0.01913
4.327	16	4.88	2.44	0.2373	0.01973
4.556	20	6.1	3.05	0.2589	0.02005
4.888	24	7.32	3.67	0.2865	0.01998
5.293	27.6	8.41	4.23	0.3139	0.01954
5.295	27.6	8.41	4.23	0.3143	0.0195
α_N = 6					
6.108	8	2.44	1.22	0.3136	0.0293
6.17	10	3.05	1.53	0.314	0.02736
6.262	12	3.66	1.83	0.3349	0.02854
6.376	14	4.27	2.14	0.3529	0.02943
6.504	16	4.88	2.44	0.3661	0.03
6.842	20	6.1	3.05	0.3926	0.03038
7.36	24	7.32	3.67	0.4389	0.03038
α_N = 8					
8.148	8	2.44	1.22	0.43	0.04293
8.182	9	2.74	1.38	0.4183	0.03921
8.233	10	3.05	1.53	0.4312	0.03958
8.352	12	3.66	1.83	0.4508	0.04135
8.496	14	4.27	2.14	0.4665	0.0426
8.657	16	4.88	2.44	0.477	0.0422
8.863	18	5.49	2.75	0.4962	0.04279
9.114	20	6.1	3.05	0.5197	0.0432
9.411	22	6.71	3.36	0.5451	0.04285

TABLE A.4 - LIFT AND DRAG DATA FOR δ_f = 0; h/c = 0.5

ngle of Attack α (deg)	Nominal Velocity U (ft/sec)	(m/s)	F_{n_c}	C_L	C_D
α_N = 0					
-0.0185	8	2.44	1.22	-0.0536	0.01257
-0.0167	10	3.05	1.53	-0.03086	0.01241
-0.0144	12	3.66	1.83	-0.01835	0.01241
-0.0137	14	4.27	2.14	-0.01284	0.01247
-0.015	16	4.88	2.44	-0.01076	0.0121
-0.007	20	6.1	3.05	-0.00521	0.01216
-0.014	24	7.32	3.67	-0.00461	0.01198
-0.033	27.6	8.41	4.21	-0.00793	0.01171
-0.035	27.6	8.41	4.21	-0.00845	0.01171
α_N = 2					
2.011	8	2.44	1.22	0.03196	0.01515
2.031	10	3.05	1.53	0.0578	0.01413
2.059	12	3.66	1.83	0.07557	0.01439
α_N = 4					
4.041	8	2.44	1.22	0.1177	0.02043
4.058	9	2.74	1.38	0.1328	0.01857
4.081	10	3.05	1.53	0.1484	0.01852
4.079	10	3.05	1.53	0.1461	0.01829
4.133	12	3.66	1.83	0.1698	0.01844
4.2	14	4.27	2.14	0.1875	0.01909
4.274	16	4.88	2.44	0.1984	0.01934
4.48	20	6.1	3.05	0.2215	0.01918
4.766	24	7.32	3.67	0.2469	0.01904
5.117	27.7	8.44	4.23	0.2709	0.0186
α_N = 6					
6.065	8	2.44	1.22	0.1887	0.0285
6.067	8	2.44	1.22	0.193	0.02874
6.092	9	2.74	1.38	0.2105	0.02566
6.124	10	3.05	1.53	0.2284	0.02512
6.204	12	3.66	1.83	0.2599	0.02603
6.3	14	4.27	2.14	0.2809	0.02716
6.407	16	4.88	2.44	0.2955	0.02755
6.714	20	6.1	3.05	0.3305	0.02789
7.146	24	7.32	3.67	0.3696	0.02748
α_N = 8					
8.097	8	2.44	1.22	0.2819	0.04023
8.13	9	2.74	1.38	0.2987	0.03622
8.172	10	3.05	1.53	0.3186	0.03528
8.274	12	3.66	1.83	0.3502	0.03634
8.397	14	4.27	2.14	0.3734	0.03741
8.548	16	4.88	2.44	0.3976	0.03820
8.94	20	6.1	3.05	0.4362	0.03866
9.489	24	7.32	3.67	0.4807	0.03782

TABLE A.5 - LIFT AND DRAG DATA FOR $\delta_{f_L} = 0$; h/c = 0.25

Angle of Attack α (deg)	Nominal Velocity U (ft/sec)	(m/s)	F_{n_c}	C_L	C_D
$\alpha_N = 0$					
-0.028	8	2.44	1.22	-0.08064	0.01195
-0.03	10	3.05	1.53	-0.05506	0.01207
-0.033	12	3.66	1.83	-0.04211	0.01187
-0.039	14	4.27	2.14	-0.03608	0.01195
-0.046	16	4.88	2.44	-0.03348	0.01184
-0.062	20	6.1	3.05	-0.0289	0.012
-0.093	24	7.32	3.67	-0.030	0.01173
-0.152	28.3	8.63	4.32	-0.0353	0.01141
-0.157	28.3	8.63	4.32	-0.03633	0.01142
$\alpha_N = 2$					
1.994	a	2.44	1.22	-0.01738	0.01348
1.994	8	2.44	1.22	-0.01762	0.01373
2.0	9	2.74	1.38	-0.00062	0.01273
2.01	10	3.05	1.53	0.0184	0.01274
2.03	12	3.66	1.83	0.039	0.01294
2.053	14	4.27	2.14	0.0498	0.01277
2.08	16	4.88	2.44	0.05826	0.01265
2.155	20	6.1	3.05	0.0721	0.0127
2.254	24	7.32	3.67	0.08196	0.0126
2.365	27.7	8.44	4.23	0.0885	0.01213
$\alpha_N = 4$					
4.009	8	2.44	1.22	0.0259	0.01714
4.021	9	2.74	1.38	0.04795	0.01543
4.048	10	3.05	1.53	0.08785	0.01545
4.091	12	3.66	1.83	0.116	0.0161
4.143	14	4.27	2.14	0.1339	0.01514
4.202	16	4.88	2.44	0.1461	0.01513
4.368	20	6.1	3.05	0.1709	0.01572
4.592	24	7.32	3.67	0.1907	0.01558
4.865	27.7	a.44	4.23	0.2095	0.01502
4.865	27.7	a.44	4.23	0.2096	0.01504
$\alpha_N = 6$					
6.032	8	2.44	1.22	0.09219	0.02162
6.033	8	2.44	1.22	0.09532	0.02165
6.052	9	2.74	1.38	0.1205	0.01902
6.078	10	3.05	1.53	0.1429	0.01908
6.141	12	3.66	1.83	0.1797	0.01998
6.214	14	4.27	2.14	0.2006	0.01998
6.3	16	4.88	2.44	0.2171	0.02009
6.552	20	6.1	3.05	0.257	0.02132
6.891	24	7.32	3.67	0.2872	0.0217
$\alpha_N = 8$					
8.052	8	2.44	1.22	0.1496	0.02867
8.077	9	2.74	1.38	0.1766	0.02548
8.11	10	3.05	1.53	0.2028	0.02573
8.195	12	3.66	1.83	0.249	0.02678
8.295	14	4.27	2.14	0.2767	0.02804
8.413	16	4.88	2.44	0.2992	0.02799
a. 748	20	6.1	3.05	0.3484	0.02925
9.178	24	7.32	3.67	0.3802	0.02756
9.618	27	a.23	4.12	0.412	0.02808
9.638	27	8.23	4.12	0.4172	0.02852

APPENDIX B

MEASURED HYDROFOIL FORCE DATA FOR FLAP DEFLECTION ANGLES δ_f = 7.5 AND 15 DEGREES

TABLE B.l - LIFT AND DUG DATA FOR δ_f = 7.5 DEGREES, 15 DEGREES; h/c = 4

Angle of Attack (deg)	Flap Deflection δ_f (deg)	Nominal Velocity U (ft/sec)	Nominal Velocity U (m/s)	F_{n_c}	C_L	C_D
α_N = 4						
4.193	7.5	8	2.44	1.22	0.5597	0.03531
4.301	7.5	10	3.05	1.53	0.5569	0.0365
4.436	7.5	12	3.66	1.83	0.5583	0.03796
4.6	7.5	14	4.27	2.14	0.5637	0.03909
4.782	7.5	16	4.88	2.44	0.5682	0.04003
5.004	7.5	18	5.49	2.75	0.5775	0.04093
5.023	7.5	18	5.49	2.75	0.5887	0.04134
5.265	7.5	20	6.1	3.05	0.5909	0.04152
5.595	7.5	22	6.71	3.36	0.6177	0.04192
α_N = 4						
4.276	15	8	2.44	1.22	0.801	0.06389
4.346	15	9	2.74	1.38	0.7971	0.06471
4.429	15	10	3.05	1.53	0.7948	0.06753
4.612	15	12	3.66	1.83	0.7844	0.06883
4.844	15	14	4.27	2.14	0.7952	0.07056
5.119	15	16	4.88	2.44	0.8145	0.07169
5.423	15	18	5.49	2.75	0.8203	0.07258
5.435	15	18	5.49	2.75	0.8277	0.07216
α_N = 8						
8.285	7.5	8	2.44	1.22	0.8273	0.078
8.36	7.5	9	2.74	1.38	0.827	0.07828
8.448	7.5	10	3.05	1.53	0.8286	0.0787
8.649	7.5	12	3.66	1.83	0.8316	0.08013
8.906	7.5	14	4.27	2.14	0.8401	0.07567
9.175	7.5	16	4.88	2.44	0.8552	0.07598
9.496	7.5	18	5.49	2.75	0.8615	0.07843
α_N = 8						
8.357	15	8	2.44	1.22	1.0358	0.1331
8.559	15	10	3.05	1.53	1.0364	0.1353
8.808	15	12	3.66	1.83	1.0371	0.1377
9.107	15	14	4.27	2.14	1.0459	0.1404
9.445	15	16	4.88	2.44	1.054	0.1403

TABLE B.2 - LIFT AND DRAG DATA FOR δ_f = 7.5 DEGREES, 15 DEGREES; h/c = 2

Angle of Attack α (deg)	Flap Deflection δ_f (deg)	Nominal Velocity U (ft/sec)	Nominal Velocity U (m/s)	F_{n_c}	C_L	C_D
α_N = 4						
4.19	7.5	8	2.44	1.22	0.5528	0.03891
4.29	7.5	10	3.05	1.53	0.5363	0.0397'9
4.416	7.5	12	3.66	1.83	0.5329	0.04075
4.58	7.5	14	4.27	2.14	0.5457	0.04164
4.746	7.5	16	4.88	2.44	0.5422	0.04179
4.969:	7.5	18	5.49	2.75	0.5566	0.04239
4.979	7.5	18	5.49	2.75	0.5626	0.04221
5.23	7.5	20	6.1	3.05	0.5744	0.04243
5.554	7.5	22	6.71	3.36	0.6006	0.04191
α_N = 4						
4.276	15	8	2.44	1.22	0.7989	0.06925
4.339	15	9	2.74	1.38	0.7785	0.07016
4.424	15	10	3.05	1.53	0.7834	0.0719
4.422	15	10	3.05	1.53	0.7822	0.07204
4.595	15	12	3.66	1.83	0.7613	0.07297
4.82	15	14	4.27	2.14	0.7723	0.07343
5.07	15	16	4.88	2.44	0.7776	0.07327
5.37	15	18	5.49	2.75	0.7881	0.07393
α_N = 8						
8.284	7.5	8	2.44	1.22	0.8233	0.07612
8.352	7.5	9	2.74	1.38	0.8094	0.07213
8.431	7.5	10	3.05	1.53	0.7983	0.07351
8.62	7.5	12	3.66	1.83	0.7946	0.07538
8.833	7.5	14	4.27	2.14	0.7846	0.07608
9.105	7.5	16	4.88	2.44	0.8047	0.07686
9.092	7.5	16	4.88	2.44	0.7953	0.07551
9.419	7.5	18	5.49	2.75	0.8178	0.07586
α_N = 8						
8.365	15	8	2.44	1.22	1.059	0.1341
8.453	15	9	2.74	1.38	1.043	0.1336
8.557	15	10	3.05	1.53	1.032	0.131
8.795	15	12	3.66	1.83	1.019	0.1329
9.08	15	14	4.27	2.14	1.018	0.1301
9.394	15	16	4.88	2.44	1.017	0.1337

TABLE B.3 - LIFT AND DRAG DATA FOR δ_f = 7.5 DEGREES, 15 DEGREES; h/c = 1

Angle of Attack α (deg)	Flap Deflection δ_f (deg)	Nominal Velocity U (ft/sec)	Nominal Velocity U (m/s)	F_{n_c}	C_L	C_D
α_N = 4						
4.156	7.5	8	2.44	1.22	0.454	0.04314
4.196	7.5	9	2.74	1.38	0.4513	0.04066
4.245	7.5	10	3.05	1.53	0.452	0.04013
4.367	7.5	12	3.66	1.83	0.4688	0.04103
4.521	7.5	14	4.27	2.14	0.4901	0.04163
4.688	7.5	16	4.88	2.44	0.4995	0.04204
4.891	7.5	18	5.49	2.75	0.5115	0.042
5.423	7.5	22	6.71	3.36	0.5494	0.04219
α_N = 4						
4.231	15	8	2.44	1.22	0.671	0.08124
4.29	15	9	2.74	1.38	0.6667	0.07668
4.359	15	10	3.05	1.53	0.6634	0.07522
4.525	15	12	3.66	1.83	0.6717	0.07517
4.733	15	14	4.27	2.14	0.689	0.07533
4.965	15	16	4.88	2.44	0.701	0.07486
5.266	15	18	5.49	2.75	0.7286	0.07528
5.61	15	20	6.1	3.05	0.7523	0.07348
α_N = 8						
8.233	7.5	8	2.44	1.22	0.6773	0.08223
8.29	7.5	9	2.74.	1.38	0.6667	0.07705
8.36	7.5	10	3.05	1.53	0.667	0.07529
8.532	7.5	12	3.66	1.83	0.6822	0.07598
8.739	7.5	14	4.27	2.14	0.6964	0.0756
8.979	7.5	16	4.88	2.44	0.712	0.07483
9.277	7.5	18	5.49	2.75	0.7347	0.0745
α_N = 8						
8.306	15	8	2.44	1.22	0.8889	0.1299
8.381	15	9	2.74	1.38	0.8768	0.1246
8.478	15	10	3.05	1.53	0.8848	0.1223
8.702	15	12	3.66	1.83	0.8988	0.1205
8.708	15	12	3.66	1.83	0.9058	0.1215
8.966	15	14	4.27	2.14	0.9099	0.1195
9.226	15	16	4.88	2.44	0.8923	0.1175
9.618	15	18	5.49	2.75	0.9315	0.1175

TABLE B.4 - LIFT AND DRAG DATA FOR δ_f = 7.5 DEGREES, 15 DEGREES; h/c = 0.5

Angle of Attack α (deg)	Flap Deflection δ_f (deg)	Nominal Velocity U (ft/sec)	(m/s)	F_{n_c}	C_L	C_D
α_N = 4						
4.109	7.5	8	2.44	1.22	0.3171	0.04312
4.144	7.5	9	2.74	1.38	0.331	0.0384
4.189	7.5	10	3.05	1.53	0.3494	0.03772
4.297	7.5	12	3.66	1.83	0.3797	0.0383
4.432	7.5	14	4.27	2.14	0.4048	0.03849
4.582	7.5	16	4.88	2.44	0.4222	0.03894
4.77	7.5	18	5.49	2.75	0.4412	0.03908
4.99	7.5	20	6.1	3.05	0.4588	0.03912
5.247	7.5	22	6.71	3.36	0.4811	0.03905
5.543	7.5	24	7.32	3.67	0.498	0.0385
α_N = 4						
4.174	15	8	2.44	1.22	0.5038	0.078
4.229	15	9	2.74	1.38	0.5265	0.07396
4.295	15	10	3.05	1.53	0.5458	0.06912
4.446	15	12	3.66	1.83	0.5704	0.07023
4.637	15	14	4.27	2.14	0.5979	0.06951
4.862	15	16	4.88	2.44	0.6255	0.06941
5.131	15	18	5.49	2.75	0.6496	0.06877
5.456	15	20	6.1	3.05	0.679	0.06924
α_N = 8						
8.157	7.5	8	2.44	1.22	0.4543	0.07161
8.211	7.5	9	2.74	1.38	0.4854	0.06915
8.277	7.5	10	3.05	1.53	0.5105	0.06678
8.425	7.5	12	3.66	1.83	0.5432	0.0676
8.611	7.5	14	4.27	2.14	0.5732	0.06729
8.813	7.5	16	4.88	2.44	0.5899	0.0657
9.084	7.5	18	5.49	2.75	0.6225	0.06558
9.402	7.5	20	6.1	3.05	0.6534	0.06549
α_N = 8						
8.222	15	8	2.44	1.22	0.6446	0.1211
8.287	15	9	2.74	1.38	0.6611	0.1141
8.369	15	10	3.05	1.53	0.6831	0.1109
8.556	15	12	3.66	1.83	0.7124	0.1073
8.79	15	14	4.27	2.14	0.7429	0.1058
9.083	15	16	4.88	2.44	0.7871	0.1064
9.415	15	18	5.49	2.75	0.8139	0.1032

APPENDIX C

BIPLANE FACTOR FOR HYDROFOIL INDUCED DRAG

The biplane factor σ_i enters the expressions for drag coefficient-due-to-lift from lifting line theory given in Equations (6) and (8), and can be seen to account, partially, for the effect of the nearby image foil for near surface operation. It is most useful for determining the limiting values of $C_{D,L}$ at both vanishing and infinite Froude numbers as indicated in Equations (8). The factor σ_i for elliptic circulation distribution only depends upon the depth-to-half span ratio $h/(b/2)$. Biplane factor values, applicable to a rectangular planform of aspect ratio A = 6, are presented in Table C.l as a function of h/c and $h/(b/2)$.

TABLE C.l - BIPLANE FACTORS FOR ELLIPTICAL CIRCULATION DISTRIBUTION

h/c	$\frac{h}{b/2}$	Biplane Factor σ_i
0.25	0.08333	0.69464
0.5	0.1667	0.53314
1.0	0.3333	0.34088
2.0	0.6667	0.16556
4.0	1.333	0.058735
A = 6		

REFERENCES

1. wu, T.Y., "A Theory for Hydrofoils of Finite Span," Journal of Mathematics and Physics, Vol. 33, pp. 207-248 (1954/1955); also California Institute of Technology Hydrodynamics Laboratory Report 26-8 (May 1953).

2. Nishiyama, T., "Linearized Steady Theory of Fully Wetted Hydrofoils," Advances in Hydroscience, Vol. 3, Edited by Ven Te Chow, Academic Press, pp. 237-342 (1966).

3. Breslin, J.P., "Application of Ship-Wave Theory to the Hydrofoil of Finite Span," Journal of Ship Research, Vol. 1, No. 1, pp. 27-35 (1957).

4. Wadlin, K.L., C.L. Shuford and J.R. McGehee, "A Theoretical and Experimental Investigation of Hydrofoils at Subcritical and Supercritical Speeds," NACA Report 1232 (1955).

5. Wilson, M.B. and J.R. Kelley, "Low Froude Number Performance of a Flat Plate Hydrofoil," DTNSRDC Ship Performance Department Report SPD-743-01 (Dec 1976).

6. Jones, C.E., "Flapped Hydrofoils in Smooth Water Subcavitating Flow," General Dynamics/Convair Report ZH-153 (Nov 1961).

7. Feldman, J., "Experimental Investigation of Near-Surface Hydrodynamic Force Coefficients for a Systematic Series of Tee Hydrofoils, DTMB Series HF-1," David Taylor Model Basin Report 1801 (Dec 1963).

8. Layne, D., "Lift and Drag Characteristics of NACA 16-309 and NACA 64A309 Hydrofoils," DTNSRDC Ship Performance Department Report SPD-326-07 (Oct 1976).

9. Dixon, R.J., M. Schmiechen, L.C. Shrout, and R.K. Watanabe, "An Experimental Investigation of the Hydrodynamic Characteristics of a Partially Cavitating Hydrofoil," Proc. 19th ATTC, University of Michigan, Ann Arbor, Michigan (Jul 1980).

10. Loftin, L.K., "Theoretical and Experimental Data for a Number of NACA 6A-Series Airfoil Sections," NACA Report 903 (1948).

11. Hoerner, S.F., "Fluid Dynamic Drag," Published by the 'Author, Midland Park, N.J. (1958).

12. Martin, M., "The Stability Derivatives of a Hydrofoil Boat-Part I," Hydronautics Inc. Report 001-10(I) (Jan 1963).

13. von Kármán, T. and J.M. Burgers, "General Aerodynamics Theory - Perfect Fluids," Vol. II of Aerodynamic Theory, Edited by W.F. Durand, Dover Publications (1963).

14. Wilson, M.B., "Lifting Line Calculations for Hydrofoil Performance at Arbitrary Froude Number and Submergence. Part I Fixed Shape Elliptical Circulation Distribution,'! DTNSRDC Ship Performance Department Report DTNSRDC/SPD-0839-01 (Jun 1978).

15. Young, A.D., "The Aerodynamic Characteristics of Flaps," British A.R.C. R&M 2622 (1953).

16. Boeing Company, "Hydrofoil Analysis and Design Program (HANDE). Theory Manual, Vol. 2," Boeing Document D321-51312-2 (Jul 1976).

17. Salvesen, N. and C. von Kerczek, "Comparison of Numerical and Perturbation Solutions of Two-Dimensional Water-Wave Problems," Journal of Ship Research, Vol. 20, No. 3 (Sept 1976).

INITIAL DISTRIBUTION

Copies	
2	CHONR 1 LIB 1 Code 438
3	USNA 1 TECH. LIB 1 Naval System Engr. Dept. 1 B. Johnson
1	NRL/LIB
1	US ARMY TRANS. R&D MARINE TRANS DIV.
1	NAVPGSCOL/LIB
3	NOSC 1 LIB 1 Hoyt. 1 Higdon
22	NAVSEA 1 SEA 03R/Kobitz 2 SEA 03R1/Dilts/Schuler 2 SEA 03R2/Benen/Sejd 1 SEA 31/Fee 1 SEA 31B/Gayle 1 SEA 3124/Spaulding 2 SEA 31242/Bebar/Kennell 1 SEA 32B/Keane 1 SEA 321/Cauldwell 1 SEA 32131/Goldstein 2 SEA 32132/Comstock/McCallum 1 SEA 32133/Sandberg 3 Det. Norfolk/Code 6660 1 LIB 1 Blount 1 Denny
3	CBC Port Hueneme, CA (CEL) 1 LIB 2 L-44/Ward/Meggit
12	DTIC
1	US COAST GUARD ACAD/LIB
1	US COAST GUARD NAVAL ENGIN.

Copies	
1	DOT/LIB, TAD-491.1
5	MARAD 1 Div. Ship Design 1 Coord Res. 1 Falls 1 Lasky 1 Siebold
2	MMA 1 LIB 1 Maritime Research Center
1	NASA HQ/LIB
1	NBS/LIB
1	NSF/Engin. Div. LIB
3	U OF CA, Berkeley/Dept. NAME 1 LIB 1 W. Webster 1 J. Wehausen
2	U OF CA, San Diego 1 A. Ellis 1 Scripps Inst. LIB
3	CIT 1 Aero LIB 1 A. Acosta 1 T. Wu
2	HARVARD U 1 Gordon McKay LIB 1 Carrier
1	U OF HAWAII/St. Denis
1	U OF ILLINOIS/J. Robertson
3	U OF IOWA 1 LIB 1 IHR/Kennedy 1 IHR/Landweber

Copies	
2	UOFMARYLAND
	1 Engin. LIB
	1 A. Plotkin, Dept. Aero Engin.
4	MIT, Dept. Ocean Engin.
	1 Barker Engin. LIB
	1 Kerwin
	1 Leehey
	1 Newman
5	U OF MINN/St. Anthony Falls
	1 LIB
	1 Arndt
	1 Silberman
	1 Song
	1 Wetzel
5	U OF MICH/Dept. NAME
	1 LIB
	1 Couch
	1 Vorus
	1 Latorre
	1 Benford
2	PENN STATE U
	1 ARL LIB
	1 Parkin
4	SIT/Davidson Lab
	1 LIB
	1 Breslin
	1 Brown
	1 Savitsky
2	SOUTHWEST RESEARCH INST.
	1 Applied Mech. Rev.
	1 Abramson
2	STANFORD U
	1 R. Street, Dept. Civil Eng.
	1 H. Ashley
1	STANFORD RES. INST./LIB
2	U OF WASHINGTON
	1 Arl. Tech. LIB
	1 D.E. Calkins

Copies	
2	VIRGINIA POLYT. INST
	1 W. Saric, Dept. Eng. Sci. and Mechs.
	1 A. Magnuson, Dept. Aero and Ocean Eng.
3	WEBB INST.
	1 LIB
	1 Hadler
	1 Ward
1	ASME/Res. Comm. Info.
1	ASNE
1	SNAME/Tech. LIB
1	AERO JET-GENERAL/LIB Azusa, CA
3	THE BOEING CO./Advanced Mar. Sys.
	1 Dixon
	1 Feifel
	1 Ray
2	BOLT, BERANEK, NEWMAN
	1 LIB
	1 N. Brown
2	DESIGNERS & PLANNERS, INC.
	1 LIB
	1 Slager
3	EDO CORP.
	1 LIB
	1 Otto
	1 Kaplan
1	GENERAL DYNAMICS CONVAIR ASW - Marine Science
2	GIBBS & COX
	1 Tech. LIB
	1 Nelson
3	GRUMMAN AEROSPACE CO., NY
	1 Tech. LIB
	1 Wright
	1 Pieroth

Copies	
1	HYDROMECHANICS, INC./Kaplan
5	HYDRONAUTICS, INC. 1 LIB 1 Hsu 1 Johnson 1 Scherer 1 Duncan
1	LOCKHEED, SUNNYVALE/Waid
3	MCDONNELL DOUGLAS, Long Beach 1 Tech. LIB 1 Hess 1 Smith
1	NEWPORT NEWS SHIPBLDG/LIB
2	ORI, INC. 1 Bullock 1 Kim
3	SCIENCE APPL. INC. 1 Skragg, La Jolla, CA 1 Von Kerczek, Annapolis, MD 1 Salvesen, Annapolis, MD
1	TETRA TECH INC., Pasadena, CA W a d e

CENTER DISTRIBUTION

Copies	Code	Name
1	0120	Jewel1
1	11	Ellsworth
1	117	Stevens
1	1102.1	Nakonechny
1	1110	Lamb
1	1150	Johnston
1	1151	O'Neill
1	15	Morgan
1	1504	Monacella
1	1506	Hawkins
1	1509	Powell
1	152	Lin
1	1521	Day
1	1521	Karafiath
1	1522	Dobay
25	1522	Wilson
1	1522	Peck
1	1522	Remmers
1	1523	Stenson
1	1523	Layne
1	154	McCarthy
1	1540	Granville
1	1541	Folb
1	1541	Rispin
1	1542	Branch Head
1	1542	Huang
1	1542	Chang
1	1542	Shen
1	1543	Santorre
1	1543	Besch
1	1543	Coder
1	1543	Jeffers
1	1543	Rood
1	1544	Brockett
1	1544	Boswell
1	156	Cieslowski
1	1560	Martin
1	1561	cox
1	1562	Moran
1	1562	Zarnick
1	1563	Smith
1	1563	Roddy
1	1564	Feldman
1	1564	Wolfe
1	16	Chaplin
1	1730.3	Buckley
1	1946	'Feller
1	2705	Gregory

Copies	Code	Name
20	5211.1	Reports Distribution
1	522.1	Unclassified Library (C)
1	522.2	Unclassified Library (C)

DTNSRDC ISSUES THREE TYPES OF REPORTS

1. DTNSRDC REPORTS, A FORMAL SERIES, CONTAIN INFORMATION OF PERMANENT TECHNICAL VALUE. THEY CARRY A CONSECUTIVE NUMERICAL IDENTIFICATION REGARDLESS OF THEIR CLASSIFICATION OR THE ORIGINATING DEPARTMENT.

2. DEPARTMENTAL REPORTS, A SEMIFORMAL SERIES, CONTAIN INFORMATION OF A PRELIMINARY, TEMPORARY, OR PROPRIETARY NATURE OR OF LIMITED INTEREST OR SIGNIFICANCE. THEY CARRY A DEPARTMENTAL ALPHANUMERICAL IDENTIFICATION.

3. TECHNICAL MEMORANDA, AN INFORMAL SERIES, CONTAIN TECHNICAL DOCUMENTATION OF LIMITED USE AND INTEREST. THEY ARE PRIMARILY WORKING PAPERS. INTENDED FOR INTERNAL USE. THEY CARRY AN IDENTIFYING NUMBER WHICH INDICATES THEIR TYPE AND THE NUMERICAL CODE OF THE ORIGINATING DEPARTMENT. ANY DISTRIBUTION OUTSIDE DTNSRDC MUST BE APPROVED BY THE HEAD OF THE ORIGINATING DEPARTMENT ON A CASE-BY-CASE BASIS.